



International Agreement Report

Validation of the CHAN-Component in TRACE using BWR Full-Size Fine-Mesh Bundle Tests

Prepared by:
M. Thieme, Dr. W. Tietsch

Westinghouse Electric Germany GmbH
Dudenstrasse 44
68167 Manheim
Germany

A. Calvo, NRC Project Manager

**Office of Nuclear Regulatory Research
U.S. Nuclear Regulatory Commission
Washington, DC 20555-0001**

August 2010

Prepared as part of
The Agreement on Research Participation and Technical Exchange
Under the Thermal-Hydraulic Code Applications and Maintenance Program (CAMP)

**Published by
U.S. Nuclear Regulatory Commission**

Validation of the CHAN-Component in TRACE using BWR Full-Size Fine-Mesh Bun- dle Tests

Manuscript Completed: December 2007

Date Published: August 2010

Prepared by:

M. Thieme, Dr. W. Tietsch
Westinghouse Electric Germany GmbH
Dudenstrasse 44
68167 Mannheim
Germany

Prepared as part of
The Agreement on Research Participation and Technical Exchange
Under the Thermal-Hydraulic Code Applications and Maintenance Program (CAMP)

**U.S. Nuclear Regulatory Commission
Washington, DC 20555-0001**



ABSTRACT

This report has been prepared at Westinghouse Electric Germany GmbH. The aim of this work is the validation of the CHAN-component for the systems code TRACE. For this purpose selected experimental NUPEC BFBT void fraction tests as well as critical power steady state and transient tests have been used to be compared to TRACE Version 5 RC 2 calculations. The NUPEC experiments contain uniquely detailed data measured not only as bundle averaged but also in a very detailed, spatial resolution down to 0.3 mm. Hence these tests are very appropriate for the validation.

In this report a description of the BFBT experimental set up, measurement technique is given. A description of the detailed TRACE modes of physical models and the steady state and transient TRACE calculations for the selected experiments as well the boundary conditions are also included in this report. A comparison between code predictions and measurements is presented and discussed.

CONTENTS

Abstract.....	iii
List of Figures.....	vi
List of Tables.....	viii
Executive Summary.....	ix
Abbreviations.....	xi
1 Introduction.....	1
2 Description of BWR Full-Size Fine Mesh Bundle Test Facility	3
2.1 Test Loop.....	3
2.2 Test Bundles.....	5
2.3 Measurement Methods	10
3 Description of the Tests.....	15
3.1 Void Distribution Tests.....	15
3.1.1 Steady State Tests	15
3.1.2 Transient Experiment 4102-001~009	16
3.2 Critical Power Tests.....	18
3.2.1 Steady State Experiments	19
3.2.2 Transient Experiment TGA10008	19
4 Short Description of TRACE.....	23
5 Modelling of the NUPEC Bundle Test for TRACE	25
6 Post-Test Calculation with TRACE.....	27
6.1 TRACE Calculation of Void Distribution Tests.....	27
6.1.1 TRACE Results for Steady State Test 1071-53.....	27
6.1.2 TRACE Results for Steady State Test 4101-53.....	31
6.1.3 Discussion of Void Fraction Steady State Results.....	34
6.1.4 TRACE Results for Transient Test 4102-001~009	50
6.2 Critical Power Calculations	53
6.2.1 Introductory Remarks	53
6.2.2 Discussion of Critical Power Steady State Results.....	55
6.2.3 TRACE Results for Transient Test TGA10008	61
7 Conclusions.....	67
8 References	69
Appendix A Input Deck Listing for Test 4101-53.....	71

LIST OF FIGURES

Fig. 2.1: Scheme of the BFBT facility [1]	4
Fig. 2.2: The test section of the BFBT facility [1]	5
Fig. 2.3: Bundle type α	6
Fig. 2.4: Bundle type β	6
Fig. 2.5: Cross section view of heater rod	7
Fig. 2.6: Schematic view of heater rod	7
Fig. 2.7: Spacer location [1].....	8
Fig. 2.8: Constructive details grid spacer (mm) [1]	9
Fig. 2.9: Constructive details ferrule spacer design (mm) [1]	9
Fig. 2.10: Void fraction measurement system [1]	10
Fig. 2.11: Definition of thermocouple position [1]	11
Fig. 2.12: Axial and radial location of thermocouples [1].....	12
Fig. 2.13: Pressure taps location for critical power measurements [1].....	13
Fig. 3.1: Cosine power distribution pattern [1].....	16
Fig. 3.2: Evolution of Flow rate [1].....	17
Fig. 3.3: Evolution of total power [1].....	17
Fig. 3.4: Pressure evolution at bundle inlet and outlet [1]	18
Fig. 3.5: Evolution of coolant temperature [1].....	18
Fig. 3.6: Inlet power distribution pattern [1]	19
Fig. 3.7: Flow rate vs. time [1]	20
Fig. 3.8: Total power vs. time [1]	20
Fig. 3.9: Pressure at the bundle inlet and outlet vs. time [1]	21
Fig. 3.10: Coolant temperature vs. time [1]	21
Fig. 5.1: TRACE model of the BFBT test section	25
Fig. 5.2: Radial heater location of bundle type α showing the different heater groups	26
Fig. 5.3: Radial heater location of bundle type β showing the different heater groups.....	26
Fig. 6.1: Comparison between BFBT data and TRACE results of test 1071-53	28
Fig. 6.2: Calculated liquid, saturation and gas temperature of test 1071-53	29
Fig. 6.3: Heater surface temperatures of each heater group of test 1071-53	29
Fig. 6.4: Heat transfer coefficient of each heater group of test 1071-53	30
Fig. 6.5: Comparison between BFBT data and TRACE results of test 4101-53	32
Fig. 6.6: Calculated liquid, saturation, gas temperature of test 4101-53	32
Fig. 6.7: Heater surface temperatures of each heater group of test 4101-53	33
Fig. 6.8: Heat transfer coefficient of each heater group of test 4101-53	33
Fig. 6.9: Comparison of predicted and measured void fraction results	34
Fig. 6.10: Void fraction C / M ratio versus inlet sub-cooling (Assembly Type 0-1)	36
Fig. 6.11: Void fraction C / M ratio versus outlet quality (Assembly Type 0-1).....	36
Fig. 6.12: Void fraction C / M ratio versus mass flow (Assembly Type 0-1)	37
Fig. 6.13: Void fraction C / M ratio versus outlet pressure (Assembly Type 0-1)	37
Fig. 6.14: Void fraction C / M ratio versus outlet quality (Assembly Type 0-2).....	38
Fig. 6.15: Void fraction C / M ratio versus mass flow (Assembly Type 0-2)	38
Fig. 6.16: Void fraction C / M ratio versus outlet pressure (Assembly Type 0-2)	39
Fig. 6.17: Void fraction C / M ratio versus outlet quality (Assembly Type 0-3).....	39
Fig. 6.18: Void fraction C / M ratio versus mass flow (Assembly Type 0-3)	40
Fig. 6.19: Void fraction C / M ratio versus outlet pressure (Assembly Type 0-3)	40

Fig. 6.20: Void fraction C / M ratio versus inlet sub-cooling (Assembly Type 1)	41
Fig. 6.21: Void fraction C / M ratio versus outlet quality (Assembly Type 1)	41
Fig. 6.22: Void fraction C / M ratio versus mass flow (Assembly Type 1)	42
Fig. 6.23: Void fraction C / M ratio versus outlet pressure (Assembly Type 1)	42
Fig. 6.24: Void fraction C / M ratio versus outlet quality (Assembly Type 2)	43
Fig. 6.25: Void fraction C / M ratio versus mass flow (Assembly Type 2)	43
Fig. 6.26: Void fraction C / M ratio versus outlet pressure (Assembly Type 2)	44
Fig. 6.27: Void fraction C / M ratio versus outlet quality (Assembly Type 3)	44
Fig. 6.28: Void fraction C / M ratio versus mass flow (Assembly Type 3)	45
Fig. 6.29: Void fraction C / M ratio versus outlet pressure (Assembly Type 3)	45
Fig. 6.30: Void fraction C / M ratio versus inlet sub-cooling (Assembly Type 4)	46
Fig. 6.31: Void fraction C / M ratio versus outlet quality (Assembly Type 4)	46
Fig. 6.32: Void fraction C / M ratio versus mass flow (Assembly Type 4)	47
Fig. 6.33: Void fraction C / M ratio versus outlet pressure (Assembly Type 4)	47
Fig. 6.34: Distribution of calculation / measurement ratio at outlet.....	48
Fig. 6.35: Distribution of calculation / measurement ratio of all void fraction tests	49
Fig. 6.36: Comparison between BFBT data and TRACE results at X-ray densitometer #3 ...	50
Fig. 6.37: Comparison between BFBT data and TRACE results at X-ray densitometer #2 ...	51
Fig. 6.38: Comparison between BFBT data and TRACE results at X-ray densitometer #1 ...	51
Fig. 6.39: Comparison between BFBT data and TRACE results at bundle outlet.....	52
Fig. 6.40: Approach to determine the critical power from results according to [1].....	54
Fig. 6.41: Ratio of prediction (C) and measurement (M) dependent on pressure	55
Fig. 6.42: Ratio of prediction (C) and measurement (M) dependent on pressure	56
Fig. 6.43: Temperature rise due to dry out of test SA510600	57
Fig. 6.44: Progression of the heat transfer coefficient of test SA510600	57
Fig. 6.45: Temperature rise due to dry out of test SA610600	58
Fig. 6.46: Progression of the heat transfer coefficient of test SA610600	58
Fig. 6.47: Temperature rise due to dry out of test SA810600	59
Fig. 6.48: Progression of the heat transfer coefficient of test SA810600	59
Fig. 6.49: Temperature rise due to dry out of test SC610500	60
Fig. 6.50: Progression of the heat transfer coefficient of test SC610500	60
Fig. 6.51: Comparison between measured inlet pressure and calculation.....	62
Fig. 6.52: Comparison between measured fluid outlet temperature and calculation.....	62
Fig. 6.53: Positions of thermocouples [1]	63
Fig. 6.54: Elevation of thermocouples [1]	63
Fig. 6.55: Temperatures of symmetric thermocouple positions to each other.....	64
Fig. 6.56: View of further comparable measured thermocouple temperatures	64
Fig. 6.57: Comparison between the averaged thermocouple temperature and calculation ...	65
Fig. 6.58: Axial temperature distribution.....	65

LIST OF TABLES

Tab. 2.1: Nichrome / Constantan properties [1]	7
Tab. 2.2: Boron Nitride properties [1]	7
Tab. 2.3: Inconel 600 properties [1].....	8
Tab. 2.4: Estimated accuracy of measured parameters [1].....	14
Tab. 3.1: Radial power pattern of bundle type α [1]	15
Tab. 3.2: Radial power pattern of bundle type β [1]	16
Tab. 3.3: Boundary conditions of the void fraction tests [1].....	16
Tab. 3.4: Boundary conditions of the selected critical power tests [1].....	19
Tab. 5.1: Power peaking factors of heater groups	26
Tab. 6.1: Comparison pressure drop over the bundle of test 1071-53.....	27
Tab. 6.2: Comparison pressure drop over the bundle of test 4101-53.....	31

EXECUTIVE SUMMARY

The aim of this work is the validation of the heat transfer models of the CHAN component in TRACE which is relevant for the modeling of fuel assemblies in boiling water reactors. In this context, measurements at the BWR full-size fine-mesh bundle test facility (BFBT) were used for TRACE validation described in this report. Four steady state experiments as well as one transient test for critical power and two steady state as well as one transient experiment for void fraction determination were selected.

For the purpose of validation, specific input decks for each of the selected BFBT tests were developed using TRACE components, specially the CHAN, the FILL and the BREAK components. Hereby all specified details of geometry, material properties and operation conditions as well as boundary conditions of the bundle and its components (heaters, spacers, wall) were considered in the TRACE-models.

Using the models developed, TRACE simulations for each test were performed on a WINDOWS PC using the version 5 RC 02.

The results of the predictions were compared to the experiment data available of the BFBT tests. Based on the comparison performed of calculation and data the following conclusion can be drawn:

- For the simulation of the BFBT steady state void fraction test, TRACE gave a good prediction on the void fraction at the bundle outlet (RSME: 0.039). But it tended to underpredict the void fraction measured at the middle of the bundle (2.73 m). Here the RSME between the prediction and the data is 0.078. But the deviation is almost within the measurement error band.
- For the transient void fraction tests representing a turbine trip transient the trends of the void fractions could be fully reproduced by TRACE in a high quality. The TRACE predictions also agree quantitatively very good with the void fraction trends except for low mass flow rates and void fractions below 0.15. For void fractions between 0.45 and 0.8 together with high mass flow rates and high heat fluxes the agreement between predictions and void fraction data is in an acceptable range with same deviations below 15 %.
- For the four selected stationary critical power tests, the predictions and data agreement is good. In general TRACE however tends to overpredict the measurement of the critical power with a RSME below 0.82 MW. For safety analysis the overprediction of critical power is not conservative!
- For the turbine trip transient critical power tests, the TRACE predictions followed qualitatively well the inlet pressure but did not follow the measured fluid temperature at the bundle outlet. The predicted limit temperature at the bundle outlet tends to increase approximately 2 s earlier than the measured one and the maximum value is about 4 K higher than the measured temperature peak. In addition, the sharp increase of the measured cladding temperature caused by the sudden increase of the

power (boundary condition) could not be reproduced by TRACE. The putter temperature increase predicted by TRACE was 6 K to a measured value of 89 K.

It should be mentioned also that attempts to simulate these tests with TRACE versions 4155, 416, 4230, 4250, 4216 and 4273 were not successful either. The obtained results did not reflect the expected physical behavior. Furthermore it was attempted to compare the CHAN with the PIPE component. Also the results with the PIPE component were in good agreement with the BFBT data but as expected a better agreement was observed with the CHAN component.

The TRACE investigations related to the stationary void fraction measurements have shown a considerable discrepancy of the TRACE predictions and of the measured data for specific conditions such as low mass flow rates and high heat flux (subcooled boiling regime). Hence further post test calculations with TRACE of relevant steady state BFBT void tests are necessary to make final conclusions about the prediction's quality.

For the final clarification of the large mismatch between the cladding temperature peak predicted by TRACE and the one measured, it is recommended to simulate further transient critical power tests. Moreover since the predicted cladding temperature is already during the steady state simulation 13 K below the measured cladding temperature, a re-evaluation of the stationary TRACE simulation combined with a parameter study is needed for the derivation of final conclusions.

ABBREVIATIONS

ATHLET	- Analysis of Thermal-Hydraulics of Leaks and Transients
BFBT	- BWR Full-Size Fine-Mesh Bundle Test
BWR	- Boiling Water Reactor
CATHARE	- code avancé de thermohydraulique pour accidents de reacteur à eau (advanced Thermohydraulic Code for the Simulation of Accidents in Light Water Reactors)
CHF	- Critical Heat Flux
CT	- Computer Tomography
GSS	- generalized steady state
LOCA	- lost of coolant Accident
LWR	- Light Water Reactor
NPP	- Nuclear Power Plant
NUPEC	- Nuclear Power Engineering Cooperation
PWR	- Pressure Water Reactor
RELAP	- Reactor loss of coolant Analysis Program
RSME	- Root Square Mean Error
TRAC	- Transient Reactor Analysis Code
TRACE	- TRAC&RELAP advanced computational Engine
US-NRC	- U. S. Nuclear Regulatory Commission

1 Introduction

Since the last decade the importance of computational simulation programs has increased in the nuclear industry. Governments which use the nuclear power in a peaceful manner prescribe regular safety evaluations of nuclear power plants (NPP) [2] [3] [4]. Safety reports especially for accident analysis describe the use of thermohydraulic system codes [6]. In addition both the NPP manufacturers and operators are always endeavouring to optimize their plant's efficiency by simulating specific transients with the help of simulation software.

A basic requirement for the use of thermohydraulic system codes is the sufficient qualification of the code, which has to be accomplished for the respective fields of application. Depending on the definition of the problem, codes like RELAP5/MOD3.3, ATHLET, CATHARE or TRAC B/P are currently used. They are well verified on the basis of extensive international longtime verification programs. Some computational programs developed by the U. S. Nuclear Regulatory Commission (U.S.-NRC), for example RELAP5 or TRAC have reached a high quality standard and they are used today as state of the art codes, however they will not be developed further because it would be too expensive to develop two codes in parallel consequence. Therefore since more than six years the U.S.-NRC has been working on the development of a new code system called TRACE (TRAC/RELAP Advanced Computational Engine). It was intended that TRACE combines the advantages of both predecessors RELAP5 and TRAC [5]. Since the development of TRACE is still ongoing. There are still comprehensive qualification and verification efforts needed to validate TRACE for industrial use as well as for safety evaluations of NPP.

TRACE has components which were developed specifically for the use for boiling water reactors (BWR) [5]. A typical example is the CHAN component. It is able to simulate fuel elements of different fuel rod and water rod configurations by using 1D hydraulic models to simulate the flow through the fuel assemblies as well as the leakage path flow from the BWR fuel assembly into the core bypass. The CHAN component can be used to represent one or more BWR fuel assemblies in a core. The CHAN component includes a number of other 1D hydraulic components, heat structures, and radiation heat transfer components for the solution of the 1D mass, energy, momentum and heat transfer equations. The CHAN component brings together all of the input required to generate a BWR fuel assembly model. TRACE internally generates (i.e. spawns) all the TRACE sub-components needed to simulate the flow and heat transfer associated with a BWR fuel assembly. The sub-components that may be utilized by a CHAN component are: powered and/or unpowered HTSTR (heat structure component), PIPE, Side-Junctions and RADENC (Radiation heat transfer enclosure component).

A detailed verification of the CHAN components is needed before it can be used with confidence for safety analyses. Hence the purpose of the report is to validate the heat transfer models of the CHAN component and thereby identify areas for possible improvements. For this purpose data from "BWR Full Size Fine Mesh Bundle test" (BFBT) [1] made by NUPEC was selected for the code validation.

2 Description of BWR Full-Size Fine Mesh Bundle Test Facility

The BFBT (BWR Full-Size Fine Mesh Bundle Test) facility from NUPEC (Nuclear Power Engineering Cooperation) in Japan has been used for the measurement of void fraction and critical power under typical BWR conditions. Experiments that simulate high-pressure and high-temperature fluid conditions; similar to present conditions of BWR can be performed. An electrically heated rod bundle has been used for the simulation of a full-scale BWR fuel assembly. The specific data of the BFBT facility [1] is discussed in this chapter.

2.1 Test Loop

Fig. 2.1 shows the main components of the BFBT facility. Pump (1) is used to circulate the coolant. The coolant is cleaned by the filter (2). The three different sized valves (3) control the flow rate. The coolant inlet temperature of the test section (5) is controlled by the pre-heater (4). The sub-cooled fluid flows from bottom to the top of the test bundle (5), where it is heated. The steam is separated from the mixture using the separator (7) and is condensed in the steam drum (8) by a spray of sub-cooled water. A part of condensed coolant in the separator is pumped into the steam-drum with spray pump (10) after the water was cooled by the two air-cooled heat exchangers (11). Four different sized valves on the spray lines (9) control the pressure. For low assembly powers the system pressure is controlled by the pressurizer (6). The return of coolant to the circulation pump closes the loop of the test facility [1]. The facility is constructed mainly of the stainless steel type SUS304. The cooling fluid used is demineralized water. The test loop can be run with a maximum pressure of 10.3 MPa, a maximum temperature of 588.15 K, a maximum power of 12 MW and a maximum flow rate of 20.83 kg/s. The facility is capable of simulating both the steady state conditions of a Boiling Water Reactor as well as various BWR operational transients.

The test section shown in Fig. 2.2 consists of a pressure vessel, electrodes and a test bundle which emulates different BWR fuel bundle. The sub-cooled coolant flows from the inlet nozzle at the bottom of the device on the side into the test section, then upwards through the test bundle and to the outlet nozzle at the device top. The heated section has an axial length of 3.708 m. At three different axial positions X-ray densitometers and at the bundle outlet an X-ray computer tomography (CT) scanner were installed for the measurement of the void fraction. The functionality of the void fraction measurements will be described in chapter 2.3. Furthermore at various positions of the bundle heater rod surfaces thermocouples for the temperature measurement were installed. Two bundle types are used for the different experiments. Chapter 2.2 provides the detailed geometry data and heater rod information of test assemblies which were used for the validation of TRACE.

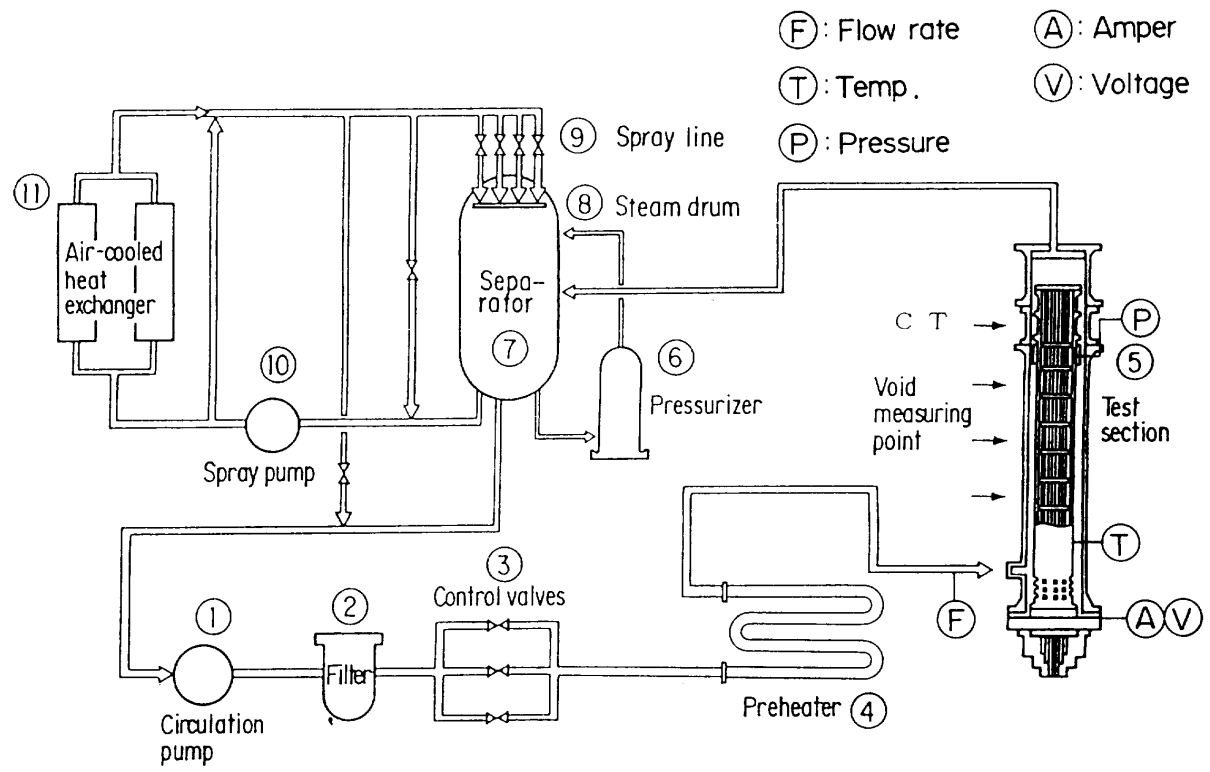


Fig. 2.1: Scheme of the BFBT facility [1]

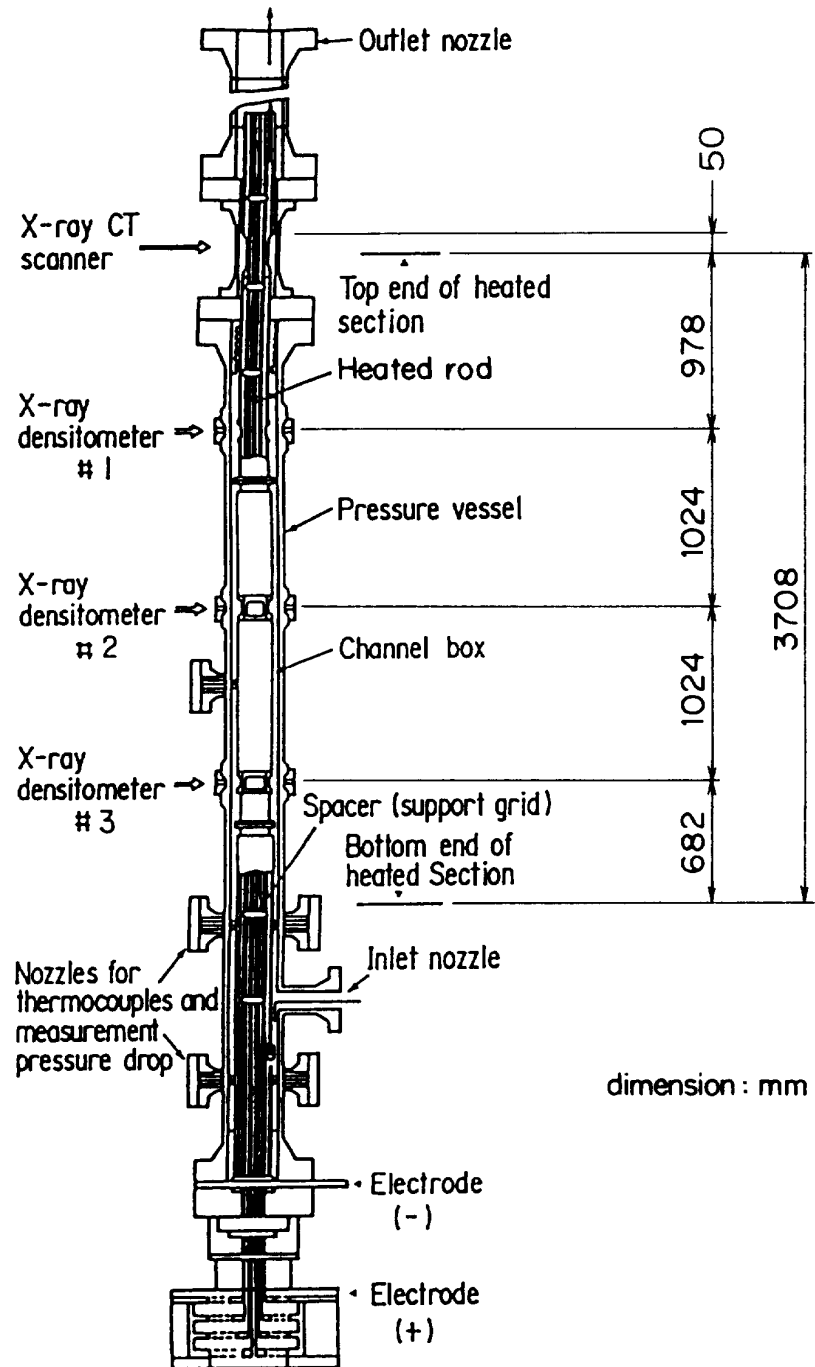


Fig. 2.2: The test section of the BFBT facility [1]

2.2 Test Bundles

Two different test bundle types were used for the BFBT experiments. Each bundle consists of a channel box, heater rods, water rods and spacers. The heater rods of both types are arranged in an 8×8 array. Furthermore both bundle types differ from the used spacer type (see chapter 2.3). Type α consisted of 62 heater rods and two water rods in a diagonal arrangement at the centre as shown in Fig. 2.3 and type β consisted of 60 heater rods and one large water rod at the bundle centre as shown in Fig. 2.4. The channel flow area of type α is $9.781 \cdot 10^{-3} \text{ m}^2$ while the flow area of type β is $9.463 \cdot 10^{-3} \text{ m}^2$. For both bundle types the

heater rods are electrically heated for the simulation of the fission power. The details of the geometry and material data are given in the next paragraphs.

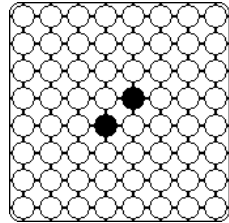


Fig. 2.3: Bundle type α

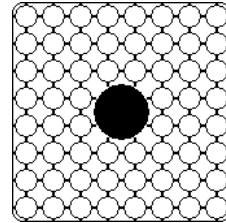


Fig. 2.4: Bundle type β

The bundle types α and β consist of the following components:

- Channel Box

The channel box has an axial heated length of 3.708 m, an inner width distance between box walls of 0.1325 m and a corner radius of 0.008 m.

- Heater Rods

The heated rods have a cylindrical shape and an outer diameter of 0.0123 m. The heated rod pitch is 0.0162 m. Fig. 2.5 shows the components of the heater rods. Fig. 2.6 provides the schematic diagram of the same. As it can be seen in Fig. 2.5 and Fig. 2.6 the heater rod consists of four material zones. The core of the heater rod and the third layer, (refer to Fig. 2.6), is the insulator material (boron nitride). The second layer is the heater (Nichrome) with an outer radius of 0.00365 m while the outer layer is the cladding (Inconel 600) with an inner radius of 0.00485 m and an outer radius of 0.00615 m. The temperature dependent density, specific heat and thermal conductivity properties of all heater rod and water rod materials are summarized in the following Tab. 2.1, Tab. 2.2 and Tab. 2.3. It is assumed that the Nichrome coils have similar properties as Constantan [1].

- Water Rods

The bundle type α has two water rods with a rod outer diameter of 0.015 m each while bundle type β has one large water rod with a rod outer diameter of 0.034 m. The water rods consist of Inconel 600. In all test assemblies there is no flow inside of the water rods [1].

- Spacers

Two types of spacers are used in the different measurements. The “grid type” spacers are used with the bundle type α and have an axial spacer length of 0.041 m. The “ferrule type” spacers are used with the bundle type β and have an axial spacer length of 0.031 m. Both spacer types have a spacer loss coefficient of 1.2 for each spacer. In all measurements there were seven spacers axially distributed along the heated bundle length in the test bundle. The spacer location is shown in Fig. 2.7. All length values on the left side, downward of “Spacer Elevation” are distances from spacer bottom face to the bottom of heated length. The constructive details of both spacer types are given in Fig. 2.8 and Fig. 2.9.

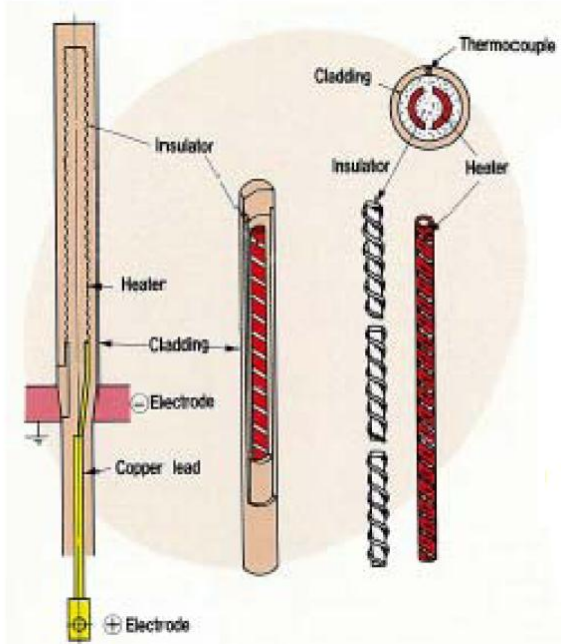


Fig. 2.5: Cross section view of heater rod

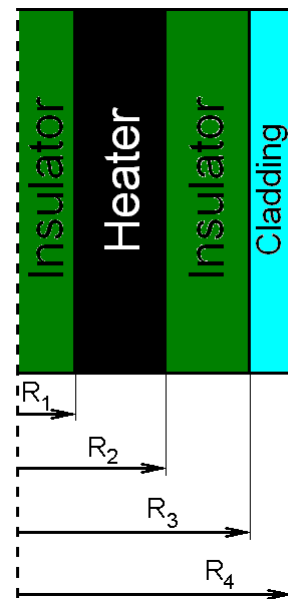


Fig. 2.6: Schematic view of heater rod

Tab. 2.1: Nichrome / Constantan properties [1]

Material	Nichrome / Constantan
Density (kg/m ³)	8393.4
Specific heat c_p (J/kg/K)	$c_p = 110 \cdot T_f^{0.2075}$ Temperature / (°F)
Thermal Conductivity k (W/m/K)	$k = 29.18 + 2.683 \times 10^{-3} \cdot T_f - 100$ Temperature / (°F)

Tab. 2.2: Boron Nitride properties [1]

Material	Boron Nitride
Density (kg/m ³)	2002
Specific heat c_p (J/kg/K)	$c_p = 760.59 + 1.7955 T_f - 8.6704 \times 10^{-4} T_f^2 + 1.7955 \times 10^{-7} T_f^3$ Temperature / (°F)
Thermal Conductivity k (W/m/K)	$k = 25.27 - 1.365 \times 10^{-3} \cdot T_f$ Temperature / (°F)

Tab. 2.3: Inconel 600 properties [1]

Material	Inconel 600
Density (kg/m³)	$\rho = 16.01846 \times (5.261008 \times 10^2 - 1.345453 \times 10^{-2} T_f - 1.194357 \times 10^{-7} T_f^2 - 2.046138 \times 10^{-8} T_f^3 + 1.7955 \times 10^{-7} T_f^4 - 2.060318 \times 10^{-13} T_f^5 + 3.682836 \times 10^{-16} T_f^6 - 2.458648 \times 10^{-19} T_f^7 + 5.597571 \times 10^{-23} T_f^8)$ Temperature / (°F)
Specific heat c_p (J/kg/K)	$c_p = 4186.8 \times (0.1014 + 4.378952 \times 10^{-5} T_f - 2.046138 \times 10^{-8} T_f^2 + 1.7955 \times 10^{-7} T_f^3 - 2.060318 \times 10^{-13} T_f^4 + 3.682836 \times 10^{-16} T_f^5 - 2.458648 \times 10^{-19} T_f^6 + 5.597571 \times 10^{-23} T_f^7)$ Temperature / (°F)
Thermal Conductivity k (W/m/K)	$k = 1.729577 \times (8.011332 + 4.643719 \times 10^{-3} T_f + 1.872857 \times 10^{-6} T_f^2 - 3.914512 \times 10^{-9} T_f^3 + 3.475513 \times 10^{-12} T_f^4 - 9.936696 \times 10^{-16} T_f^5)$ Temperature / (°F)

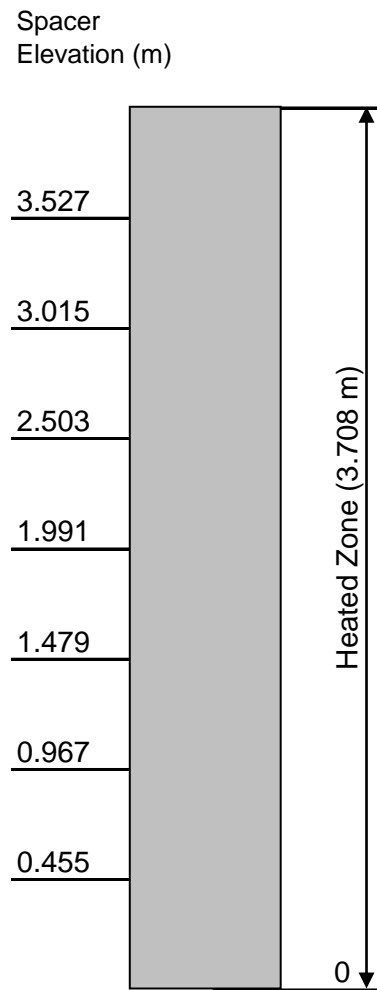


Fig. 2.7: Spacer location [1]

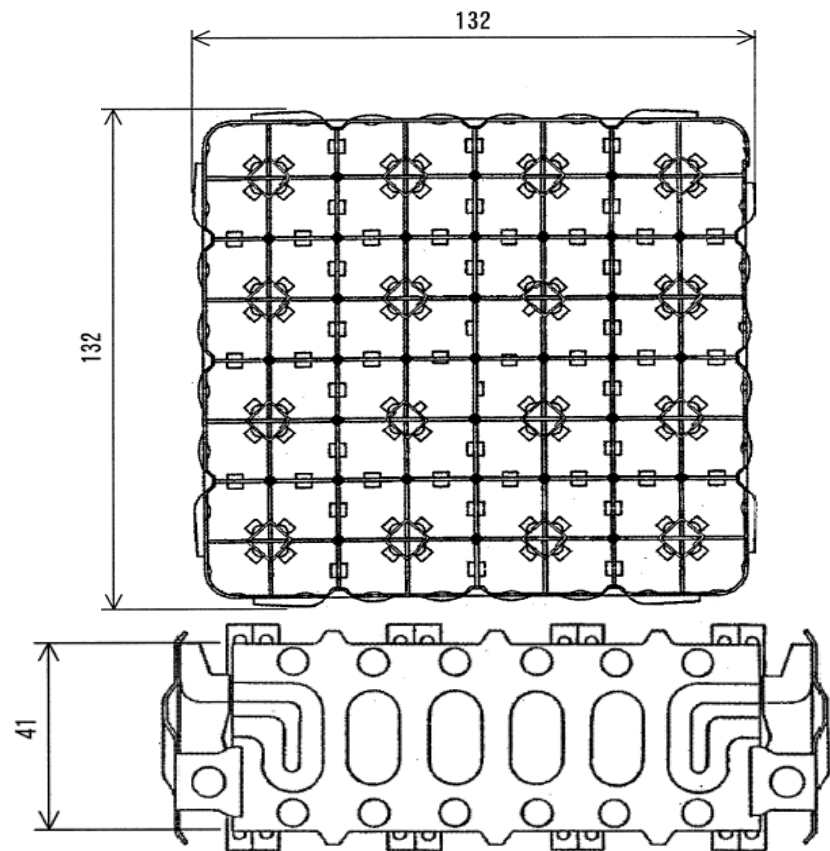


Fig. 2.8: Constructive details grid spacer (mm) [1]

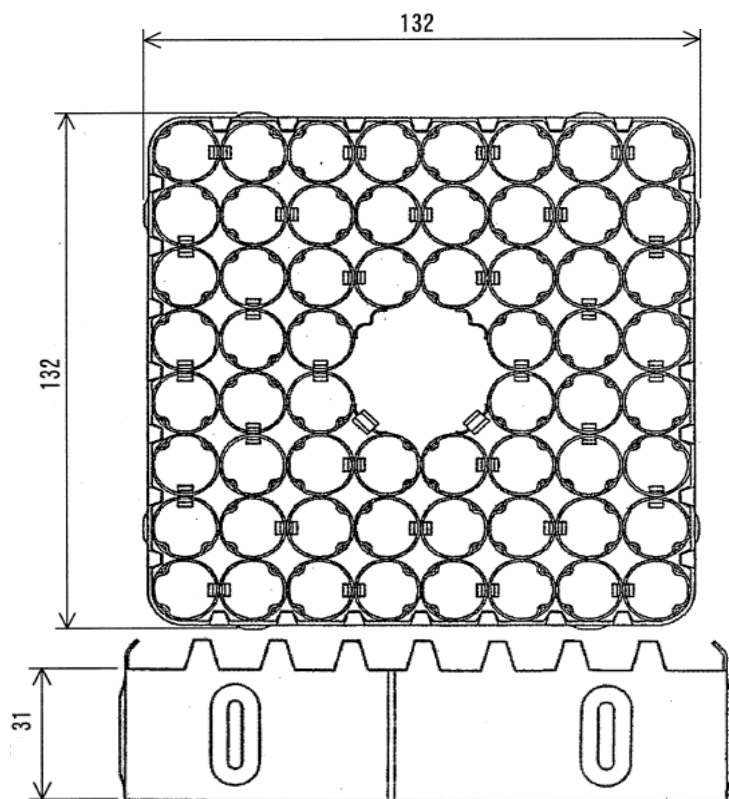


Fig. 2.9: Constructive details ferrule spacer design (mm) [1]

2.3 Measurement Methods

Two different systems of void distribution measurements were applied in the BFBT bundle tests. The fine mesh void distributions were measured using the X-ray computer tomography (CT) scanner 0.05 m above the heated zone. In addition three different axial bundle positions were measured with the so-called X-ray densitometers. Both measurements are based on the same physical principles, which are used in medicine as well. In this case, the fact that x-rays are absorbed in different amounts by water and steam was used. The bundle section was moved in the x-ray beam and the void fraction was measured with a x-ray detector. In addition the x-ray CT scanner is 360° rotatable, (refer to Fig. 2.10 (b)), and this enabled the determination of the void fraction distribution with an accuracy of 0.3 mm x 0.3 mm at the bundle outlet. Therefore the results of the x-ray CT scanner can be used to validate CFD-programs as well. The scanning time of the X-ray CT scanner is 15 s and of X-ray densitometer is up to 60 s. The positions of the X-ray densitometers and X-ray CT scanners are shown in Fig. 2.2 and Fig. 2.10 (a).

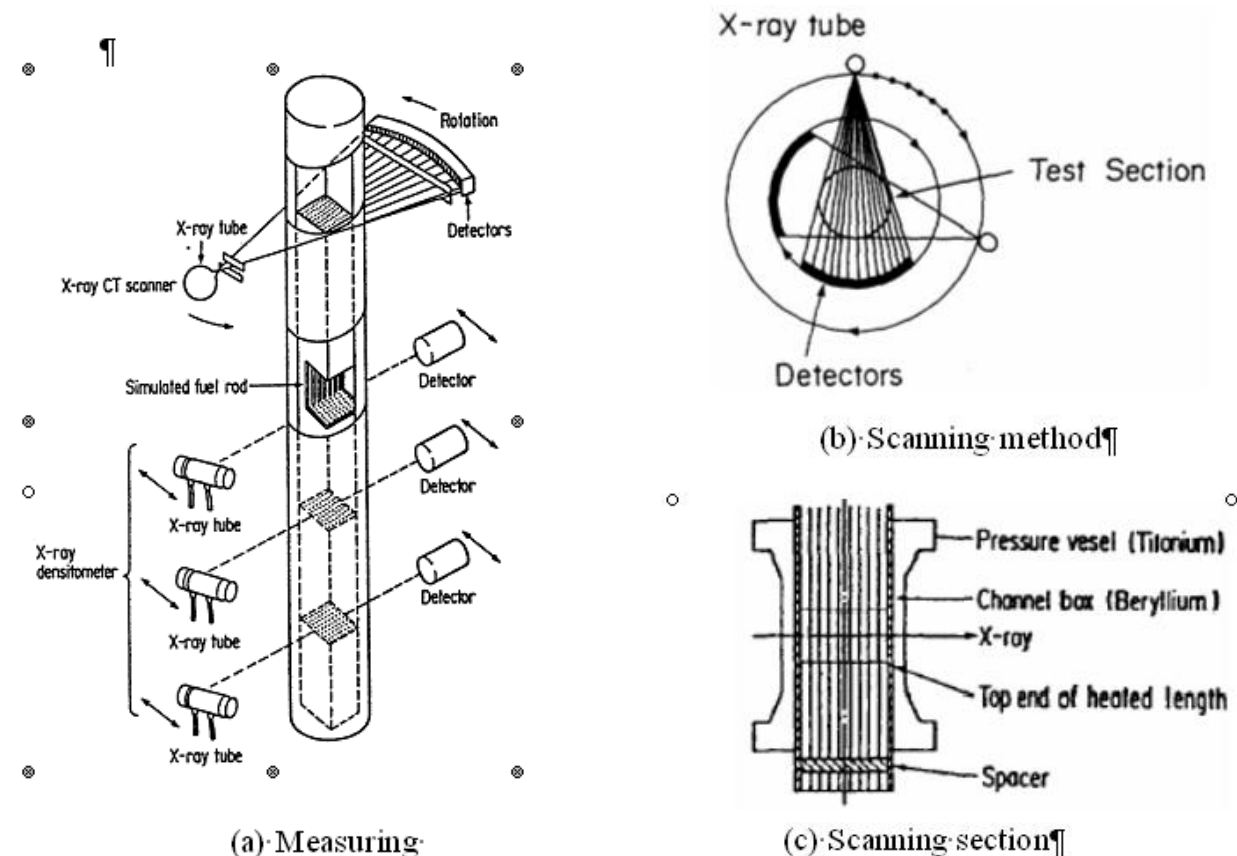


Fig. 2.10: Void fraction measurement system [1]

The critical power was determined when the peak rod surface temperature became 14 °C higher than the steady state temperature level before dry-out occurred [1], at which the temperature measurements were determined with thermocouples on specific heater rod surfaces. The critical power was measured by a slow increase of the bundle power while monitoring the individual heater thermocouple signals.

Each thermocouple position is identified in the following notation:

ROD NUMBER – AXIAL LOCATION – ROTATIONAL ANGLE

Fig. 2.11 describes the thermocouple position notation as it was used for the results of the BFBT experiments for the example 16 – B – 270. The first number represented the rod number as it is shown in Fig. 2.11. The letter gives the axial level of thermocouple position. Fig. 2.12 provides the meaning of the various axial location letters. All thermocouples are located 6 mm under one of the four highest spacers. The last number means the surface location angle in degree (Fig. 2.11).

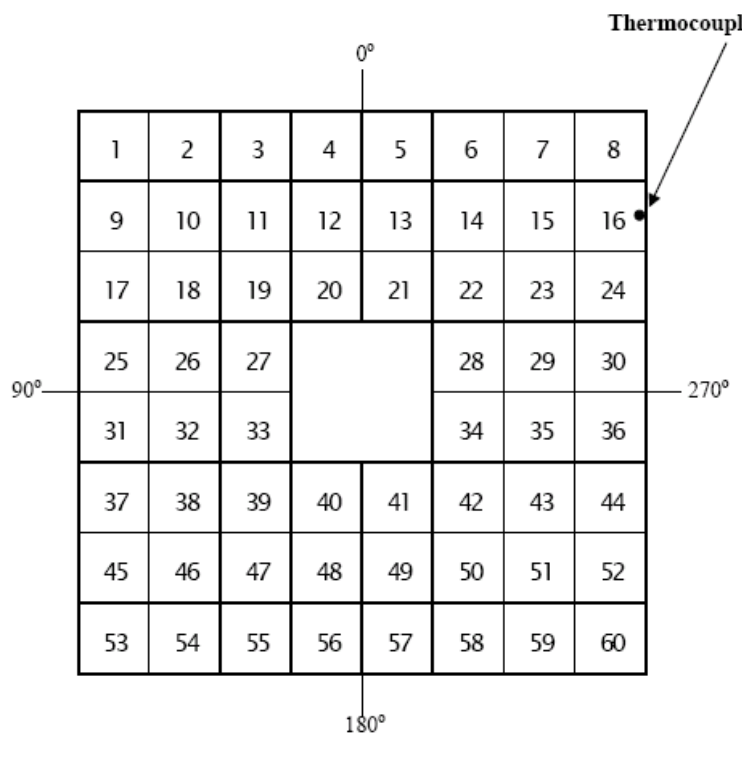


Fig. 2.11: Definition of thermocouple position [1]

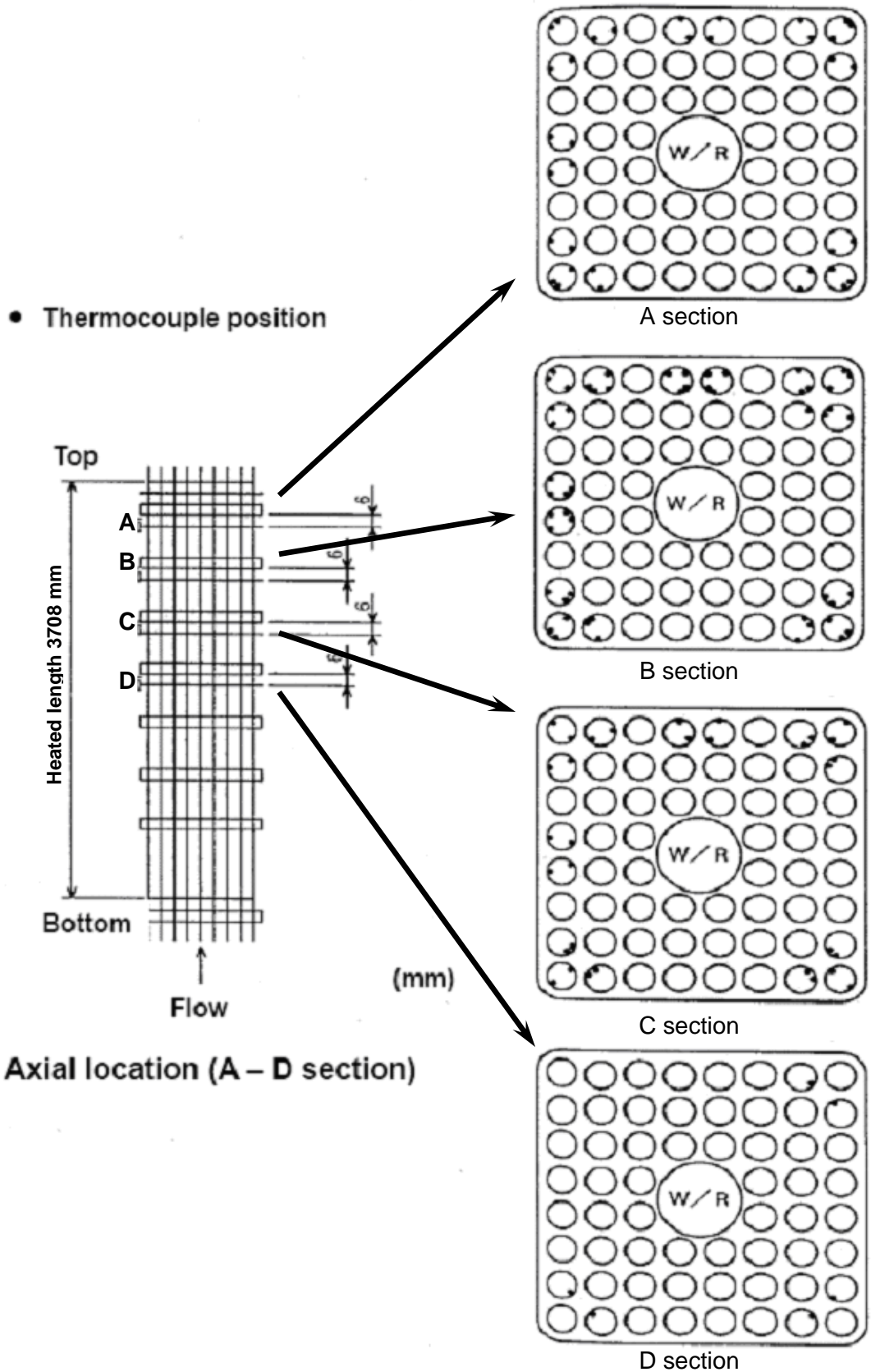


Fig. 2.12: Axial and radial location of thermocouples [1]

Furthermore differential and absolute pressures were measured using diaphragm transducers. The bundle pressure drop was monitored at several locations as depicted in Fig. 2.13.

The sub-cooled water conditions at the inlet were measured using double thermistors. The inlet flow rate was measured using turbine flow meter. On the heater rods, the surface temperature was monitored at positions just upstream of the spacers by the 0.5 mm diameter chromel-alumel thermocouples, which were located in the heater rod cladding [1].

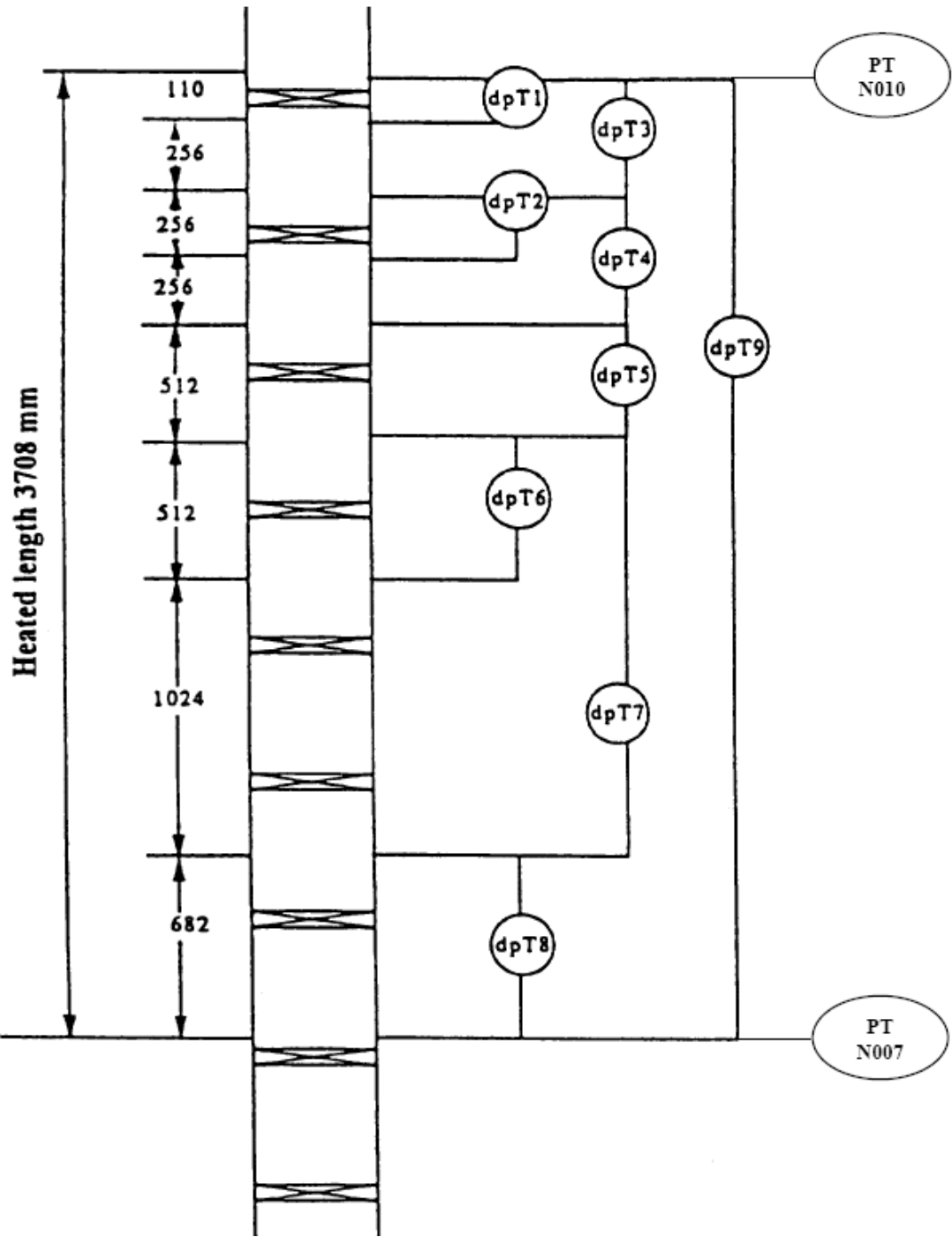


Fig. 2.13: Pressure taps location for critical power measurements [1]

The estimated accuracy of the various measurements is shown in Tab. 2.4. There were three types of void fraction measurements: the sub-channel-average void fraction, which was more than 400 pixel elements, the local void fraction on a $0.3 \text{ mm} \times 0.3 \text{ mm}$ square pixel element, and the cross-sectional average void fraction which was more than 10^5 pixel elements. The accuracy of these void fraction measurements depends on the photon statistics of the X-ray

source, the detector non-linearity and the accuracy of the known fluid conditions (temperature and pressure) measurements [1].

Tab. 2.4: Estimated accuracy of measured parameters [1]

	Quantity	Accuracy
Generals	Pressure	1 %
	Flow	1 %
	Power	1.5 %
	Inlet fluid temperature	1.5 °C
X-ray tubes	Local void fraction	8 %
	Sub-channel void fraction measurements	3 %
	Cross-sectional void fraction measurements	2 %

3 Description of the Tests

The selected void distribution tests are described in chapter 3.1 and the critical power tests are described in chapter 3.2. All selected radial bundle profiles in this report emulate a fuel assembly at the beginning of the operation cycle of a NPP. The test numbers from BFBT [1] were adopted in this report for a better understanding.

3.1 Void Distribution Tests

Two different test assemblies (number 1 and 4) of the void distribution tests were selected for investigations. Test assembly number 1 consists of the bundle type α , (refer to Fig. 2.3), with a cosines-shape axial power profile whereas the test assembly number 4 consists of bundle type β , (refer to Fig. 2.4), with a uniform-shape axial power profile.

3.1.1 Steady State Tests

This chapter describes the BFBT tests: 1071-53 and 4101-53. Test 1071-53 has a radial power pattern as given in Tab. 3.1 and the radial power pattern Tab. 3.2 was used for test 4101-53. The axial power distribution profile which was used in the test 1071-53 is shown in Fig. 3.1. A uniform axial power distribution profile was used in test 4101-53. The test boundary conditions which include the pressure at the outlet, the temperature at the inlet, the mass flow and the power for both tests are given in Tab. 3.3.

Tab. 3.1: Radial power pattern of bundle type α [1]

1.15	1.30	1.15	1.30	1.30	1.15	1.30	1.15
1.30	0.45	0.89	0.89	0.89	0.45	1.15	1.30
1.15	0.89	0.89	0.89	0.89	0.89	0.45	1.15
1.30	0.89	0.89	0.89		0.89	0.89	1.15
1.30	0.89	0.89		0.89	0.89	0.89	1.15
1.15	0.45	0.89	0.89	0.89	0.89	0.45	1.15
1.30	1.15	0.45	0.89	0.89	0.45	1.15	1.30
1.15	1.30	1.15	1.15	1.15	1.15	1.30	1.15

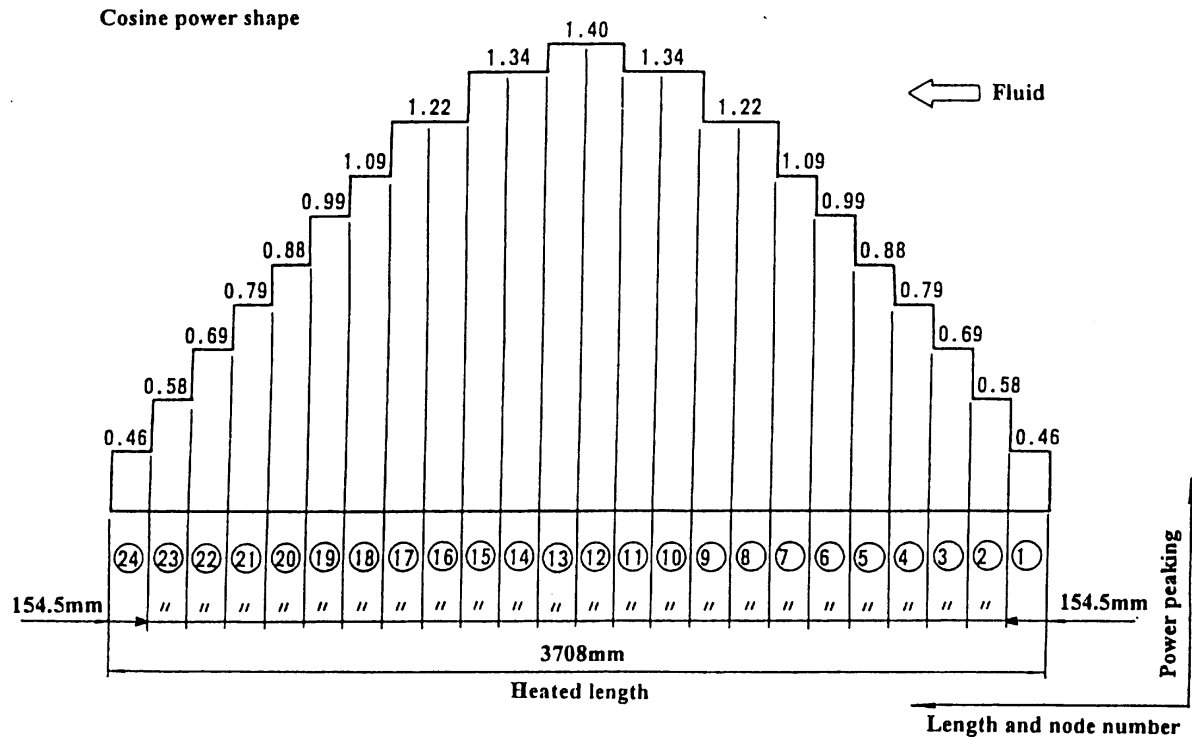


Fig. 3.1: Cosine power distribution pattern [1]

Tab. 3.2: Radial power pattern of bundle type β [1]

1.15	1.30	1.15	1.30	1.30	1.15	1.30	1.15
1.30	0.45	0.89	0.89	0.89	0.45	1.15	1.30
1.15	0.89	0.89	0.89	0.89	0.89	0.45	1.15
1.30	0.89	0.89			0.89	0.89	1.15
1.30	0.89	0.89			0.89	0.89	1.15
1.15	0.45	0.89	0.89	0.89	0.89	0.45	1.15
1.30	1.15	0.45	0.89	0.89	0.45	1.15	1.30
1.15	1.30	1.15	1.15	1.15	1.15	1.30	1.15

Tab. 3.3: Boundary conditions of the void fraction tests [1]

Test	1071-53	4101-53
Outlet Pressure (Pa)	7 160 000	7 170 000
Inlet Temperature (K)	551.55	551.35
Total Mass Flow (kg/s)	15.16111	15.18056
Total Power (W)	1 230 000	1 240 000

3.1.2 Transient Experiment 4102-001~009

The test simulates the heat transfer and flow conditions of a turbine trip transient of a BWR. The test has a radial power pattern as given in Tab. 3.2. A uniform axial power distribution profile was used in this test. The heated range is split in 24 parts in the axial direction. The

length of one part is 0.1545 m. The time dependent boundary conditions are given in Fig. 3.2, Fig. 3.3, Fig. 3.4 and Fig. 3.5.

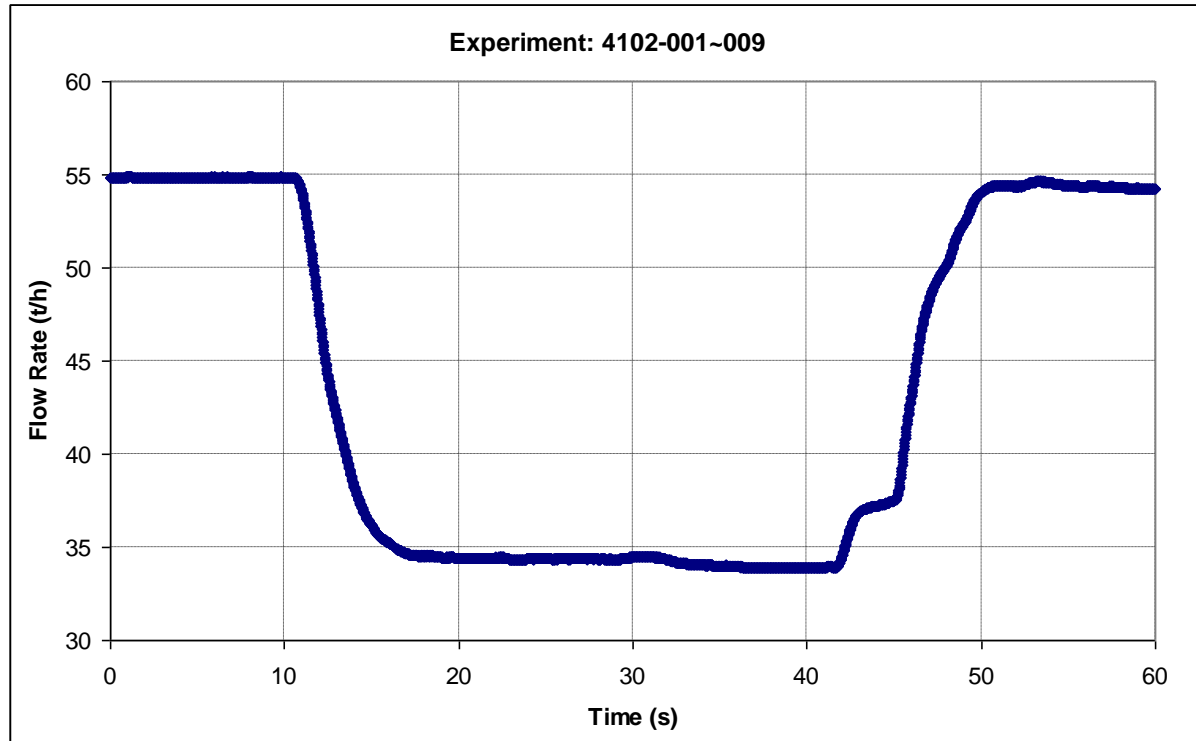


Fig. 3.2: Evolution of Flow rate [1]

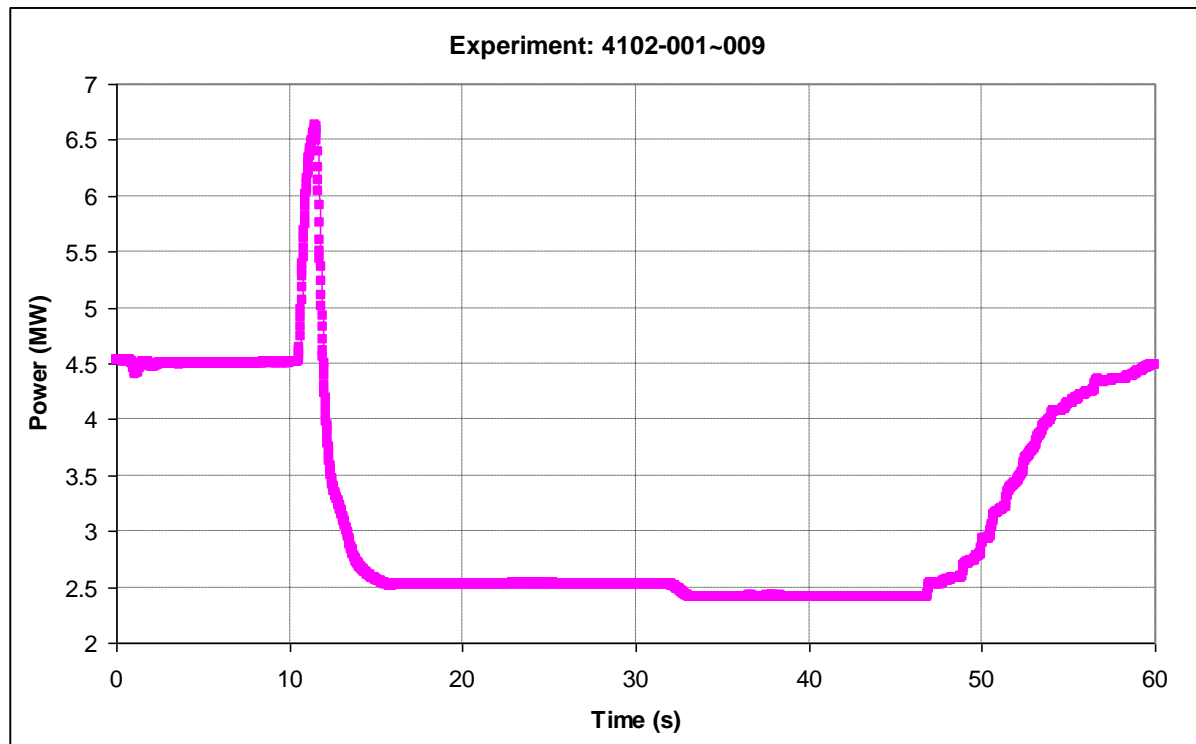


Fig. 3.3: Evolution of total power [1]

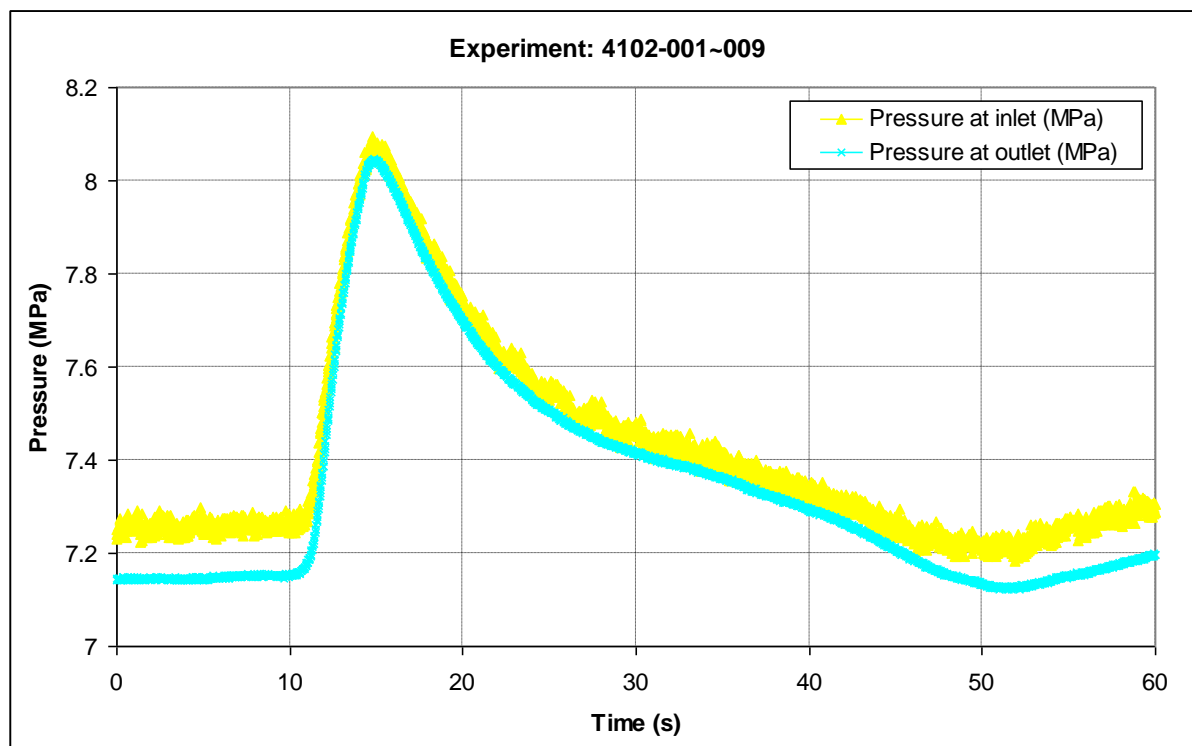


Fig. 3.4: Pressure evolution at bundle inlet and outlet [1]

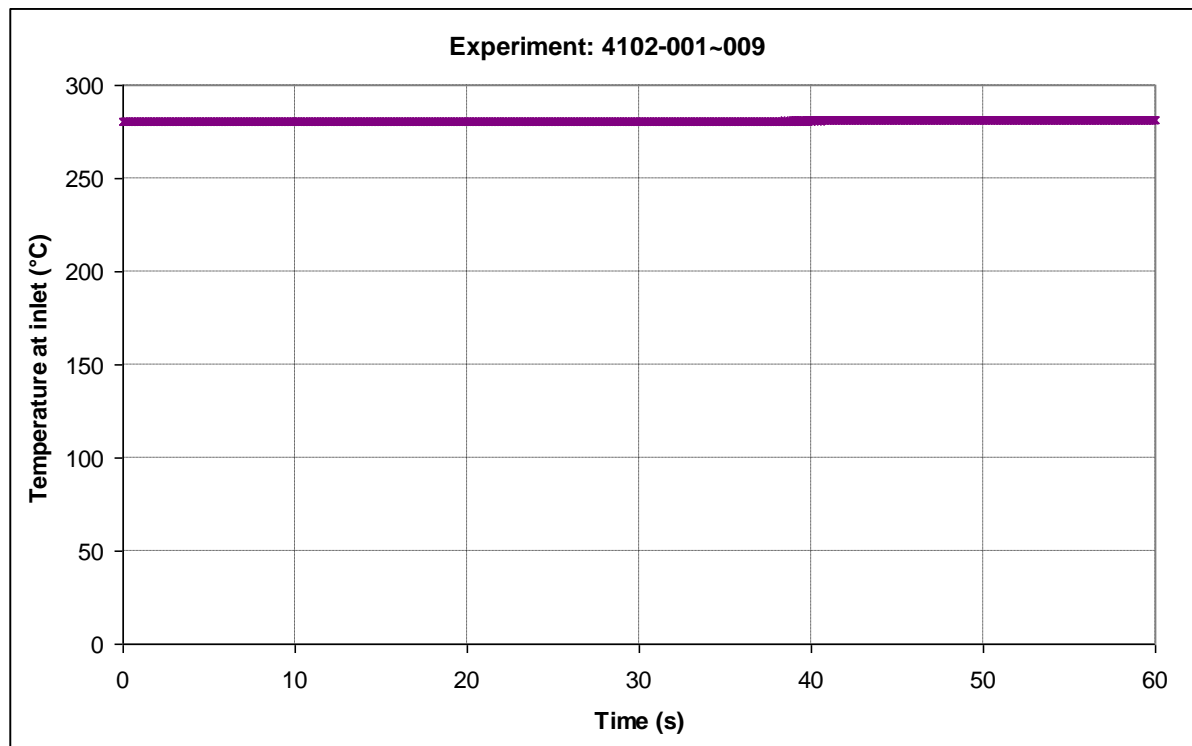


Fig. 3.5: Evolution of coolant temperature [1]

3.2 Critical Power Tests

Two different test assemblies are considered for the simulation of the Critical Power tests. Both selected test assemblies consist of bundle type β , (refer to Fig. 2.4). Assembly C2A has

a cosines-shape axial power profile whereas the assembly C3 has an inlet-peak shape axial power profile.

3.2.1 Steady State Experiments

Four tests with different heater rod arrangements were selected for the code validation. The tests have a radial power pattern as given in Tab. 3.2. The axial power distribution profile which was used in the first three tests: SA510600, SA610600 and SA810600 are shown in Fig. 3.1 whereas the axial power distribution profile for last test SC610500 is shown in Fig. 3.6. The test boundary conditions for all these steady state experiments are given in Tab. 3.4.

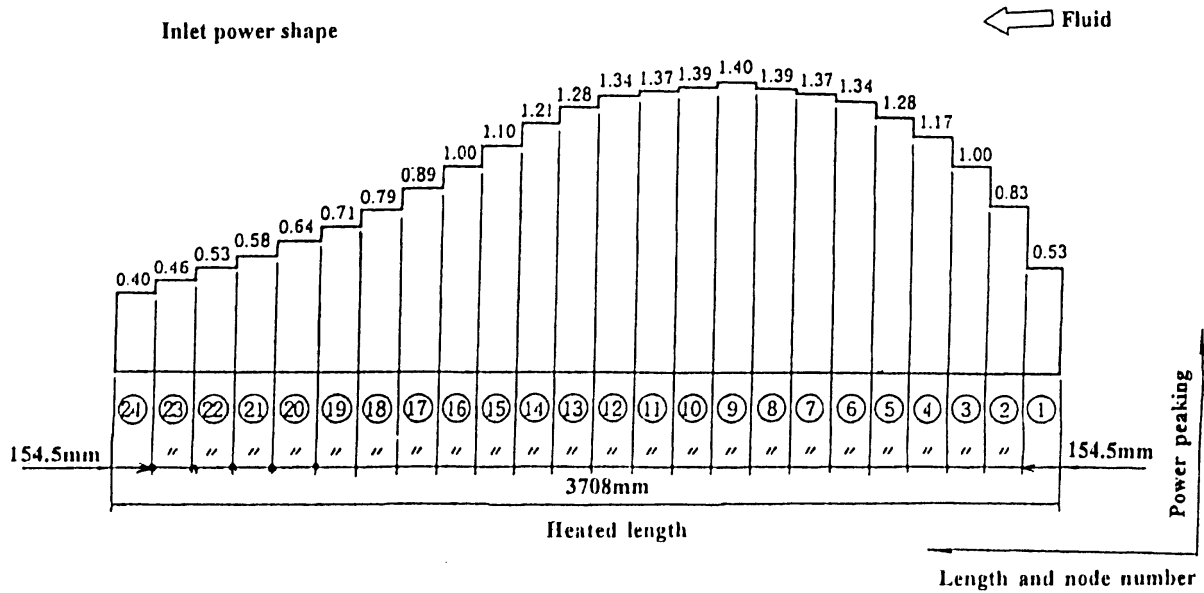


Fig. 3.6: Inlet power distribution pattern [1]

Tab. 3.4: Boundary conditions of the selected critical power tests [1]

Test	SA510600	SA610600	SA810600	SC610500
Outlet Pressure (Pa)	5 510 000	7 180 000	8 560 000	7 190 000
Inlet Temperature (K)	523.918	543.668	557.739	551.297
Total Mass Flow (kg/s)	15.19444	15.29667	15.27778	15.25

3.2.2 Transient Experiment TGA10008

This test simulates the core conditions corresponding to a turbine trip transient. The test has a radial power pattern as given in Tab. 3.2. The axial power distribution profile which was used in this test is shown in Fig. 3.1. The test boundary conditions as a function of the time are given in Fig. 3.7, Fig. 3.8, Fig. 3.9 and Fig. 3.10.

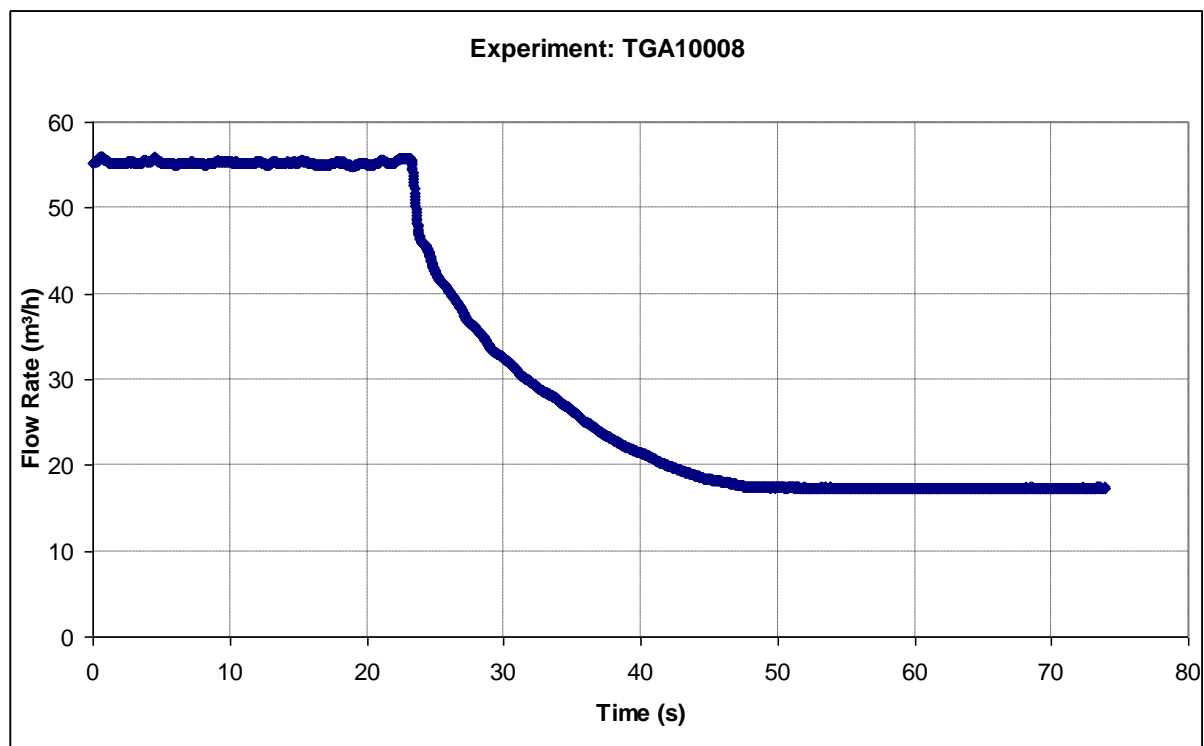


Fig. 3.7: Flow rate vs. time [1]

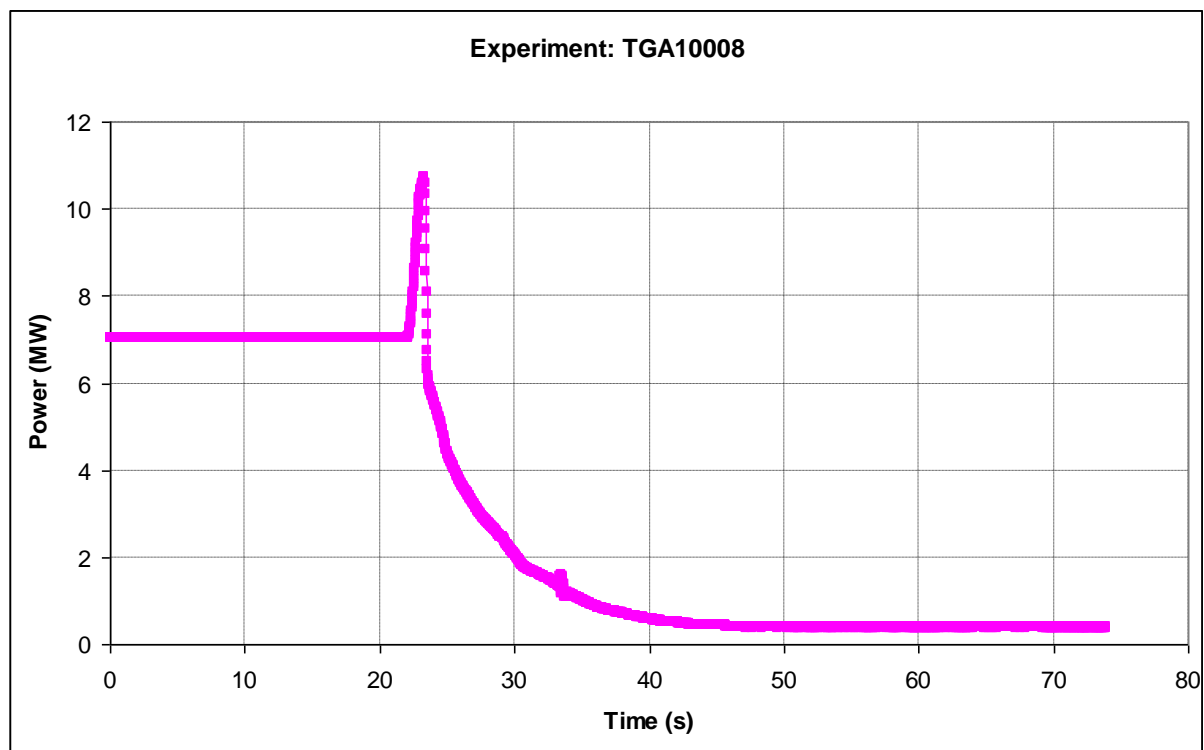


Fig. 3.8: Total power vs. time [1]

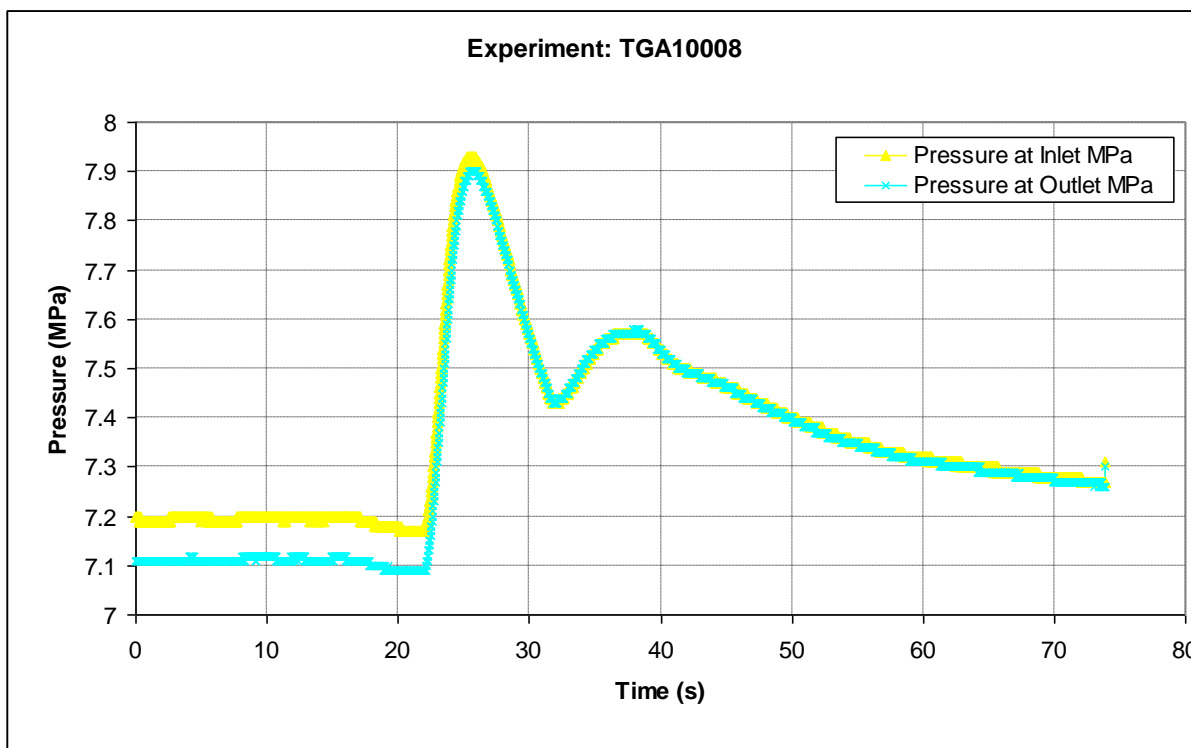


Fig. 3.9: Pressure at the bundle inlet and outlet vs. time [1]

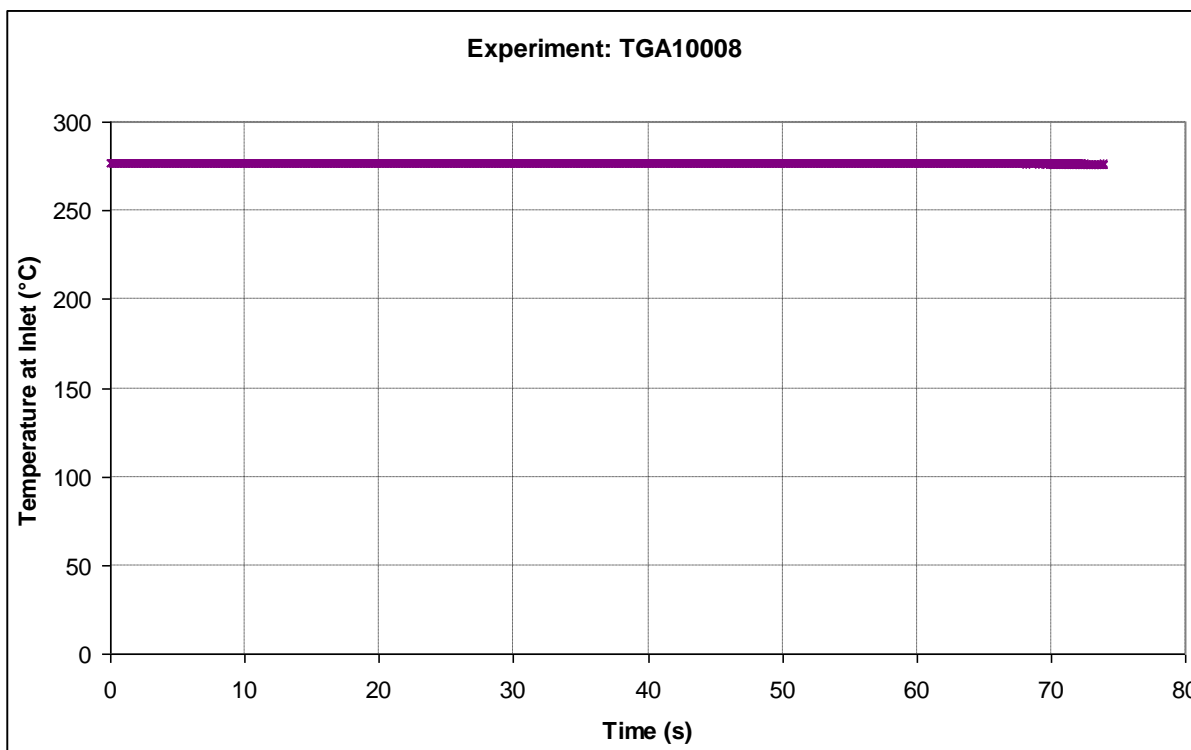


Fig. 3.10: Coolant temperature vs. time [1]

4 Short Description of TRACE

TRACE (TRAC/RELAP Advanced Computational Engine) is a best-estimate thermohydraulic reactor system code which is being developed by the U.S. Nuclear Regulatory Commission (NRC) since about 6 years. The code allows the analysis of both transient and steady-state neutronic thermal-hydraulic behaviour of light water reactors (LWR) [5]. This code is a result of long term effort to combine the capabilities of the NRC's four main system codes (TRAC-P, TRAC-B, RELAP5 and RAMONA) into one modernised computational tool. TRACE has been designed to perform best-estimate analysis of loss-of-coolant accidents (LOCAs) and operational transients in pressurized light-water reactors (PWRs) and boiling light-water reactors (BWRs). Furthermore it can also model phenomena occurring in experimental facilities designed to simulate transients of reactor systems. The TRACE code includes models like multidimensional two-phase flow, generalized heat transfer, heat conduction, nonequilibrium thermodynamics, level tracking, reflood, and reactor kinetic models. The code architecture is completely modular. The TRACE code includes components like: BREAKs, FILLs, CHANs (BWR fuel channels), HEATRs (feed water heaters), HTSTRs (heat structure), JETPs (jet pumps), POWERs, PUMPs, TEEs, VALVEs, and VESSELs. Generally the models used in TRACE can be classified in 1D hydraulic models, with exception of the VESSEL component. It uses three dimensional fluid-dynamics models.

5 Modelling of the NUPEC Bundle Test for TRACE

For the envisaged investigations with TRACE only the test section (see Fig. 2.2) including the heater and water rods and the upper plenum was modelled. The bundle conditions at the inlet and outlet are presented in the model by TRACE components FILL and BREAK. The boundary conditions at the inlet and outlet for each test are given by the components FILL Number 100 in Fig. 5.1 and BREAK Number 300 in Fig. 5.1. The channel box wall with all heaters is modelled with the CHAN component, Fig. 5.1. Each heater rod is axial subdivided in 24 heated and one unheated cell. The cell elevation of each heated cell is 0.1545 m and of the unheated cell is 0.1 m. The CHAN wall was split in three mesh points and the inside perimeter was calculated as 0.516 m. Furthermore adiabatic boundary conditions at the channel wall outer surface were assumed. The seven spacers were modelled by an additive pressure drop at the respective locations (Fig. 2.7). Refer to chapter 2.2 for more spacer details. The pitch to diameter ratio was calculated as 1.317. Since there are four groups of heater rods with the same radial power, they were explicitly considered in the CHAN component. Also the water rods of the different test arrangements are presented separately in the model utilizing the capability of CHAN components (refer to Fig. 5.2 and Fig. 5.3). The heater rods of the CHAN-component, Fig. 2.6, are nodalized with 22 radial mesh points. Particularly both boron nitride and the nichrome regions are nodalized with five radial mesh points and the outer inconel 600 region is nodalized with two radial mesh points. Furthermore the power of all heater groups is defined in the POWER-component.

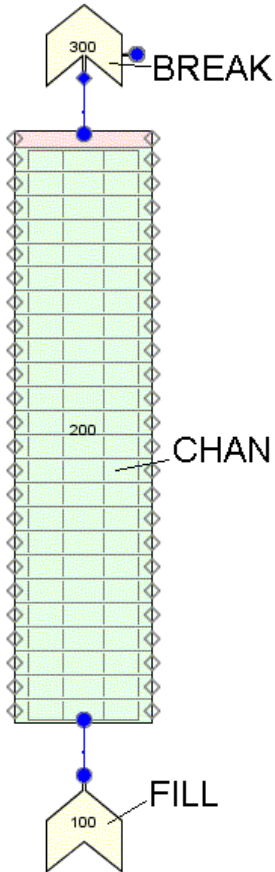


Fig. 5.1: TRACE model of the BFBT test section

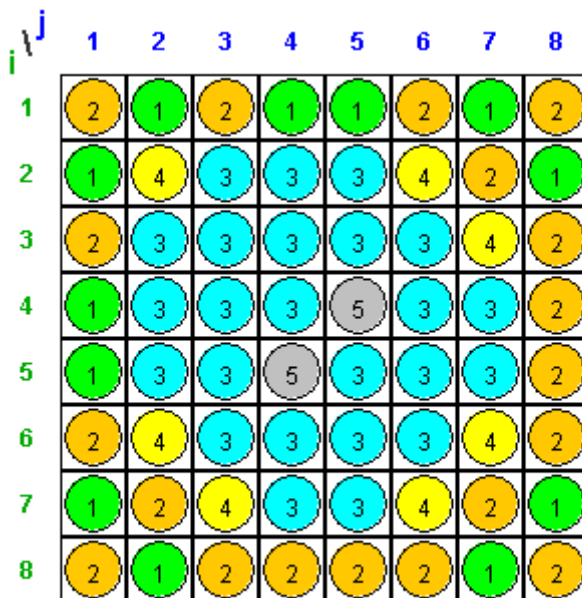


Fig. 5.2: Radial heater location of bundle type α showing the different heater groups

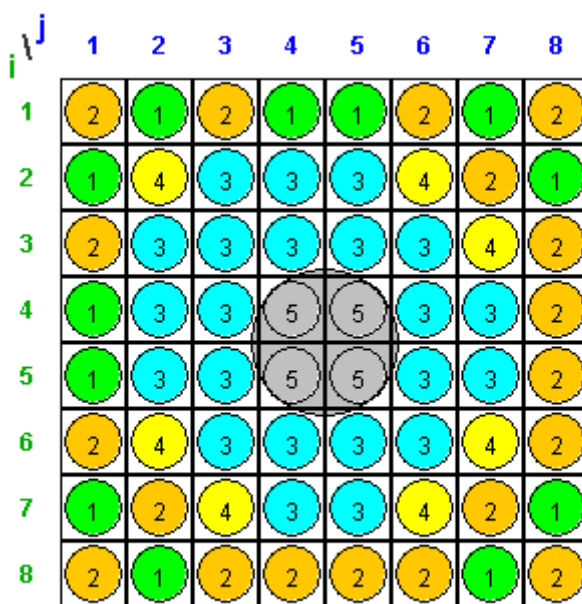


Fig. 5.3: Radial heater location of bundle type β showing the different heater groups

Tab. 5.1: Power peaking factors of heater groups

Group Number	Group Type	Power Peaking Factor
1	Heater Rods	1.30
2	Heater Rods	1.15
3	Heater Rods	0.89
4	Heater Rods	0.45
5	Water Rod	0.00

6 Post-Test Calculation with TRACE

Two steady-state calculations the one tests transient calculation selected from both void distribution test row and critical power test row of the BFBT tests were performed. The TRACE calculations were performed on Dual Core PC with Windows @1.66 GHz using the TRACE Version V5.0RC2. For each specific calculation the boundary and initial conditions, given in chapter 3, were used.

6.1 TRACE Calculation of Void Distribution Tests

In this chapter the void distribution post-test calculations will be presented. They include both steady state and transient calculations. The minimum/maximum time step was set to 0.0001 s / 0.001 s in the steady state and transient calculations.

6.1.1 TRACE Results for Steady State Test 1071-53

The following calculation was performed using the generalized steady-state calculation (GSS) mode. A convergence criterion of 10^{-6} was selected. The CPU time for this calculation was approximately 9 s.

The comparison of pressure drop between the measured BFBT data and the TRACE calculation results is given in Tab. 6.1. The relative deviation of calculation from the test data is less than 1 % which indicates a good agreement. The calculated pressure is in the error band of the measured pressure. The relative deviation was computed by the difference between the measured data and the TRACE result divide by the measured data.

Tab. 6.1: Comparison pressure drop over the bundle of test 1071-53

	Data / MPa	TRACE / MPa
Pressure Drop Δp	0.06	0.0597
Measurement Error	± 0.14	-
Deviation / %		0.57%

The comparison of calculated and measured void fraction is shown in Fig. 6.1. The graph shows a good agreement of measured and predicted the void fraction at the outlet of the bundle. However, in the middle area of the bundle the computed void fraction is observed to be approximately 20 % less (relative deviation) than the test data. But it is still within the uncertainty error band. The liquid, gas and saturation temperatures are shown in Fig. 6.2. It can clearly be seen that the liquid temperature is rising from inlet temperature to the saturation temperature and then equals the saturation temperature. A comparison of Fig. 6.1 and Fig. 6.2 shows clearly subcooled boiling regime between the bundle elevation at 1.4 m and 2.3 m. In the next figure, (Fig. 6.3), the computed surface temperatures of the four heater groups

are shown. As expected the group with the higher heat power shows also the highest surface temperatures (see Tab. 5.1). Fig. 6.4 represents the corresponding heat transfer coefficients for each of the heater group.

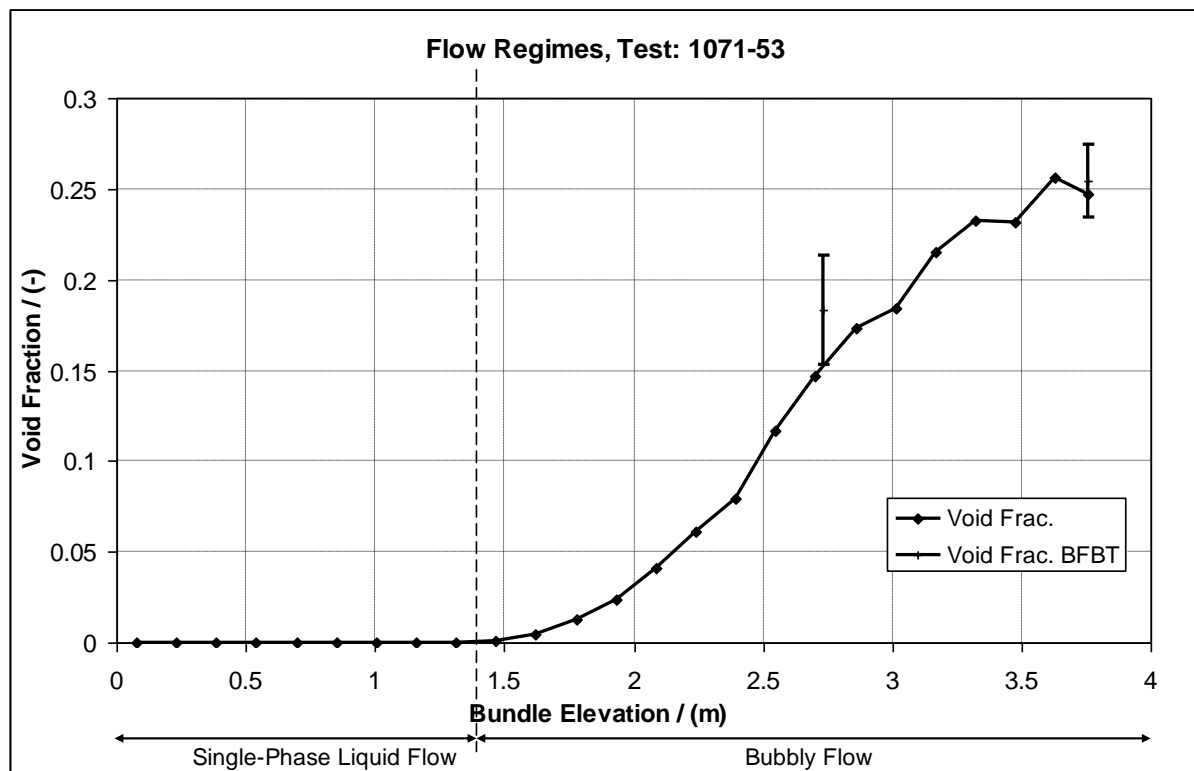


Fig. 6.1: Comparison between BFBT data and TRACE results of test 1071-53

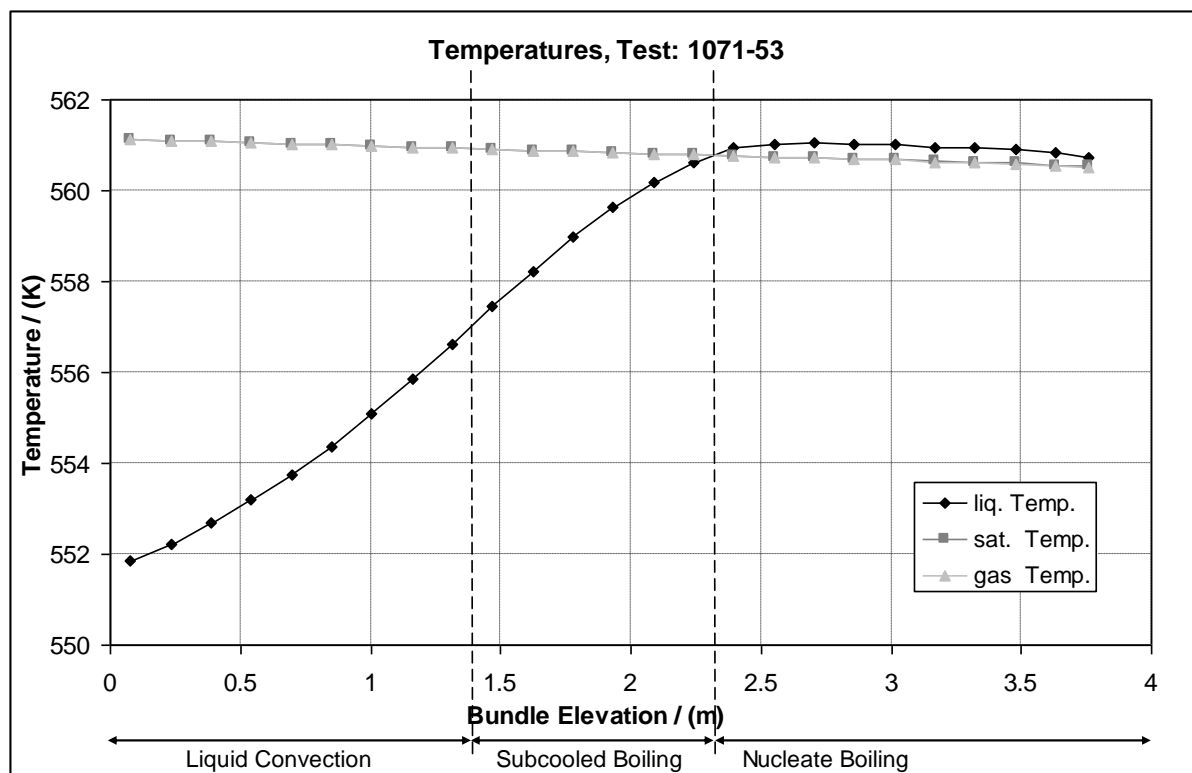


Fig. 6.2: Calculated liquid, saturation and gas temperature of test 1071-53

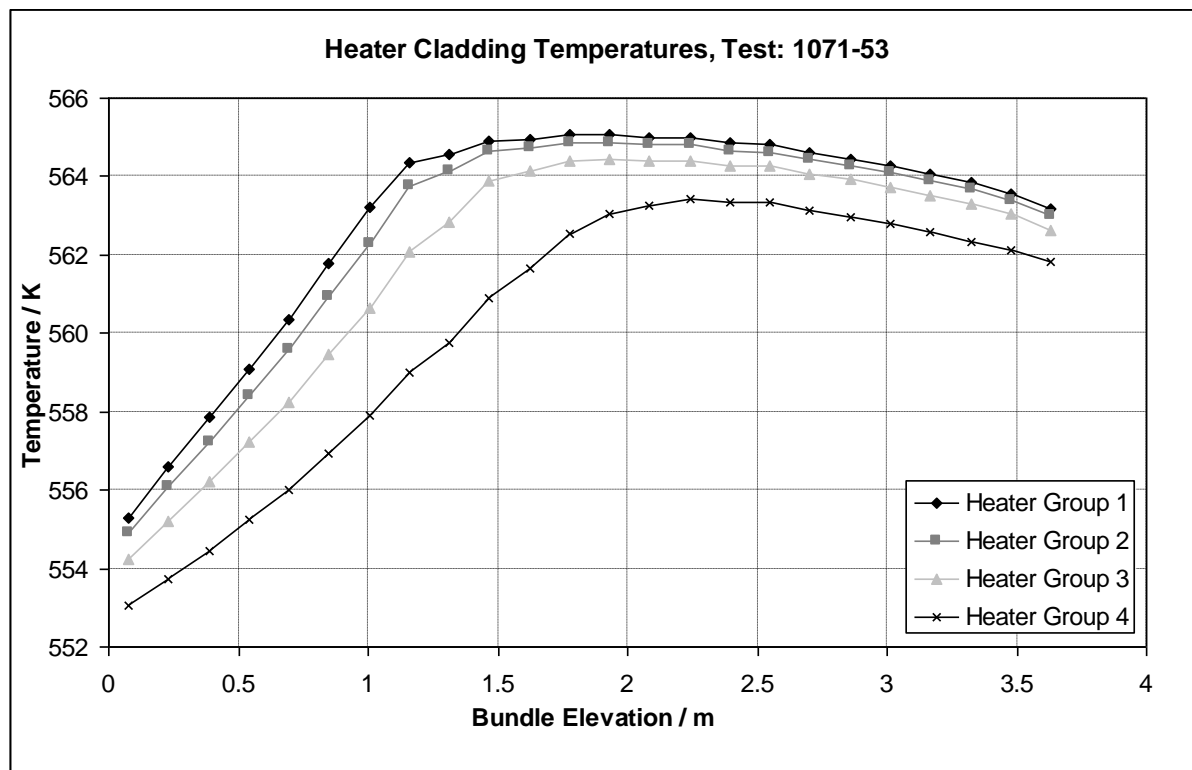


Fig. 6.3: Heater surface temperatures of each heater group of test 1071-53

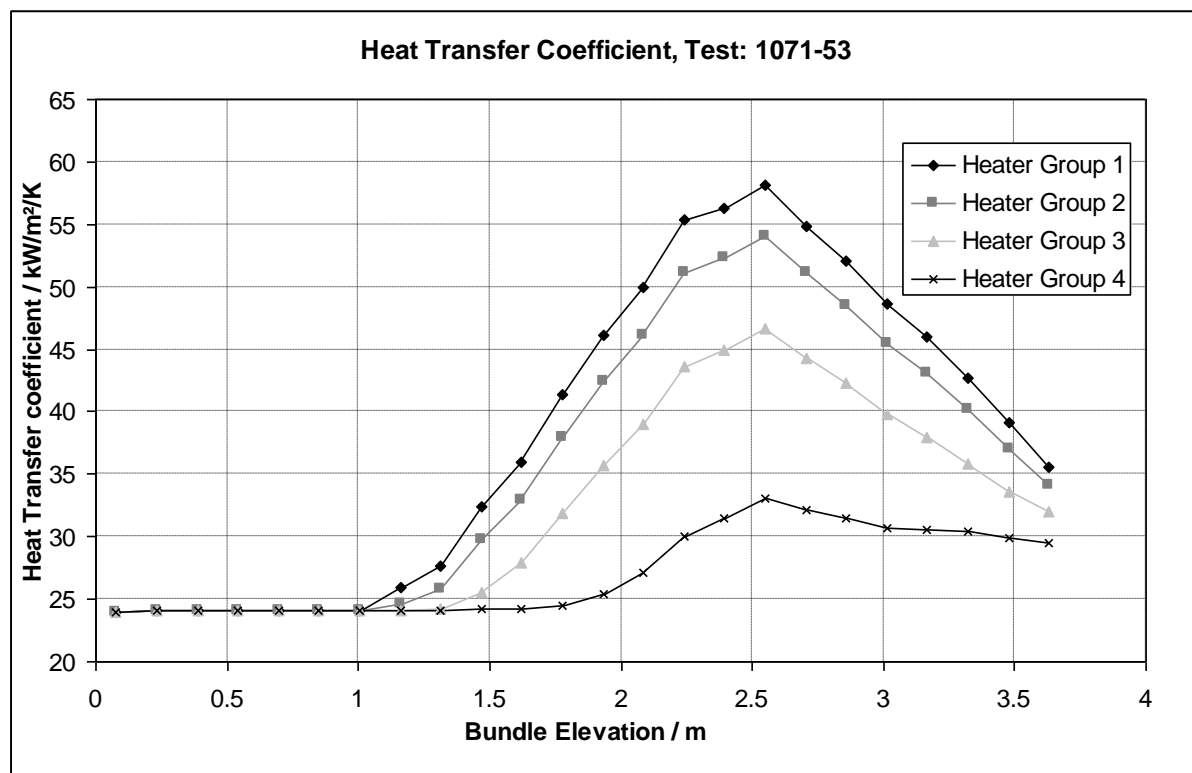


Fig. 6.4: Heat transfer coefficient of each heater group of test 1071-53

6.1.2 TRACE Results for Steady State Test 4101-53

The TRACE calculation was performed in the generalized steady-state calculation (GSS) mode. In this mode the calculation is terminated when the convergence criterion of 0.001 was satisfied for all physical parameters. The CPU time needed for this calculation was approximately 8 s.

The comparison of the measured and calculated pressure drop (TRACE) is given in Tab. 6.2. Clearly there is a good correlation between the measured BFBT data and the TRACE calculation.

Tab. 6.2: Comparison pressure drop over the bundle of test 4101-53

	Data / MPa	TRACE / MPa
Pressure Drop Δp	0.06	0.0616
Measurement Error	± 0.14	-
Deviation / %		2.7%

The comparison of calculated and measured void fraction, shows also a very good agreement at the outlet of the bundle, Fig. 6.5. At the axial elevation of 2.730 m (X-ray densitometer) TRACE underpredicts the measured void fraction by 27 % but the calculated value is still within the measurement uncertainty band. The liquid, gas and saturation temperatures are shown in Fig. 6.6. As expected the behaviour of these parameters is similar to the behaviour obtained in the previous calculation. Here the rise of liquid temperature has a more linear shape, due to the setting of a uniform axial power distribution. The heater rod surface temperatures of the heater groups, shown in Fig. 6.7, have a gradual decrease by comparison with the previous test calculation which show a rapid decrease. The computed heat transfer coefficients for each heater group are shown in Fig. 6.8. By comparison with the previous test calculation, the heat transfer coefficients are decreasing above a bundle elevation of about 2.5 m, Fig. 6.4, and the behaviour of the heat transfer coefficients is strictly monotonically increasing which is physical sound.

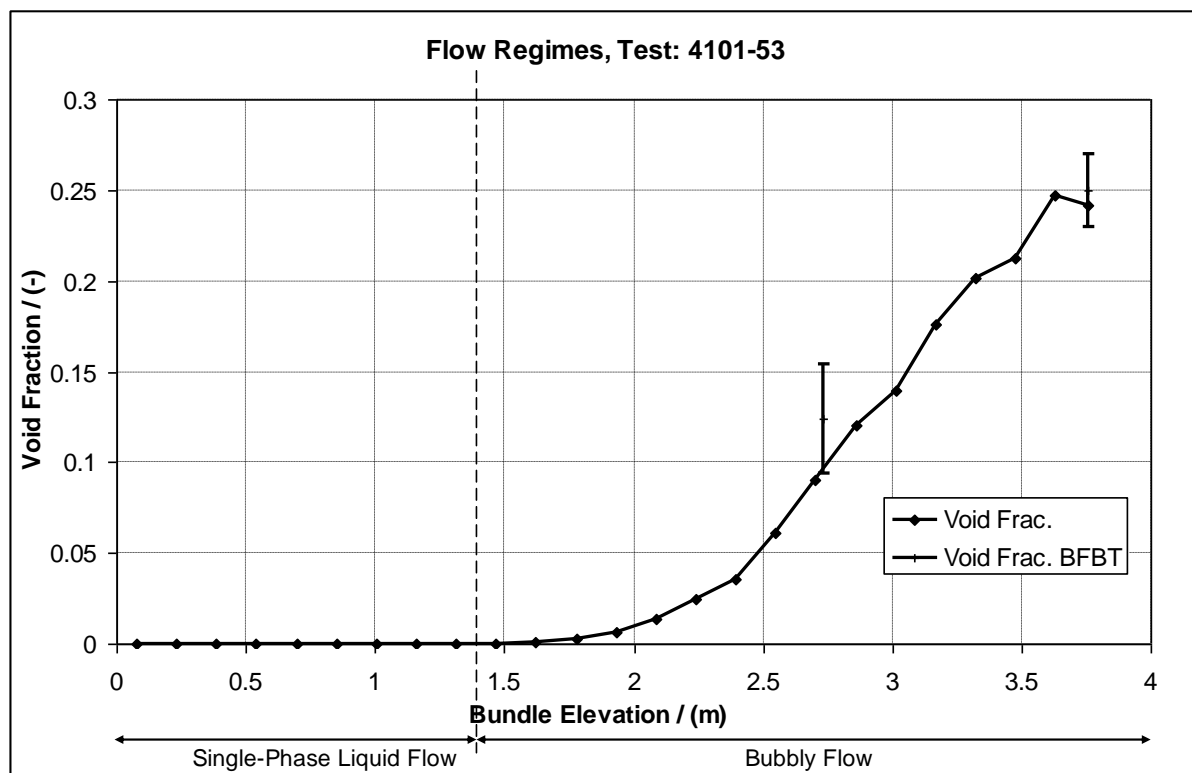


Fig. 6.5: Comparison between BFBT data and TRACE results of test 4101-53

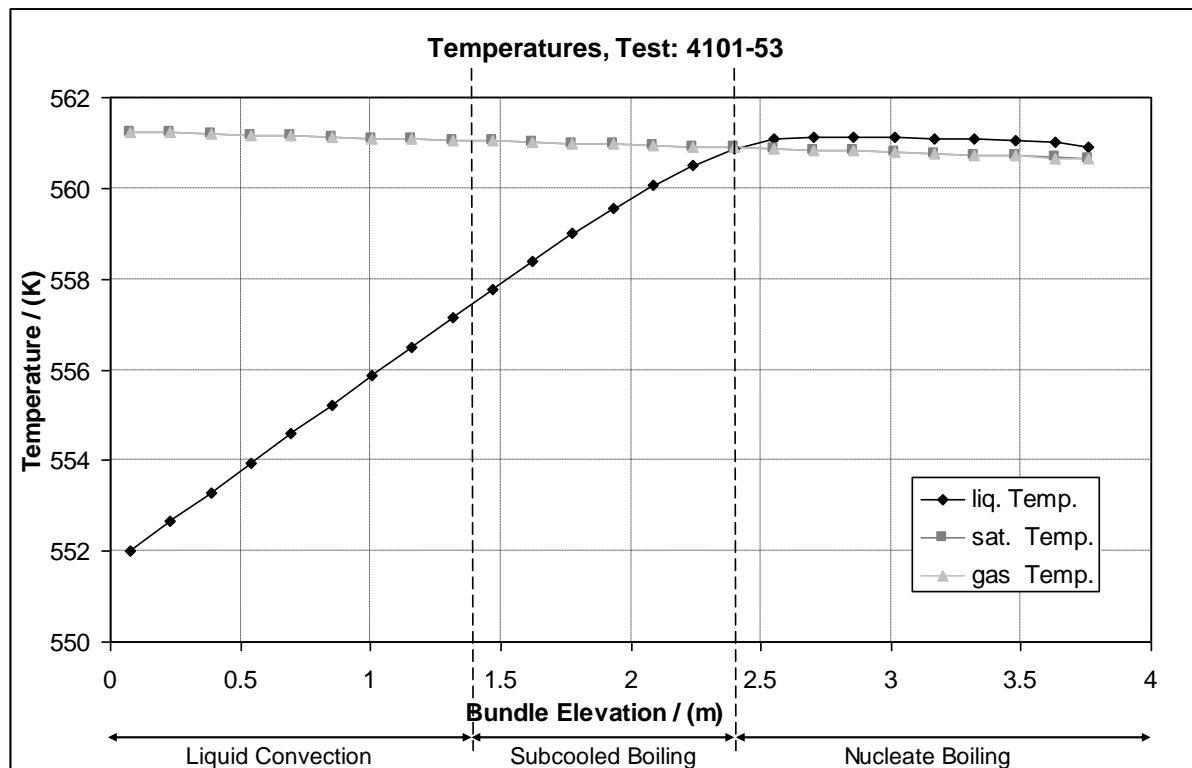


Fig. 6.6: Calculated liquid, saturation, gas temperature of test 4101-53

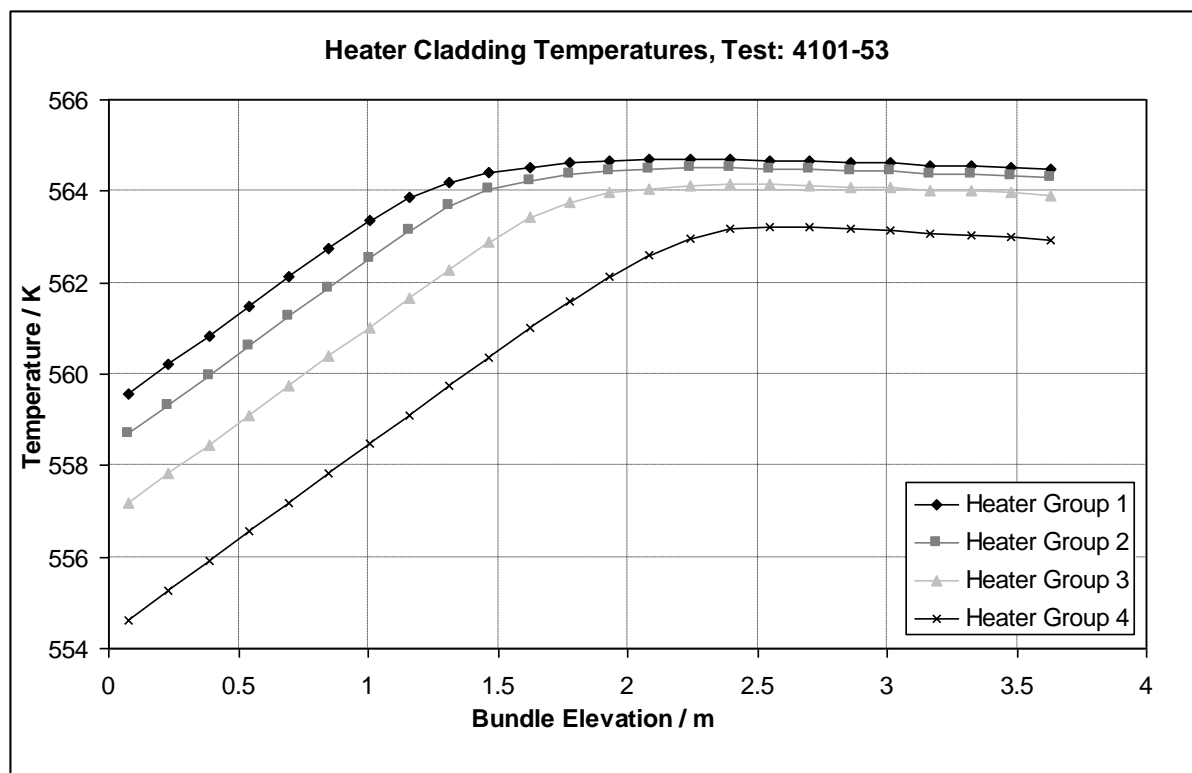


Fig. 6.7: Heater surface temperatures of each heater group of test 4101-53

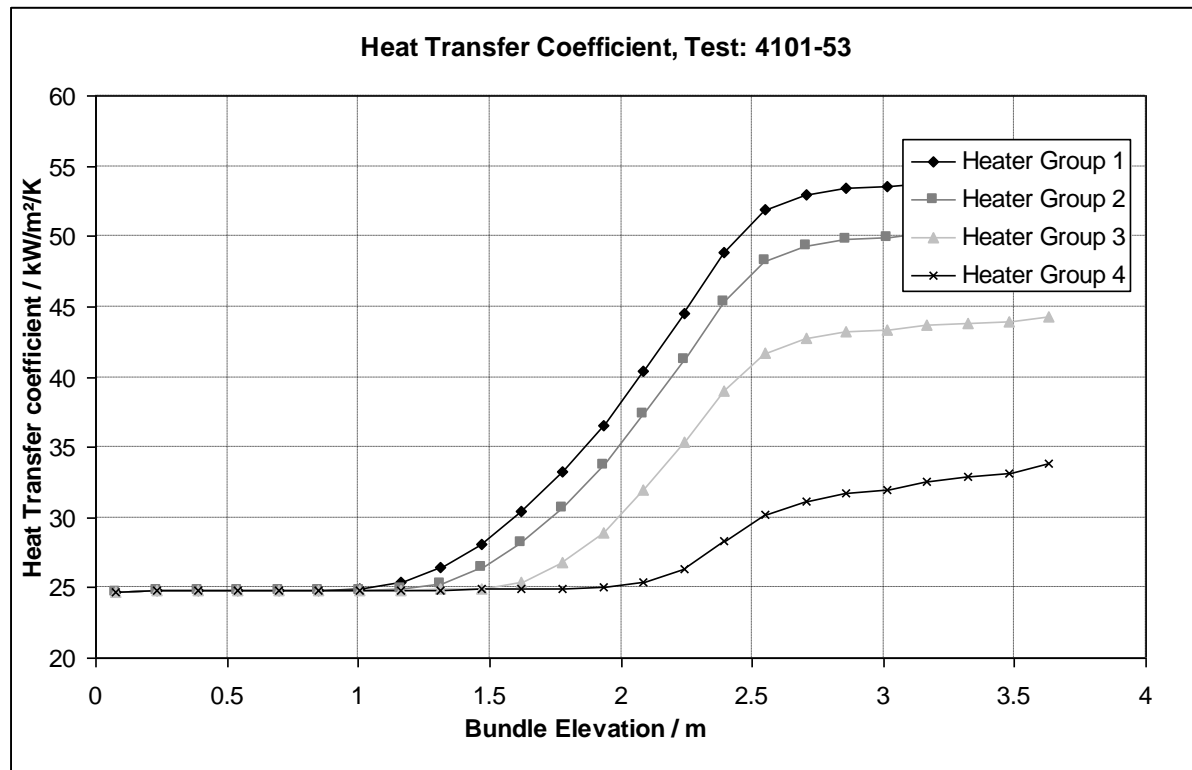


Fig. 6.8: Heat transfer coefficient of each heater group of test 4101-53

6.1.3 Discussion of Void Fraction Steady State Results

The comparison between the predicted void fraction and the calculated data at four elevations is summarized in Fig. 6.9. TRACE tends in general to underpredict the void fraction. It is worth to note that the predictions of TRACE at the elevation 3.758 m are very close to the experimental data, (RSME: 0.039) while the calculations at the other elevations deviate from the measurements by an RSME up to 0.064.

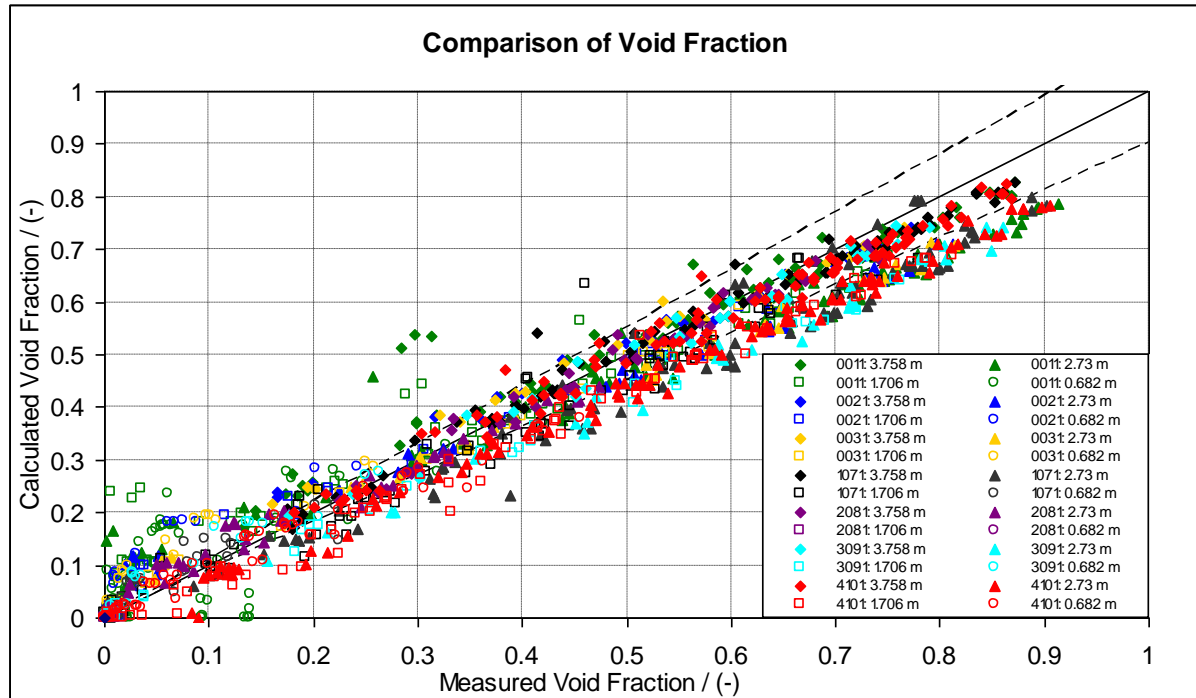


Fig. 6.9: Comparison of predicted and measured void fraction results

Furthermore an uncertainty analysis according to the guidelines of the Exercise 4, Phase I of [1] was performed in this report. Thereby the influence of the four input parameters outlet pressure, outlet quality, flow rate and inlet sub-cooling were investigated. Therefore the void fraction deviation versus each input parameter was plotted in which all other input parameters were chosen constant (Fig. 6.10 to Fig. 6.33). The uncertainty analysis confirms the earlier observation that the TRACE accuracy is not so good for low quality and mass flow conditions. The sub-cooling dependent ratio of calculated and measured outlet void fraction for the assembly type 0-1, (refer to [1]), is given in Fig. 6.10. The sub-cooling is independent of the void fraction deviation in the region between 20 kJ / kg and 120 kJ / kg.

The dependence of the deviation between calculated and measured results on the outlet quality for the assembly type 0-1 is presented in the same way in Fig. 6.11. It is good to see that the deviation of the void fraction is higher for low outlet quality conditions.

The ratio of the calculated and measured results is plotted against the flow rate in Fig. 6.12.

In Fig. 6.13 the ratio of calculated and measured results depending on the outlet pressure for the assembly type 0-1 is shown. Fig. 6.14 represents the ratio of calculated and measured results depending on the outlet quality for the assembly type 0-2. The C / M deviation is higher for low outlet quality conditions. The flow rate dependent ratio of calculated and measured outlet void fraction for the assembly type 0-2 is given in Fig. 6.15. In this diagram the deviation of outlet void fraction is higher for low mass flow conditions. The dependence of the deviation between calculated and measured results on the outlet pressure for the assembly type 0-2 is presented in Fig. 6.16. The ratio of the calculated and measured results is plotted against the outlet quality in Fig. 6.17. In Fig. 6.18 is shown the ratio of calculated and measured results depending on the flow rate for the assembly type 0-3. Fig. 6.19 represents the ratio of calculated and measured results depending on the outlet pressure for the assembly type 0-3. The inlet sub-cooling dependent ratio of calculated and measured outlet void fraction for the assembly type 1 is given in Fig. 6.20. The dependence of the deviation between calculated and measured results on the outlet quality for the assembly type 1 is presented in Fig. 6.21. The ratio of the calculated and measured results is plotted against the flow rate in Fig. 6.22. The deviation of the outlet void fraction is higher for low mass flow conditions. In Fig. 6.23 is shown the ratio of calculated and measured results depending on the outlet pressure for the assembly type 1. Fig. 6.24 represents the ratio of calculated and measured results depending on the outlet quality for the assembly type 2. The flow rate dependent ratio of calculated and measured outlet void fraction for the assembly type 2 is given in Fig. 6.25. The dependence of the deviation between calculated and measured results on the outlet pressure is presented in Fig. 6.26 for the assembly type 2. The ratio of the calculated and measured results is plotted against the outlet quality in Fig. 6.27. In Fig. 6.28 is shown the ratio of calculated and measured results depending on the flow rate for the assembly type 3. Fig. 6.29 represents the ratio of calculated and measured results depending on the outlet pressure for the assembly type 3. The inlet sub-cooling dependent ratio of calculated and measured outlet void fraction for the assembly type 4 is given in Fig. 6.30. The dependence of the deviation between calculated and measured results on the outlet quality is presented in Fig. 6.31 for the assembly type 4. The ratio of the calculated and measured results is plotted against the flow rate in Fig. 6.32. In Fig. 6.33 is shown the ratio of calculated and measured results depending on the outlet pressure for the assembly type 4.

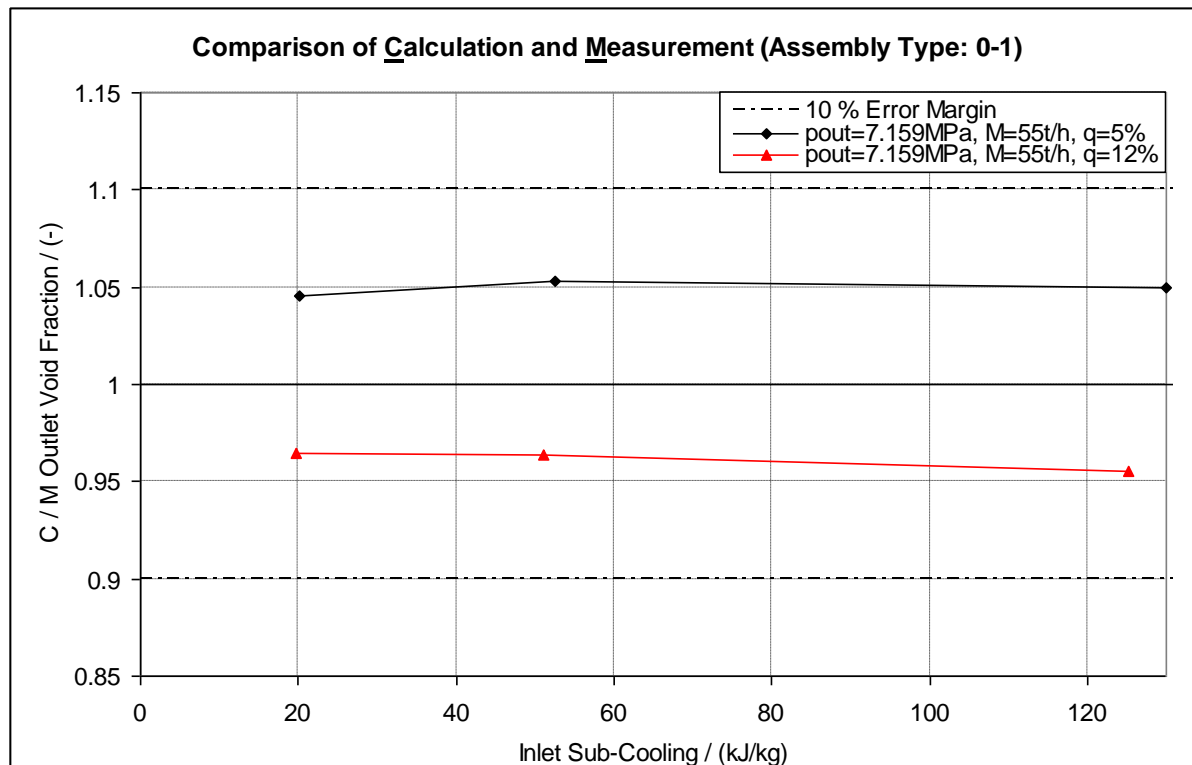


Fig. 6.10: Void fraction C / M ratio versus inlet sub-cooling (Assembly Type 0-1)

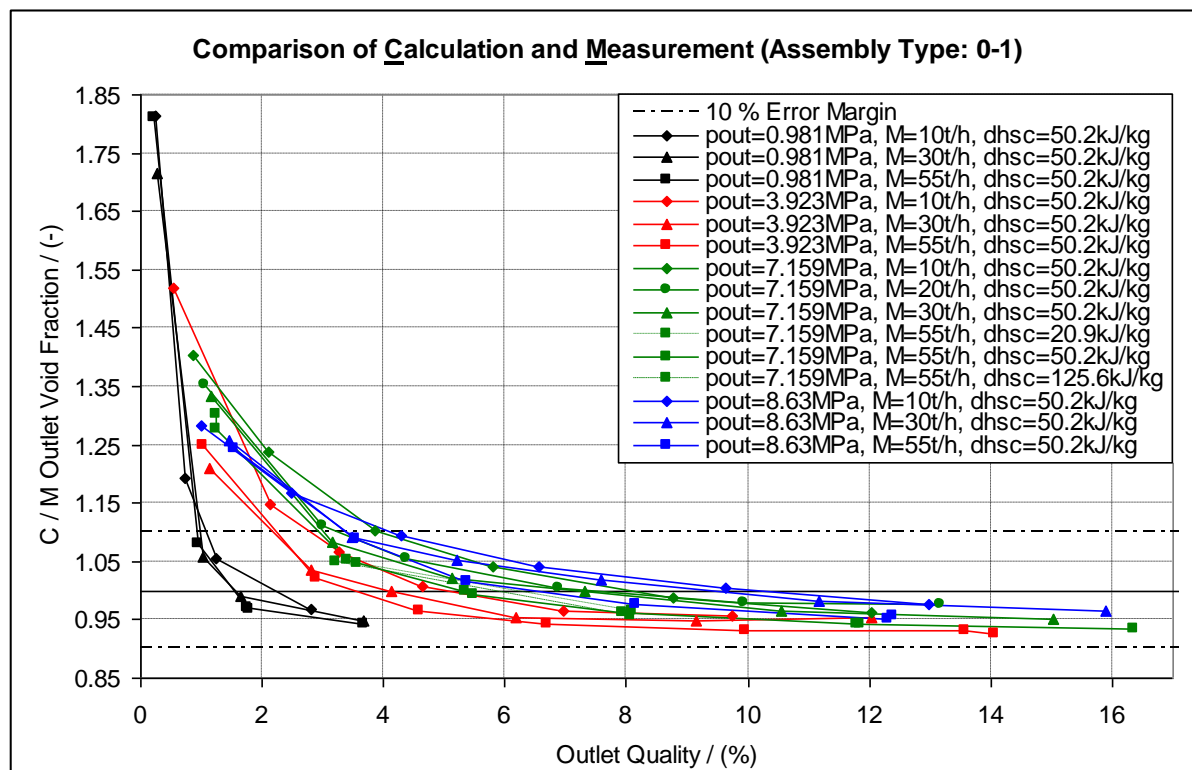


Fig. 6.11: Void fraction C / M ratio versus outlet quality (Assembly Type 0-1)

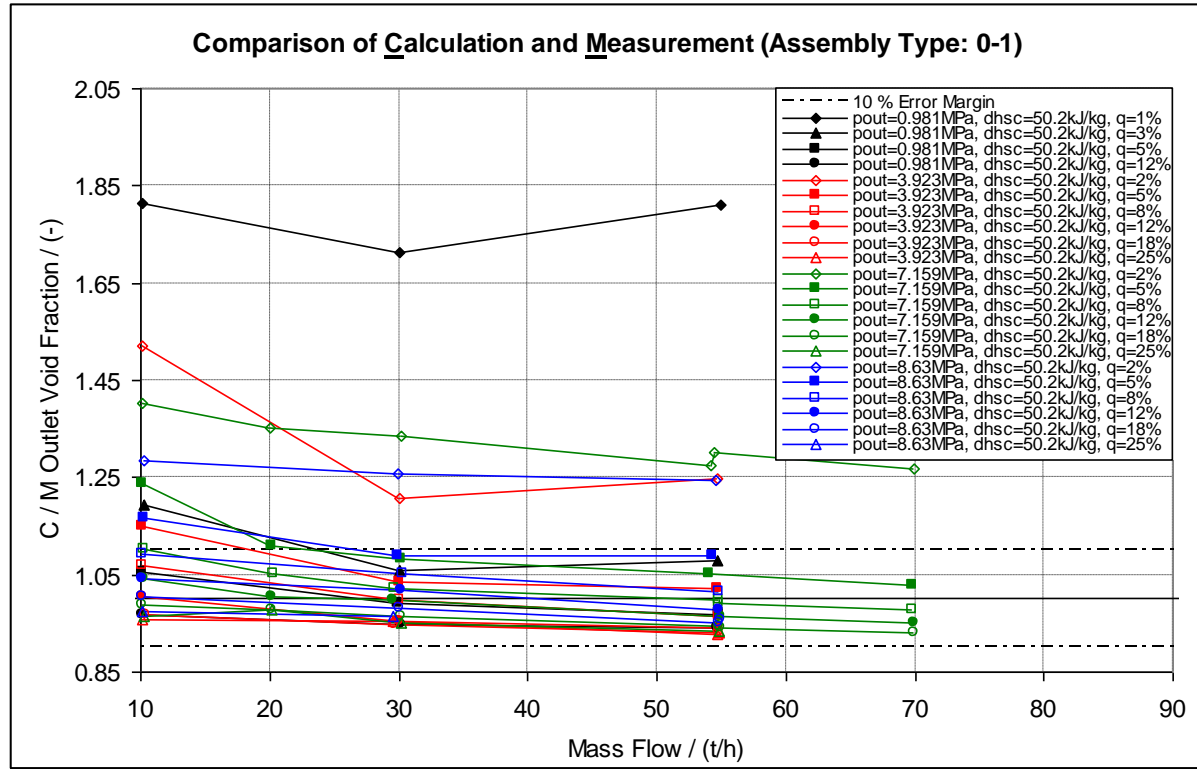


Fig. 6.12: Void fraction C / M ratio versus mass flow (Assembly Type 0-1)

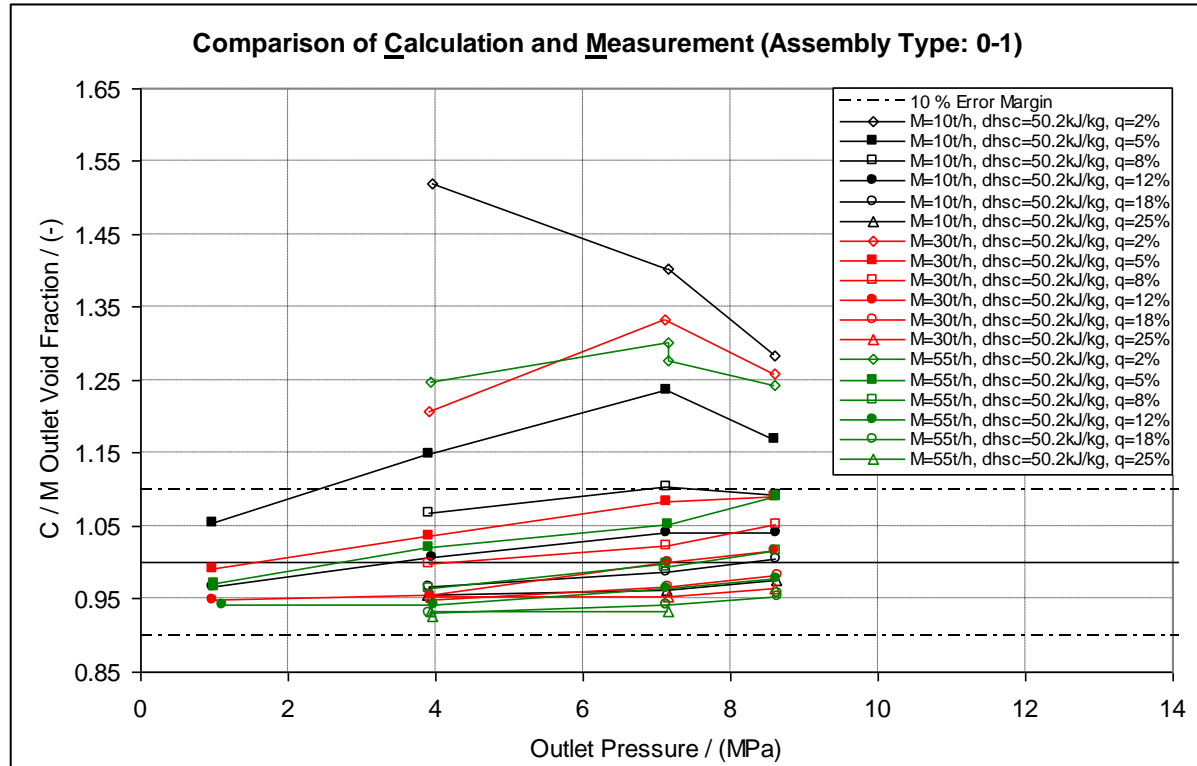


Fig. 6.13: Void fraction C / M ratio versus outlet pressure (Assembly Type 0-1)

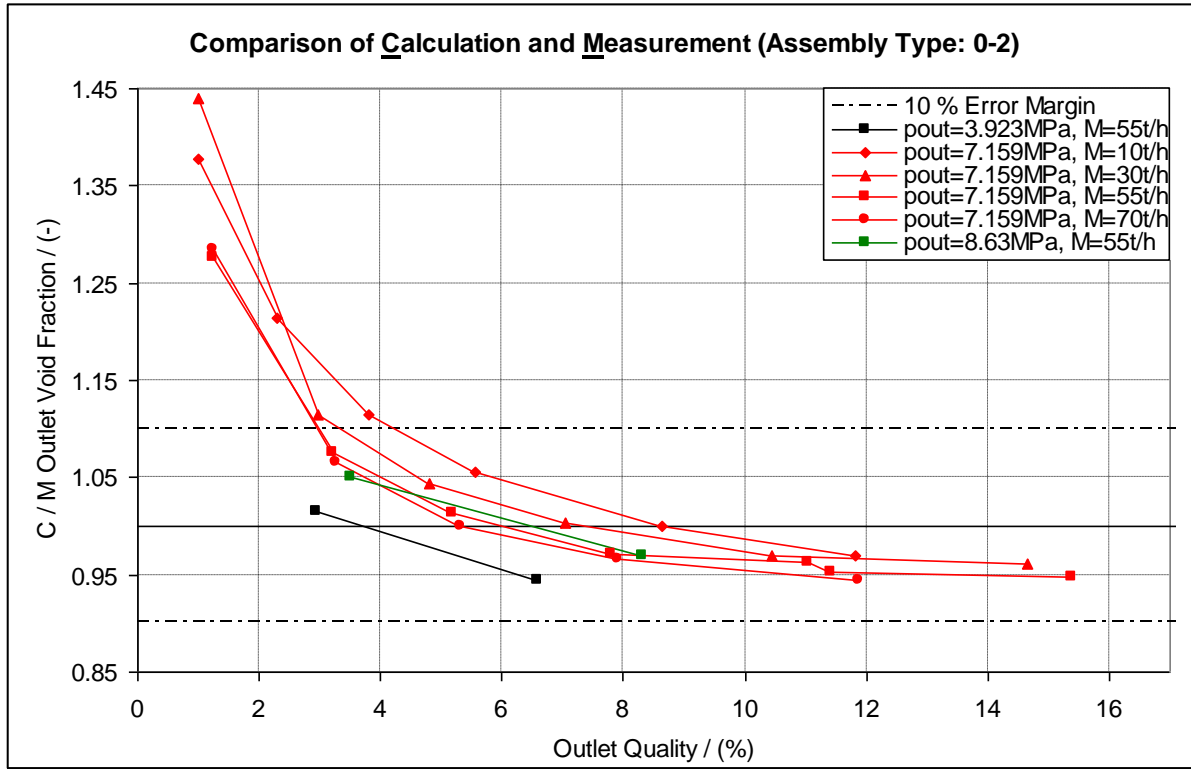


Fig. 6.14: Void fraction C / M ratio versus outlet quality (Assembly Type 0-2)

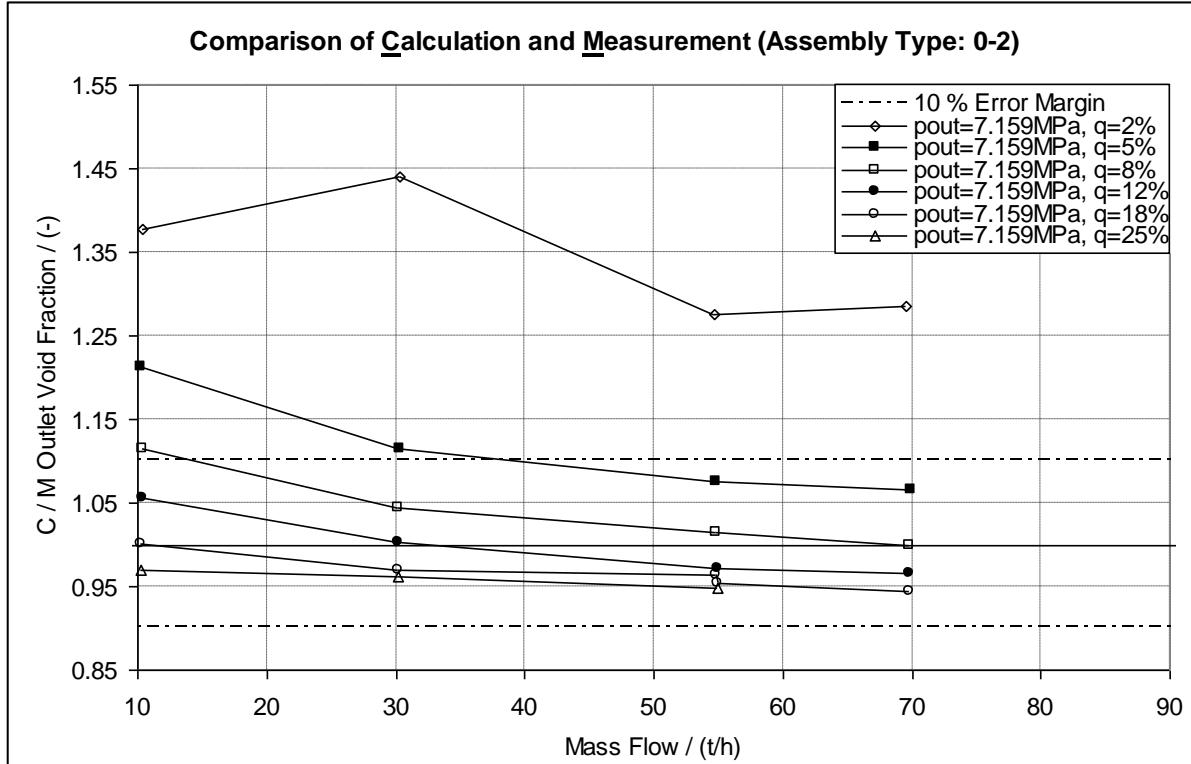


Fig. 6.15: Void fraction C / M ratio versus mass flow (Assembly Type 0-2)

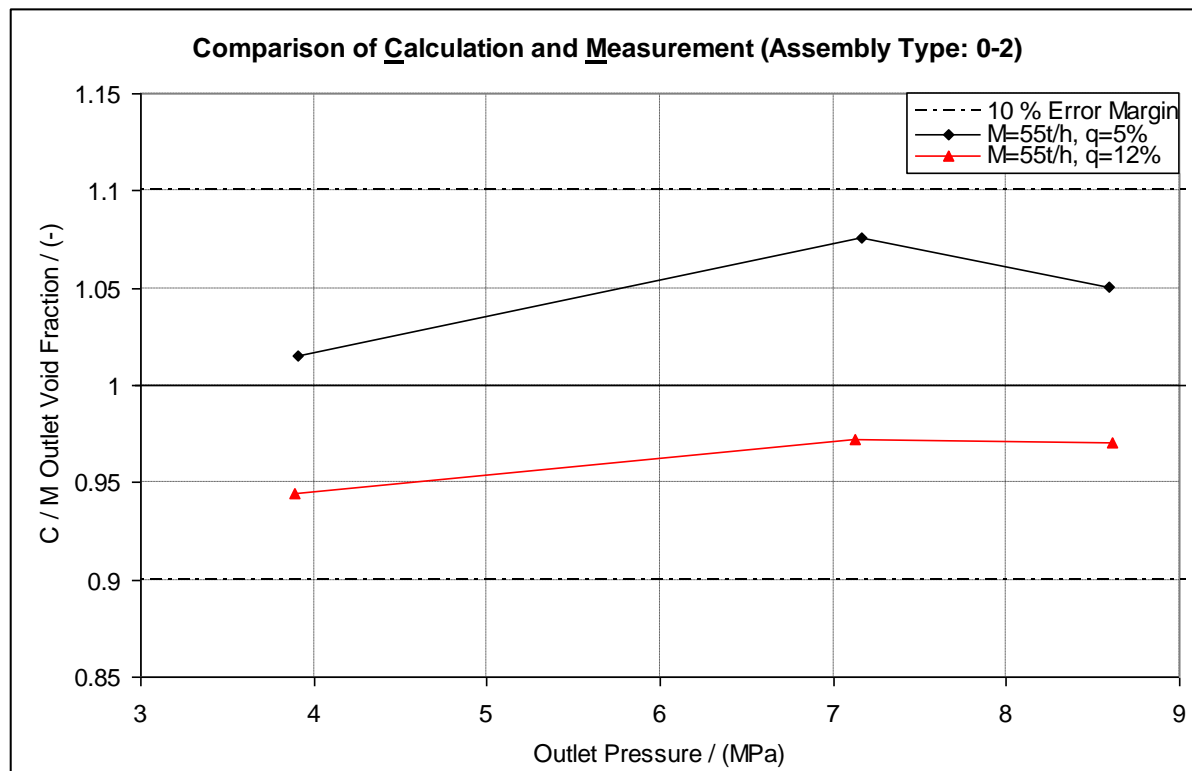


Fig. 6.16: Void fraction C / M ratio versus outlet pressure (Assembly Type 0-2)

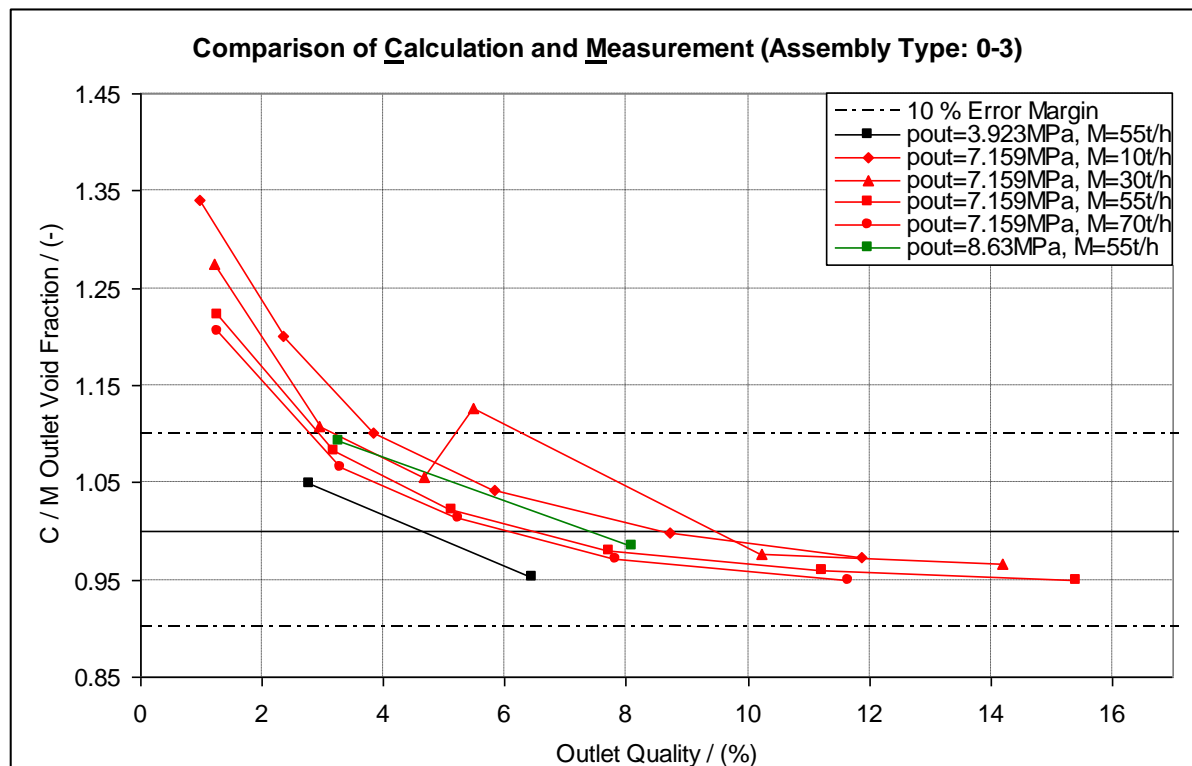


Fig. 6.17: Void fraction C / M ratio versus outlet quality (Assembly Type 0-3)

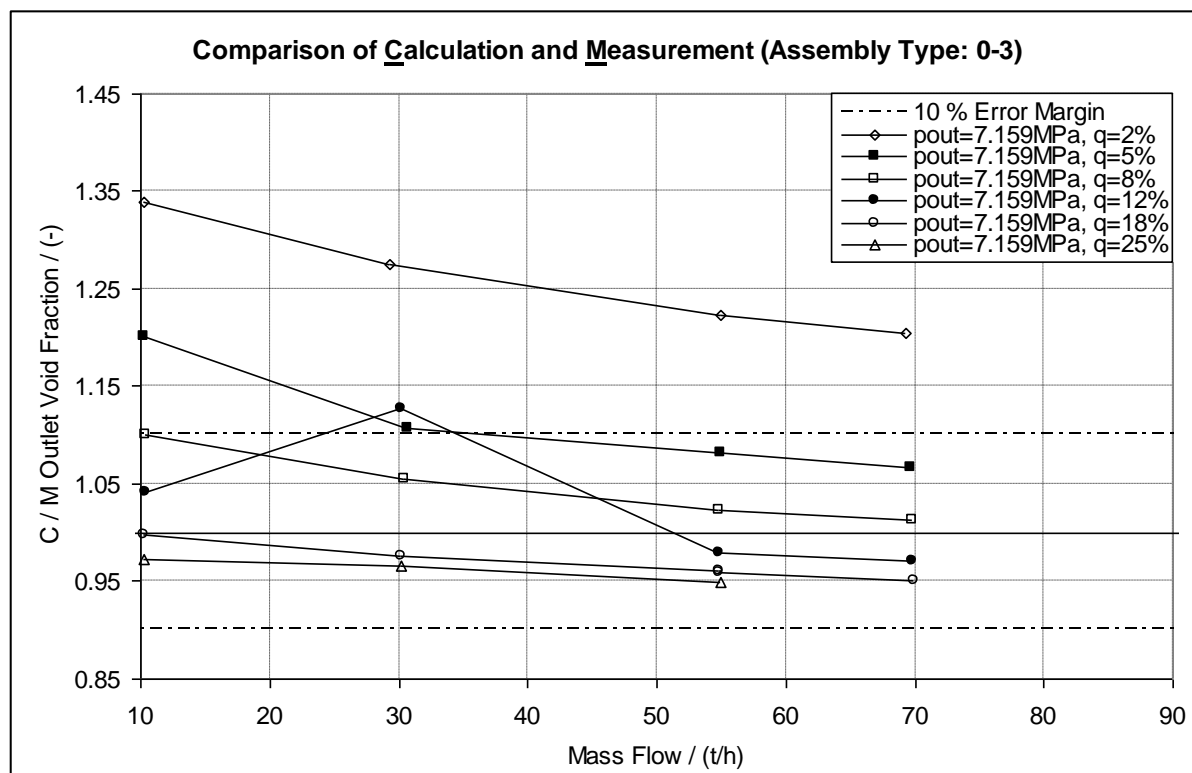


Fig. 6.18: Void fraction C / M ratio versus mass flow (Assembly Type 0-3)

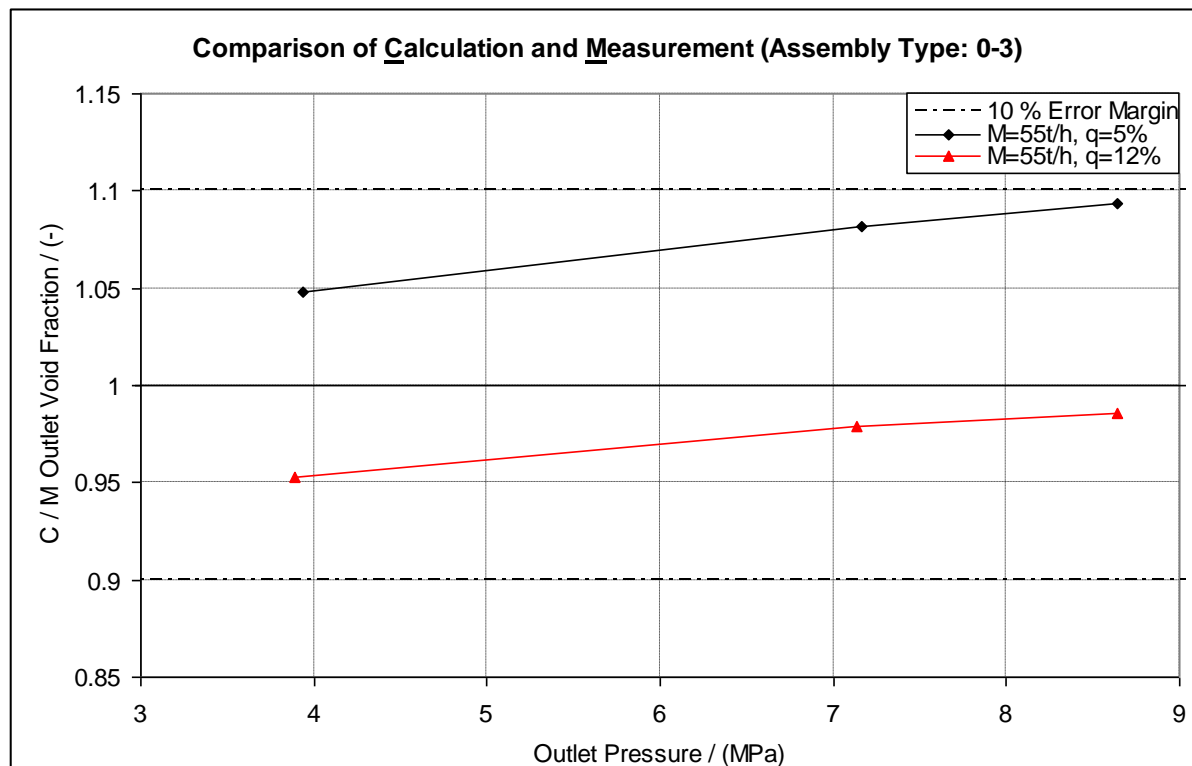


Fig. 6.19: Void fraction C / M ratio versus outlet pressure (Assembly Type 0-3)

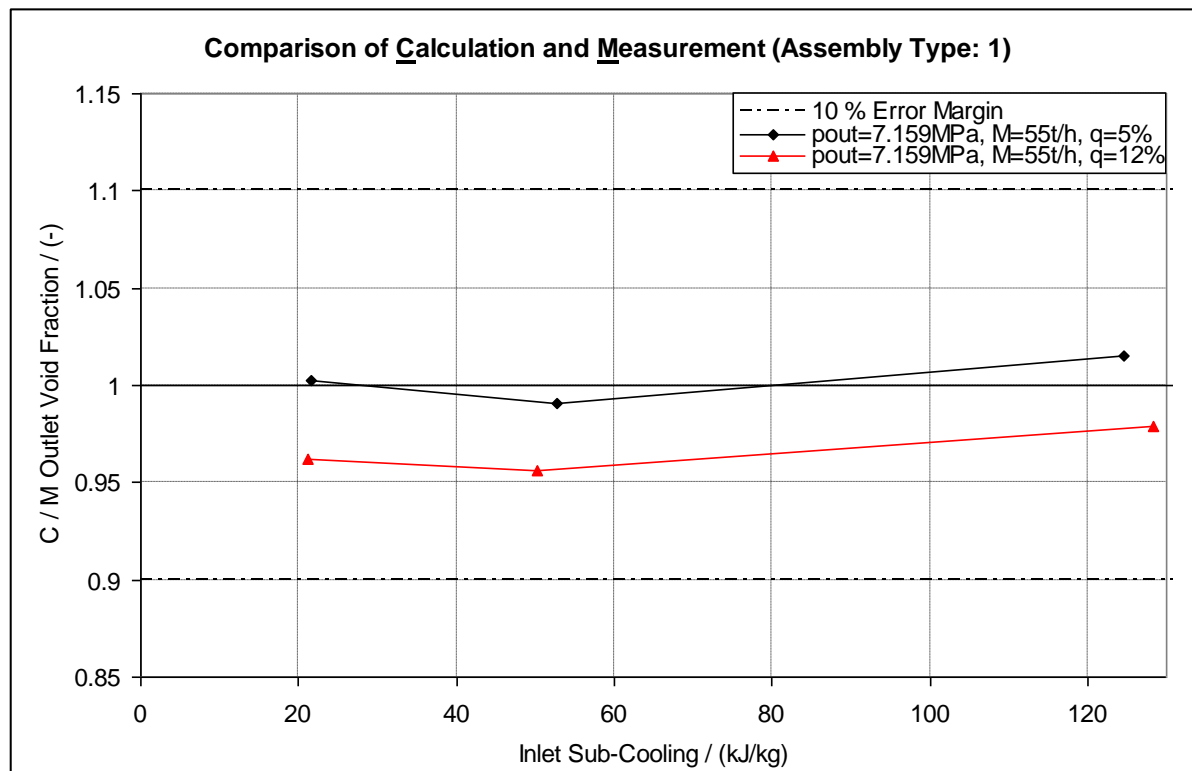


Fig. 6.20: Void fraction C / M ratio versus inlet sub-cooling (Assembly Type 1)

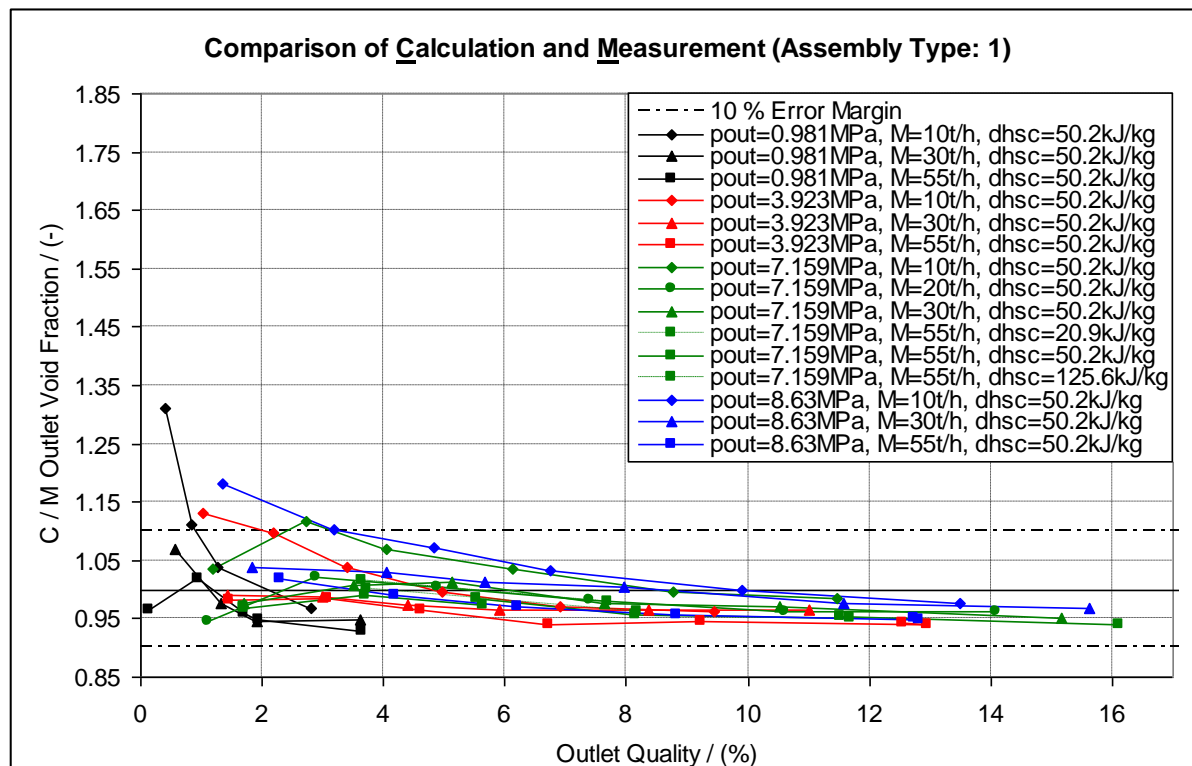


Fig. 6.21: Void fraction C / M ratio versus outlet quality (Assembly Type 1)

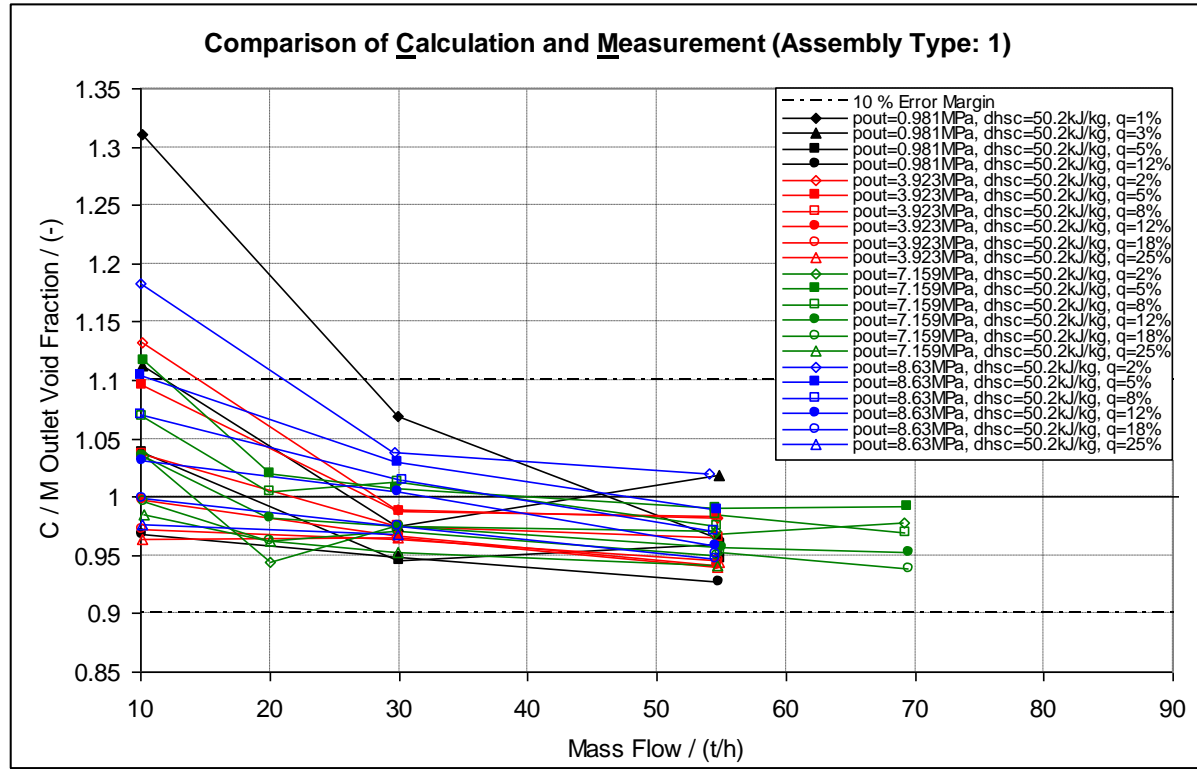


Fig. 6.22: Void fraction C / M ratio versus mass flow (Assembly Type 1)

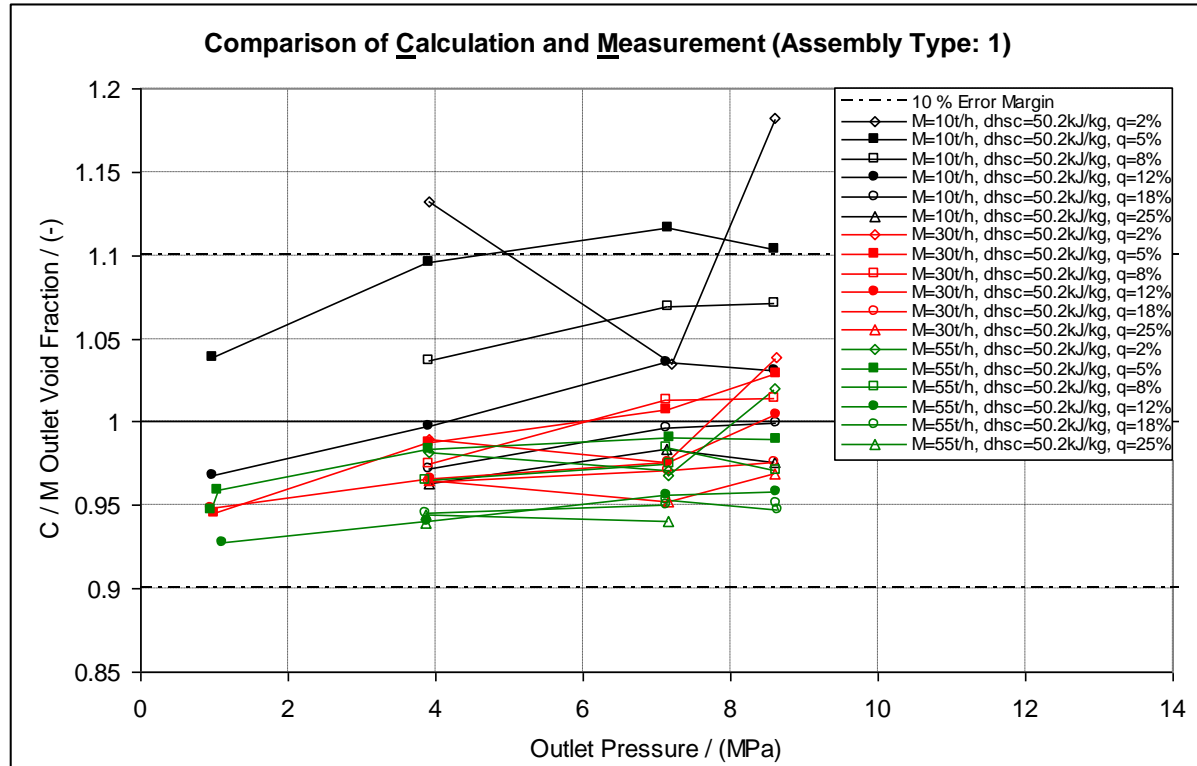


Fig. 6.23: Void fraction C / M ratio versus outlet pressure (Assembly Type 1)

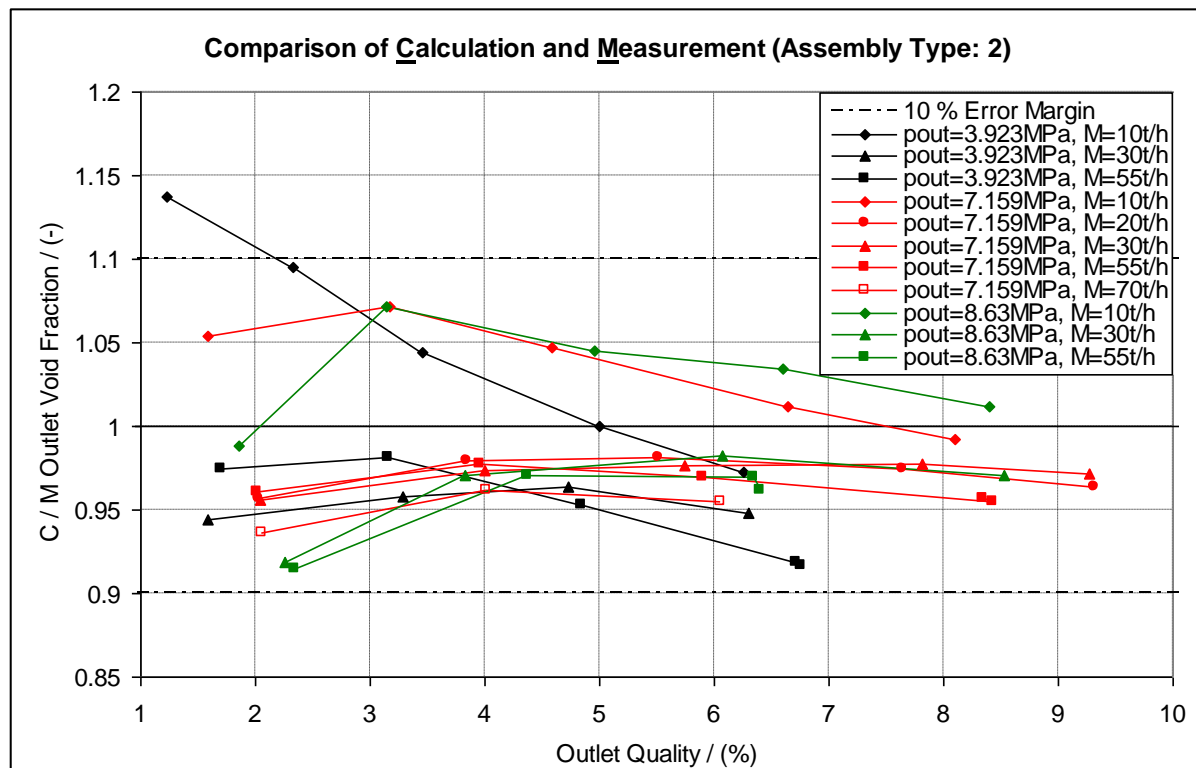


Fig. 6.24: Void fraction C / M ratio versus outlet quality (Assembly Type 2)

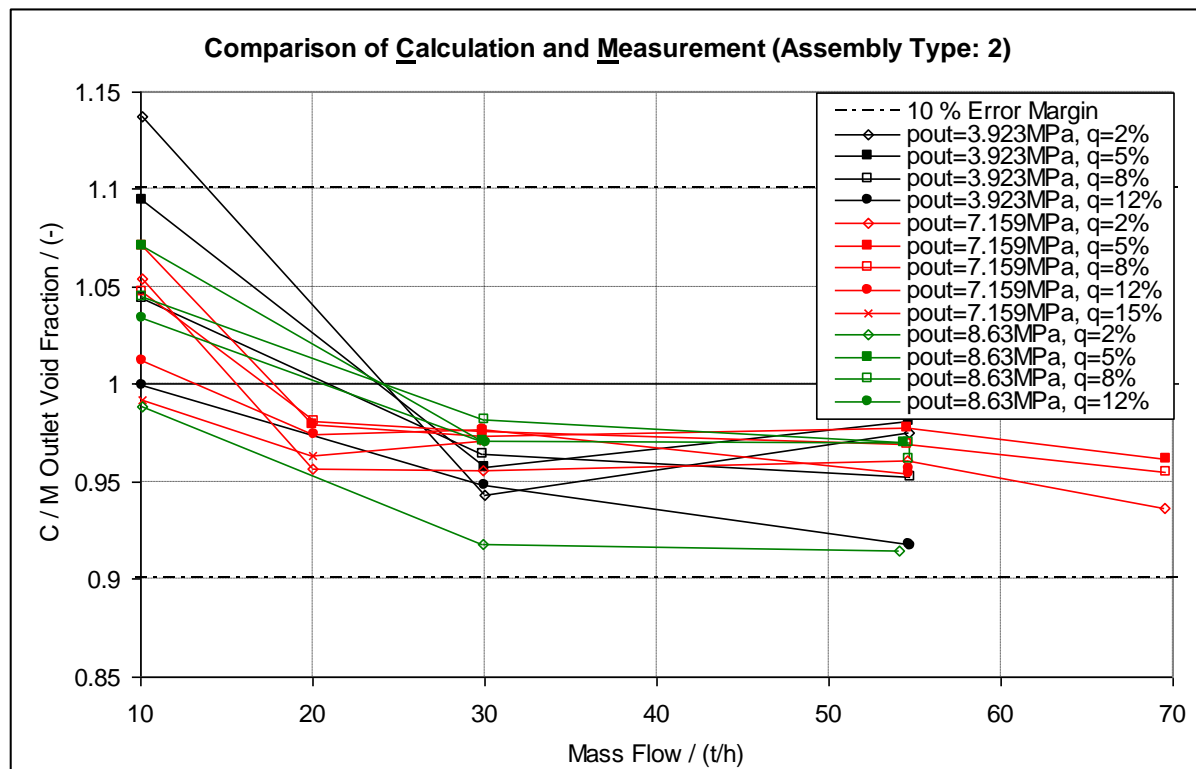


Fig. 6.25: Void fraction C / M ratio versus mass flow (Assembly Type 2)

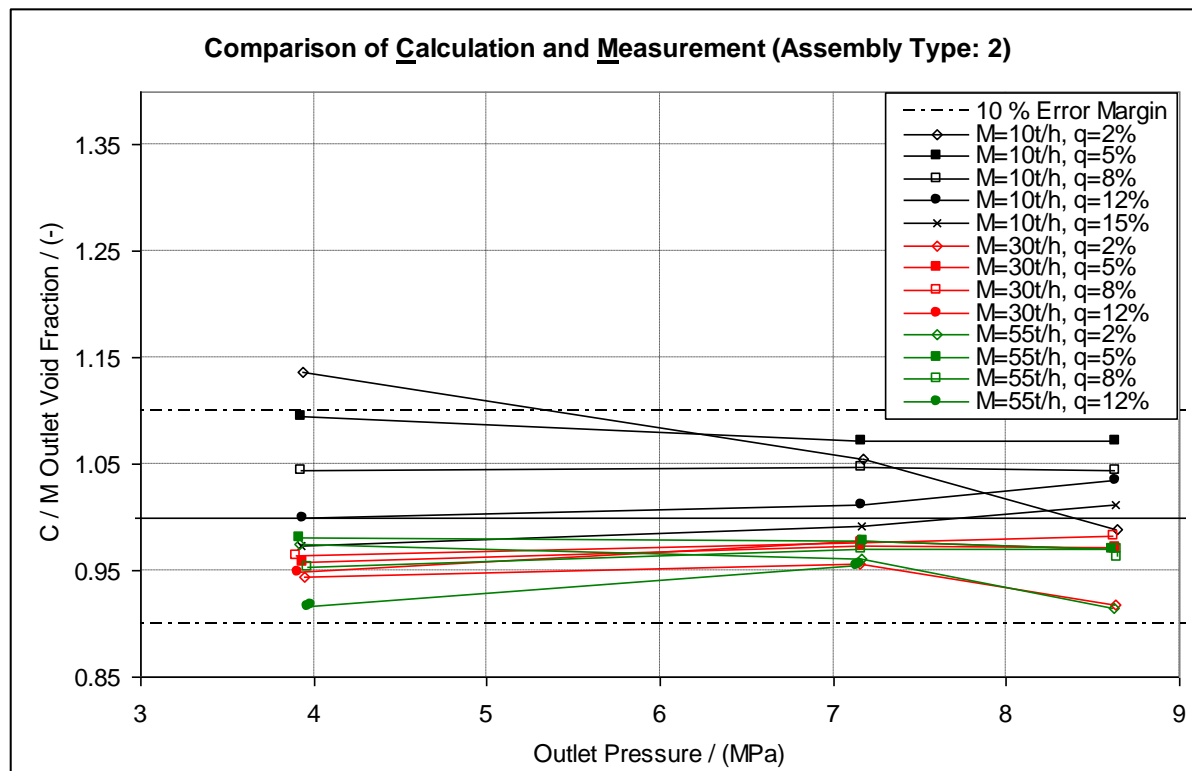


Fig. 6.26: Void fraction C / M ratio versus outlet pressure (Assembly Type 2)

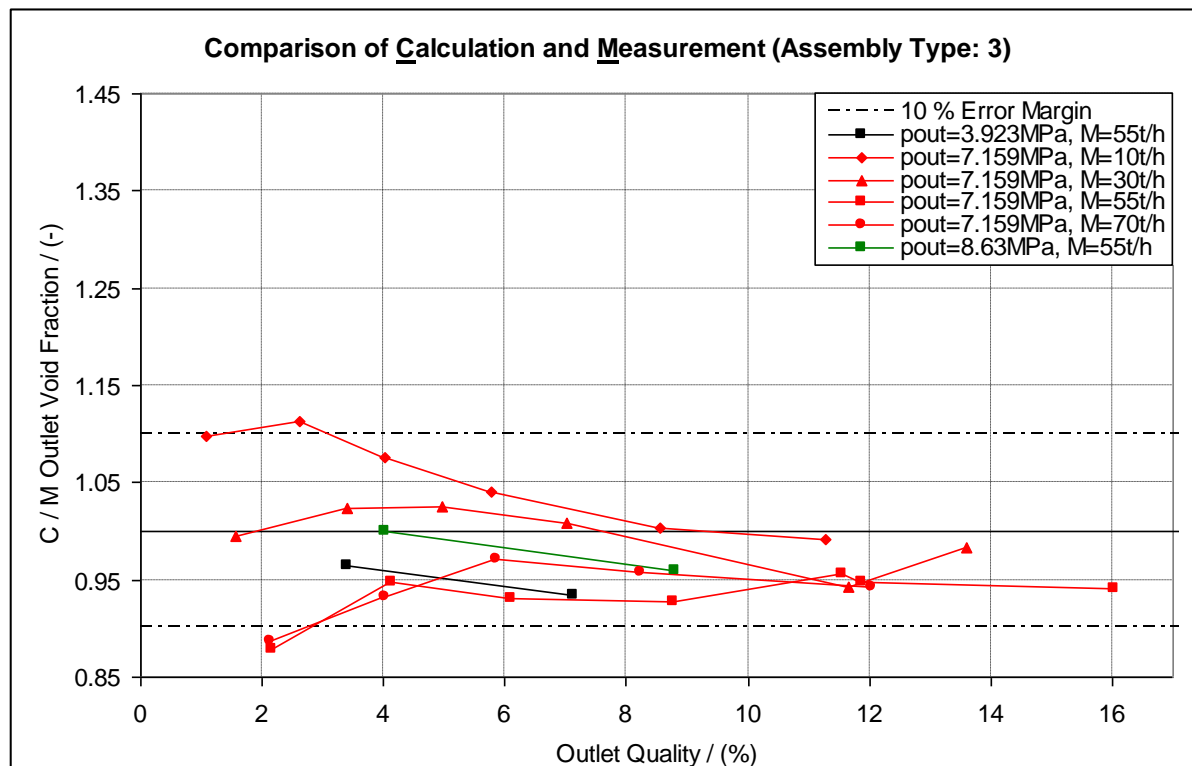


Fig. 6.27: Void fraction C / M ratio versus outlet quality (Assembly Type 3)

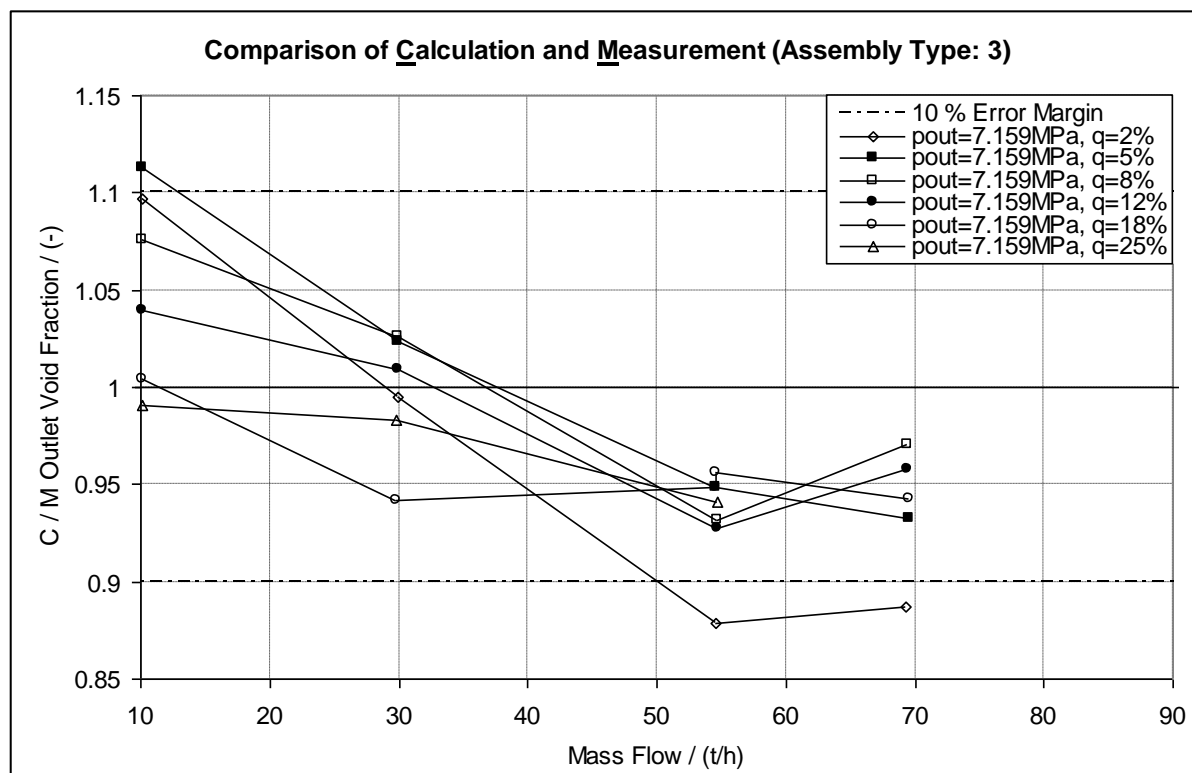


Fig. 6.28: Void fraction C / M ratio versus mass flow (Assembly Type 3)

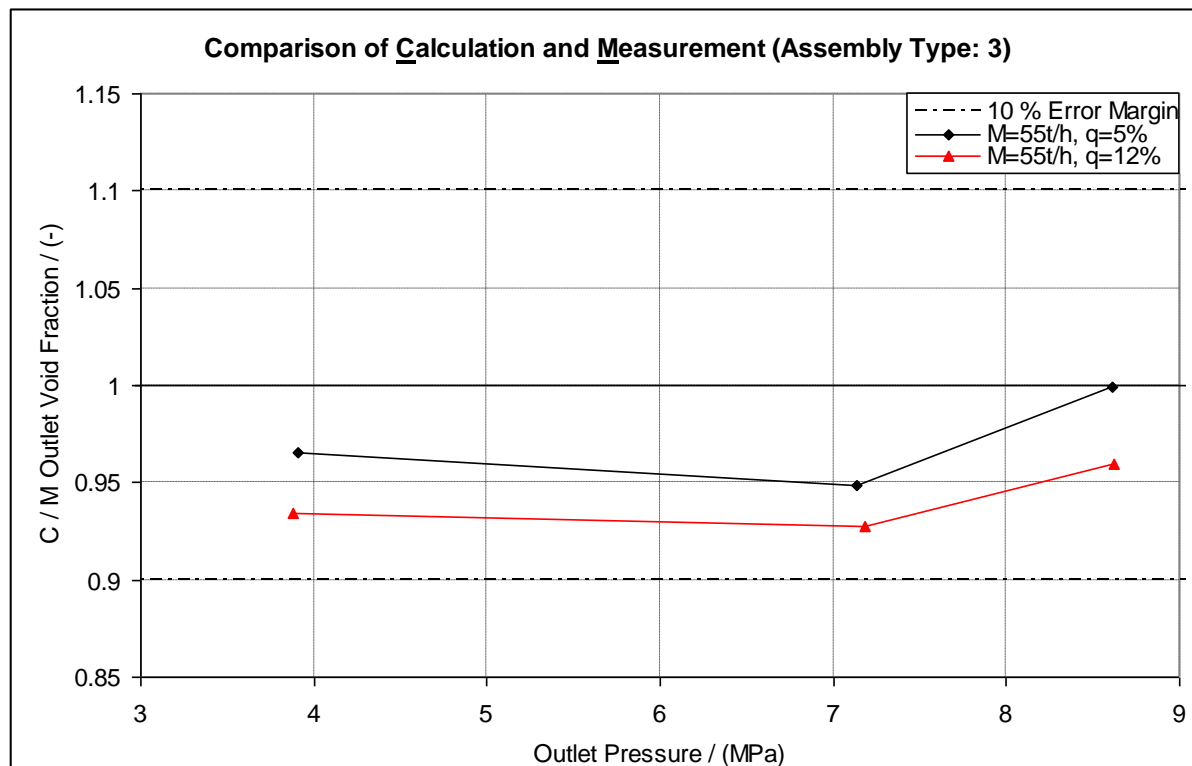


Fig. 6.29: Void fraction C / M ratio versus outlet pressure (Assembly Type 3)

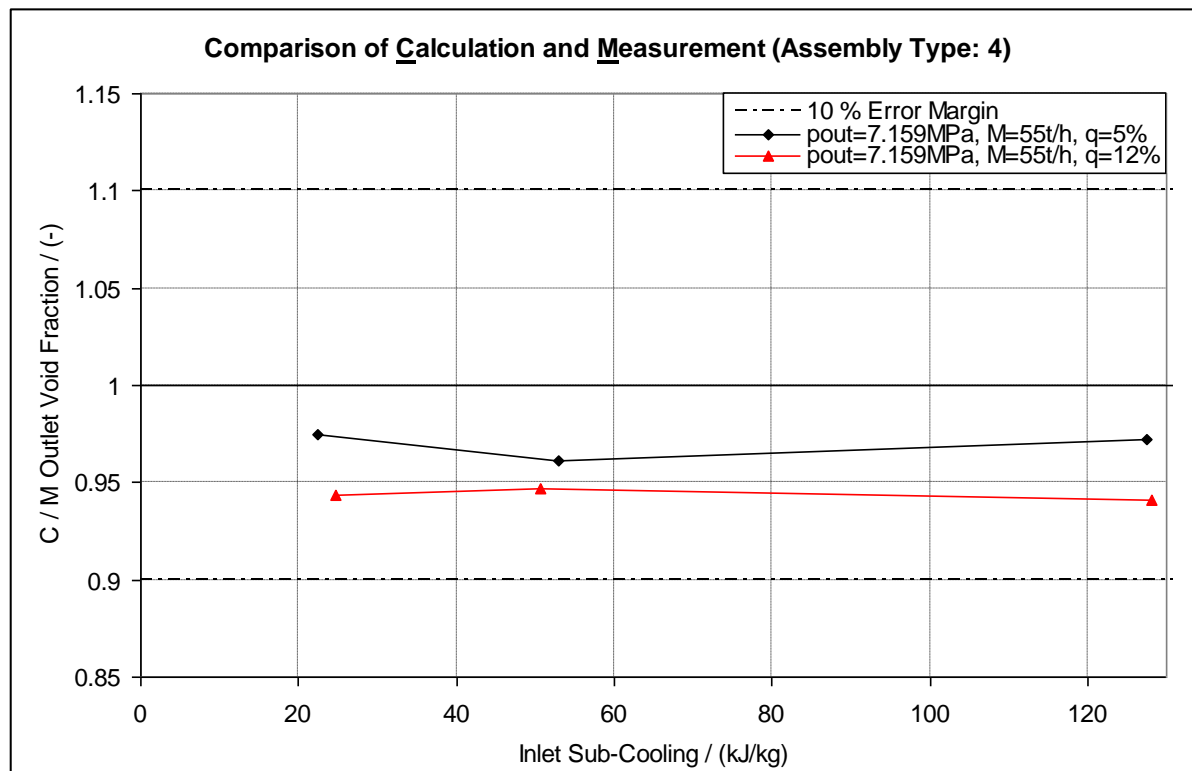


Fig. 6.30: Void fraction C / M ratio versus inlet sub-cooling (Assembly Type 4)

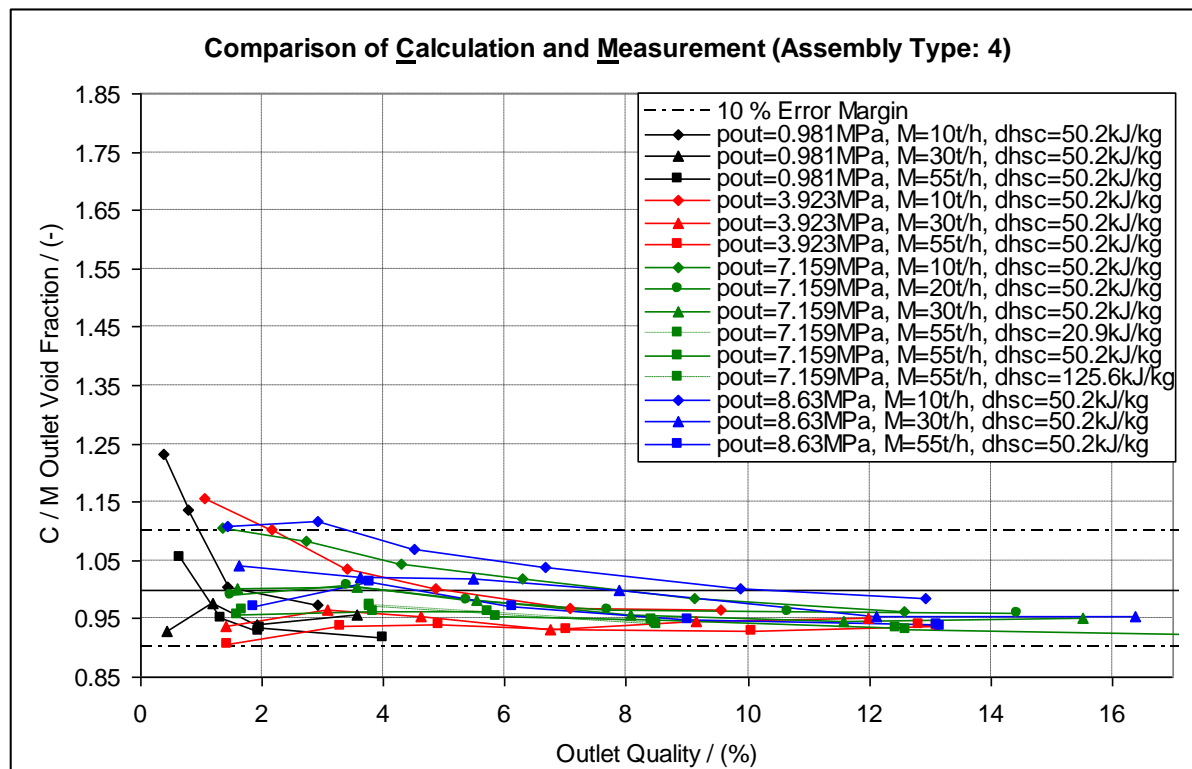


Fig. 6.31: Void fraction C / M ratio versus outlet quality (Assembly Type 4)

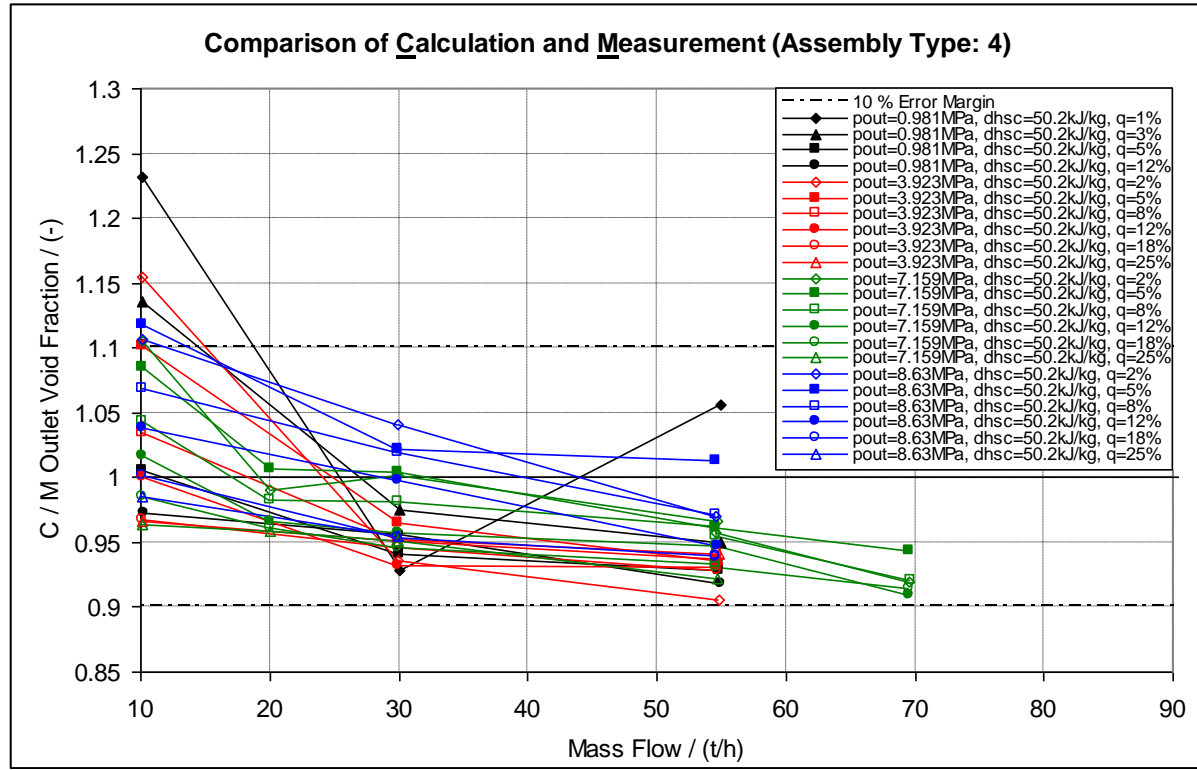


Fig. 6.32: Void fraction C / M ratio versus mass flow (Assembly Type 4)

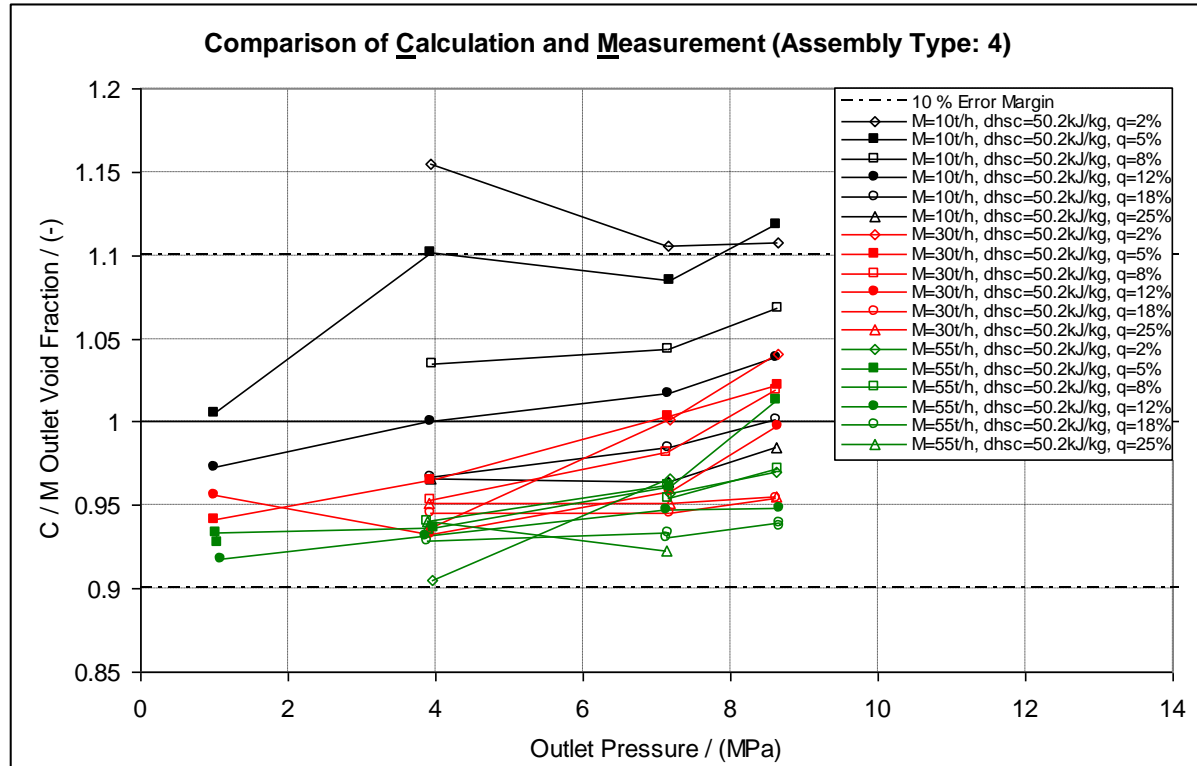


Fig. 6.33: Void fraction C / M ratio versus outlet pressure (Assembly Type 4)

Summarizing all of the calculational results in Fig. 6.34 a histogram of the void fraction deviation at the bundle outlet is shown in which the test clusters as function of calculation / prediction ratio is plotted. As a general result of the most post test calculations showed a poor comparison to the measurements. In Fig. 6.35 the void fraction ratio distributions of all four measured bundle elevations is plotted. This graph clearly indicates that at the upper bundle levels the deviations between the TRACE calculation and measurement are bigger.

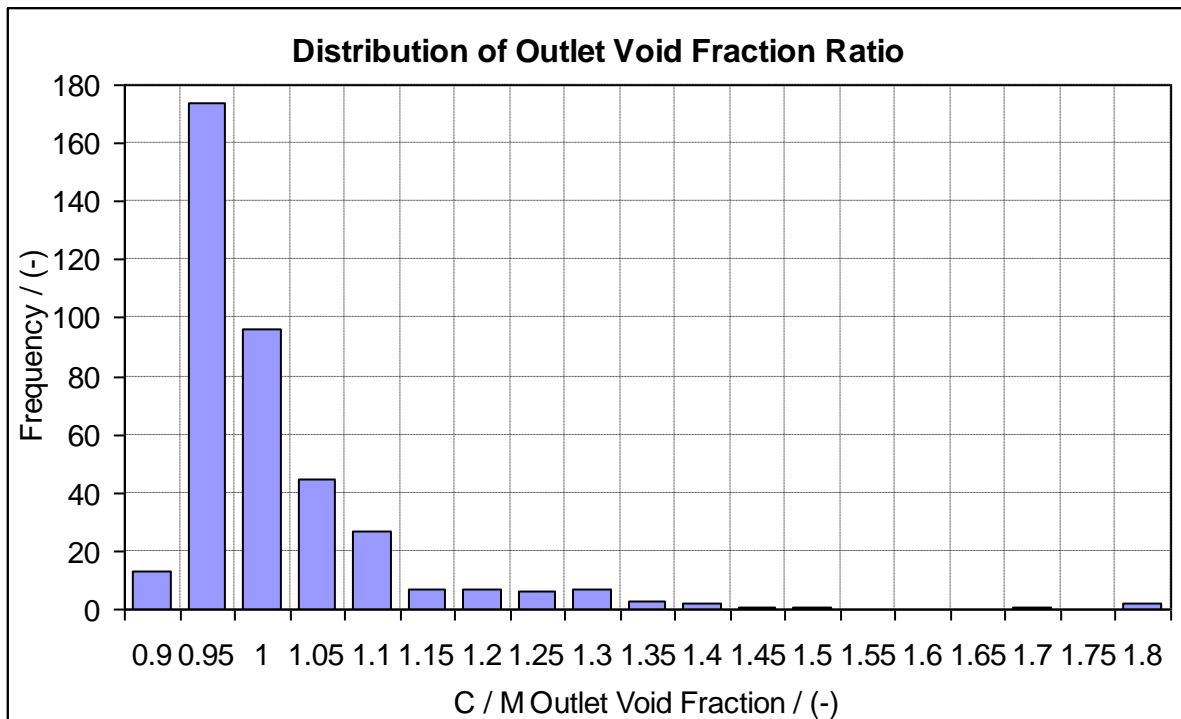


Fig. 6.34: Distribution of calculation / measurement ratio at outlet

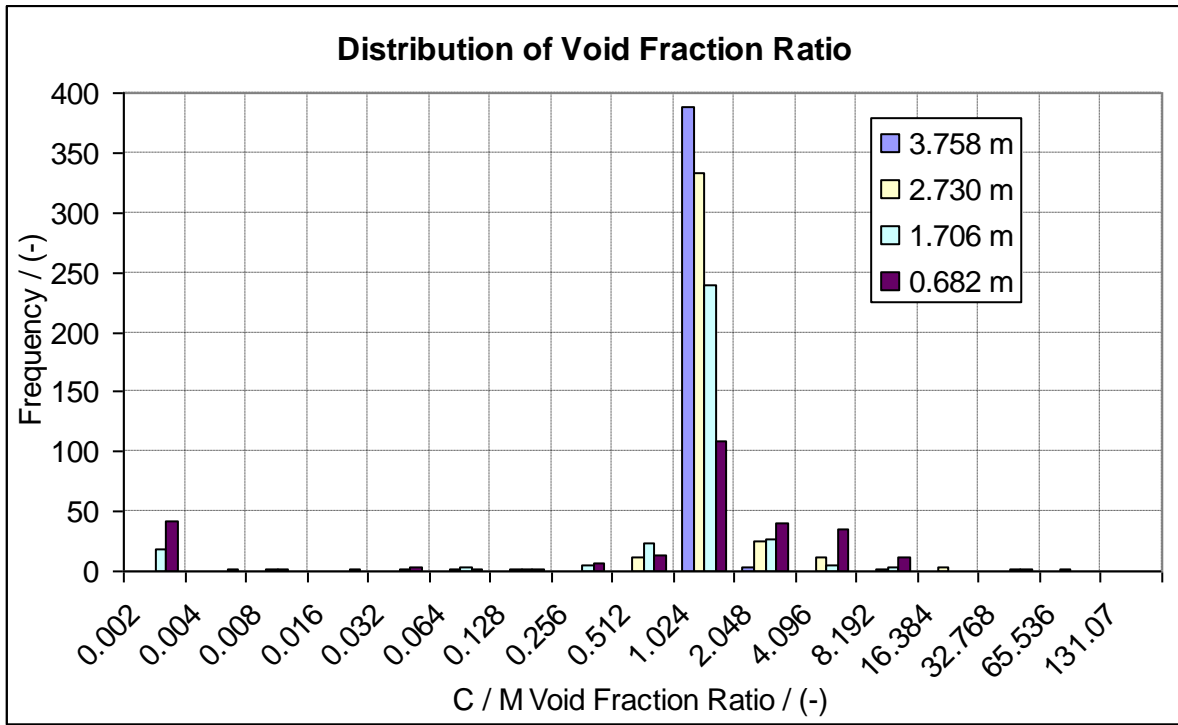


Fig. 6.35: Distribution of calculation / measurement ratio of all void fraction tests

6.1.4 TRACE Results for Transient Test 4102-001~009

For the simulation of this transient test a steady state calculation was performed initially to get the steady state solution. Then, a transient TRACE calculation was performed using the model described in chapter 3.1.2 and 0 and the time dependent boundary conditions given in Fig. 3.2, Fig. 3.3, Fig. 3.4 and Fig. 3.5. The CPU time for this calculation was approximately 191 s.

A comparison of predicted and measured void fractions evolution for four different axial positions is given in Fig. 6.36, Fig. 6.37, Fig. 6.38 and Fig. 6.39. As can be observed in the figures, the predicted void trends follow very well the measured void evolution at all four measured positions for the turbine trip transient. The agreement between the TRACE results and the data is very good except for low mass flow rates and void fractions below 0.15 (i.e. in the subcooled boiling zone), where TRACE overpredicts the void fraction, Fig. 6.36. For void fractions between 0.45 and 0.8 and high mass flow rates and heat fluxes the agreement between predictions and data is reasonable good with deviations below 15 %. It is worth to note that by a void fraction between 0.45 and 0.5 the bubbly slug flow regime exist, between 0.75 and 0.8 the annular flow is present whereas between 0.5 and 0.75 there is churn flow which is determining in TRACE by an interpolation scheme. Here TRACE trends to underpredict the void fraction.

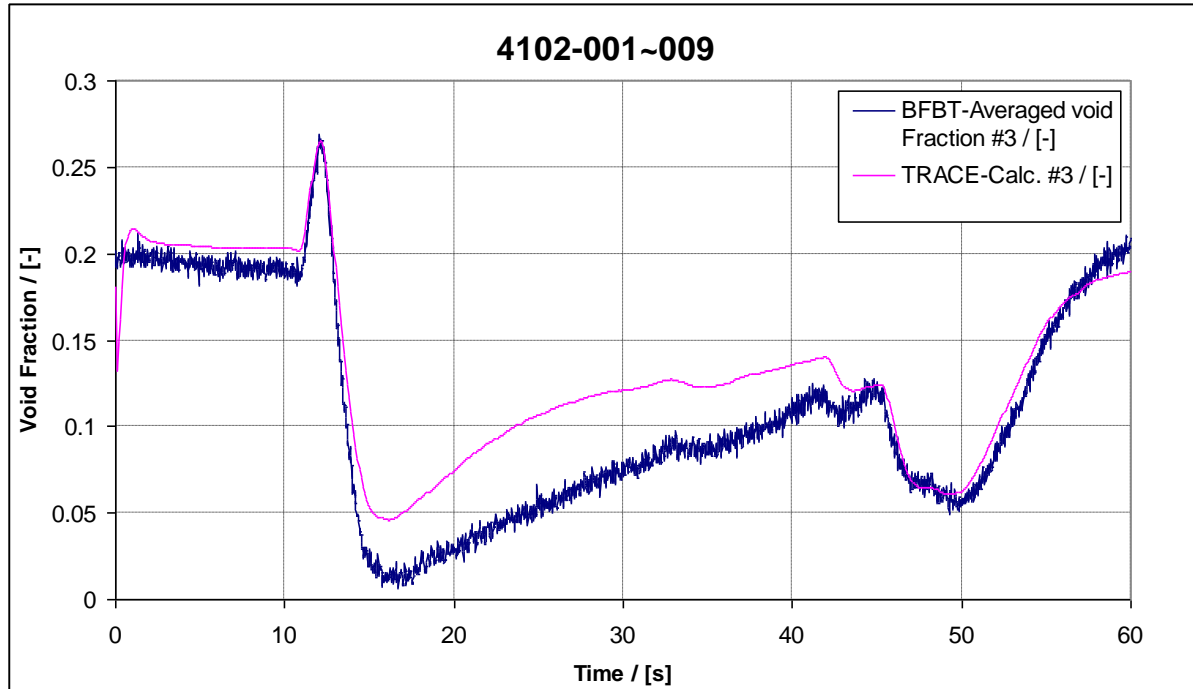


Fig. 6.36: Comparison between BFBT data and TRACE results at X-ray densitometer #3

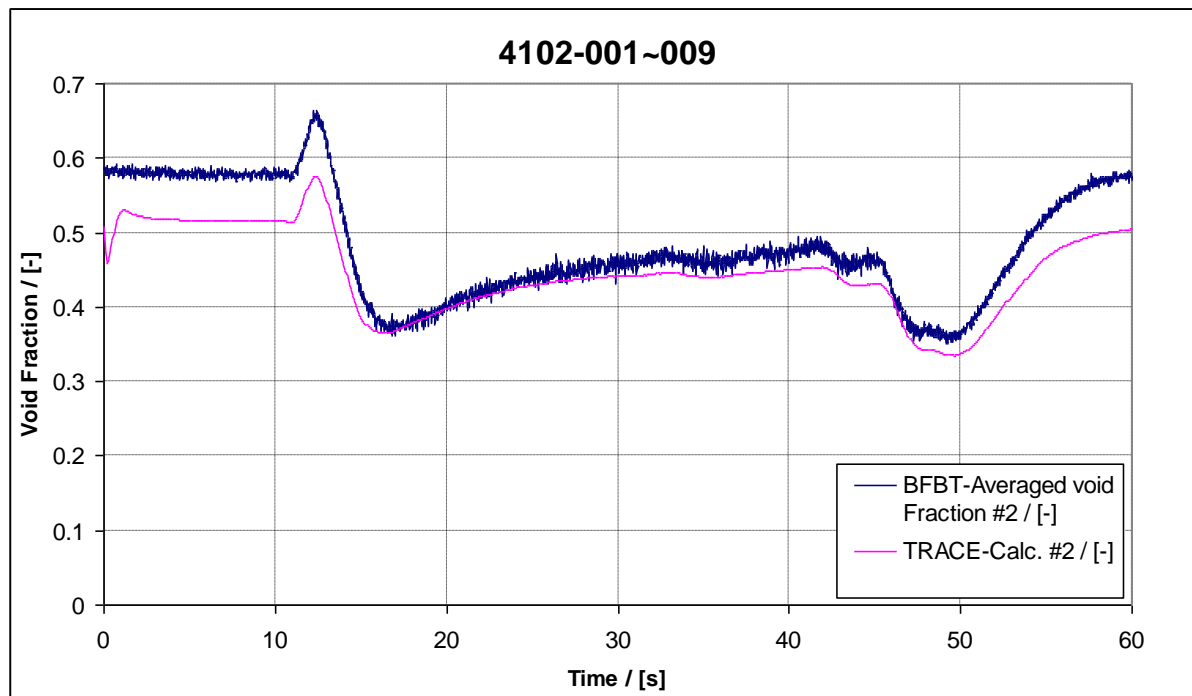


Fig. 6.37: Comparison between BFBT data and TRACE results at X-ray densitometer #2

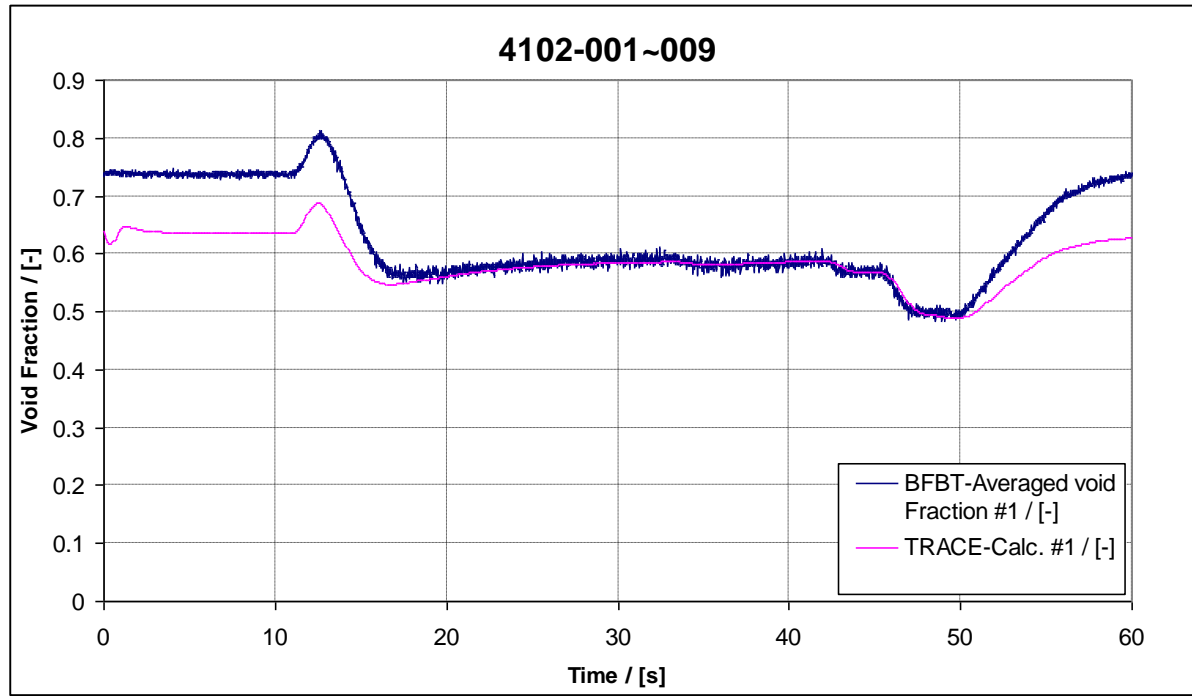


Fig. 6.38: Comparison between BFBT data and TRACE results at X-ray densitometer #1

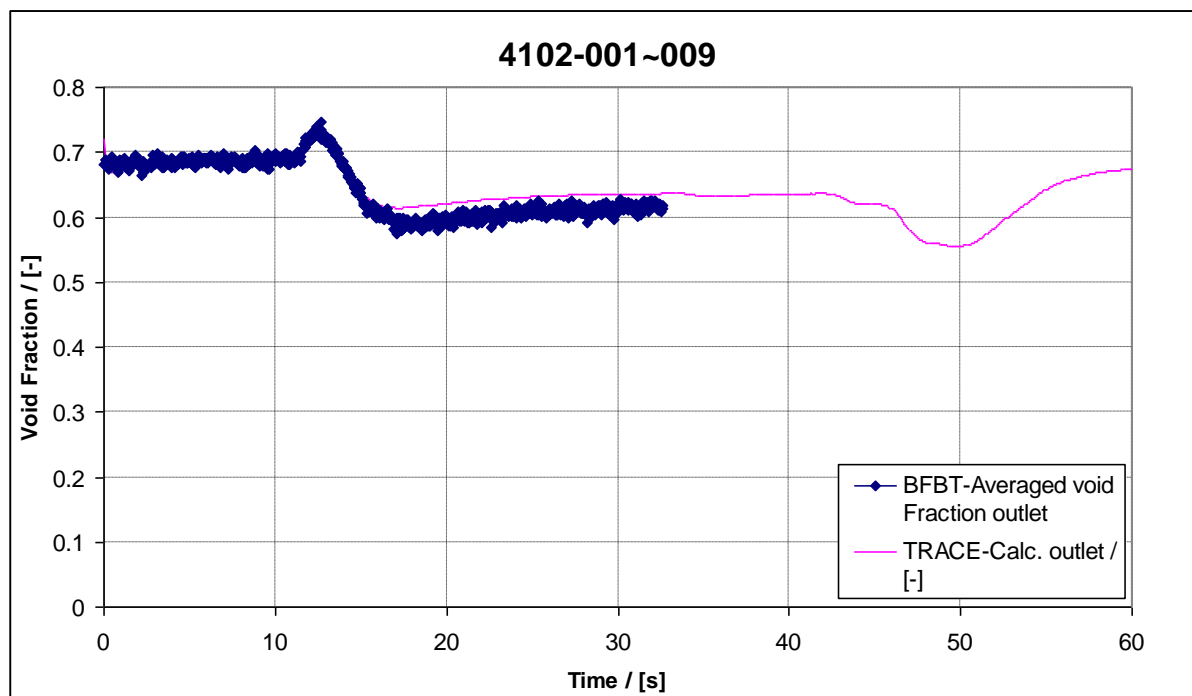


Fig. 6.39: Comparison between BFBT data and TRACE results at bundle outlet

6.2 Critical Power Calculations

6.2.1 Introductory Remarks

In this chapter selected results of the critical power post-test calculation are presented. It includes both steady state and transient calculations. The minimum/maximum time step was set to 0.0001 s/0.05 s for the steady state calculations and 0.0001 s/0.001 s for the transient calculations.

Four steady state critical power tests of the NUPEC test series, (see Tab. 3.4), were selected for the TRACE simulations. The boundary conditions of each test used in the simulations are given in Tab. 3.4.

First a steady state TRACE simulation was performed to initialize the subsequent transient calculation. To simulate the critical power test, a transient TRACE calculation was carried out in which the power was slowly increased with a ramp by 15 W/s. This was given as a time dependent boundary condition. In Fig. 6.40 the approach used to determine the critical power from the simulation's results is shown. For the derivation of the critical power from the TRACE simulation the following steps are necessary:

step 1: The outer surface temperature of all heater groups versus time are plotted for the axial elevation of 3.009 m which corresponds to the position of the thermocouples.

step 2: The temperature evolution with the highest increase rate is identified. This corresponds to the heater rod group 1. Then the time (T_{crit}) at which the heater temperatures has increased by 14 K is determined.

step 3: The bundle power is plotted against the time. On this plot, the power corresponding to the time " T_{crit} " is read as the critical power (P_{crit}).

This approach has been applied to estimate the critical power from the TRACE results for the four tests.

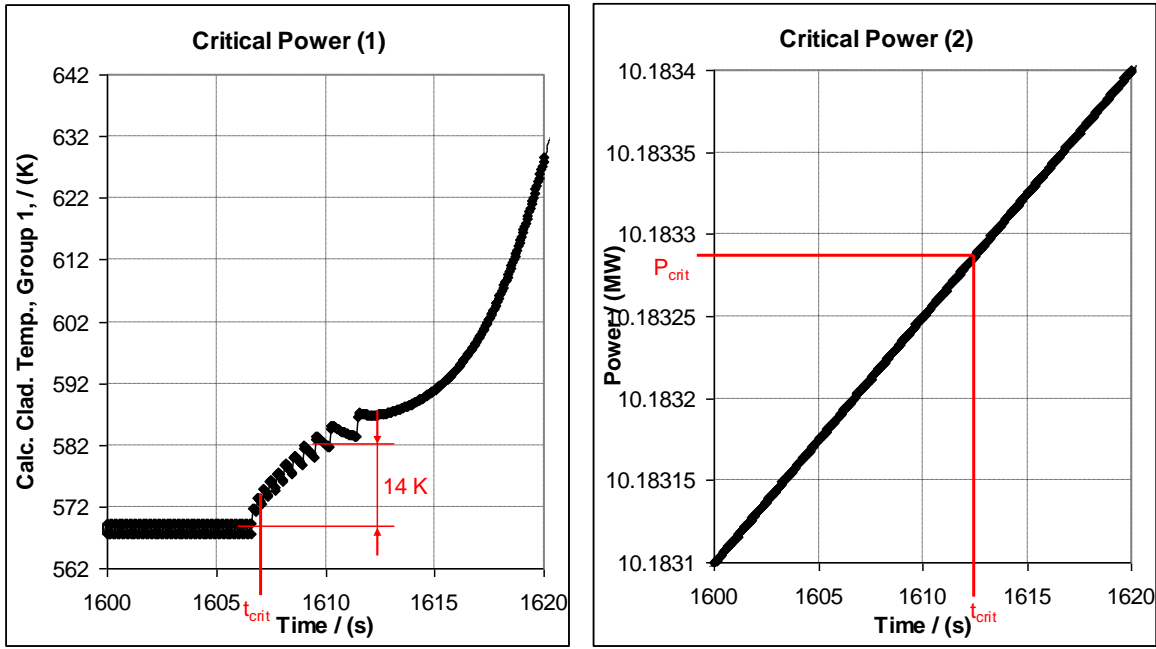


Fig. 6.40: Approach to determine the critical power from results according to [1]

6.2.2 Discussion of Critical Power Steady State Results

In Fig. 6.41 the ratio of predicted (C) and measured (M) critical power is given for the tests as function of the bundle pressure. In Fig. 6.41 it is shown that P_{crit} is overpredicted by TRACE but the RSME is below 0.82 MW. Moreover the deviation of the predictions compared to the measurements becomes larger the higher with increasing bundle pressure. For a pressure of 7.2 MPa different values of P_{crit} were predicted by TRACE because the axial power profile of the test assemblies C2A and C2B are different from C3. The axial power profile has a skewed peak shape for C3 and is cosine shaped for C2A, C2B. Furthermore different radial power profiles exist between C2A and C2B [1].

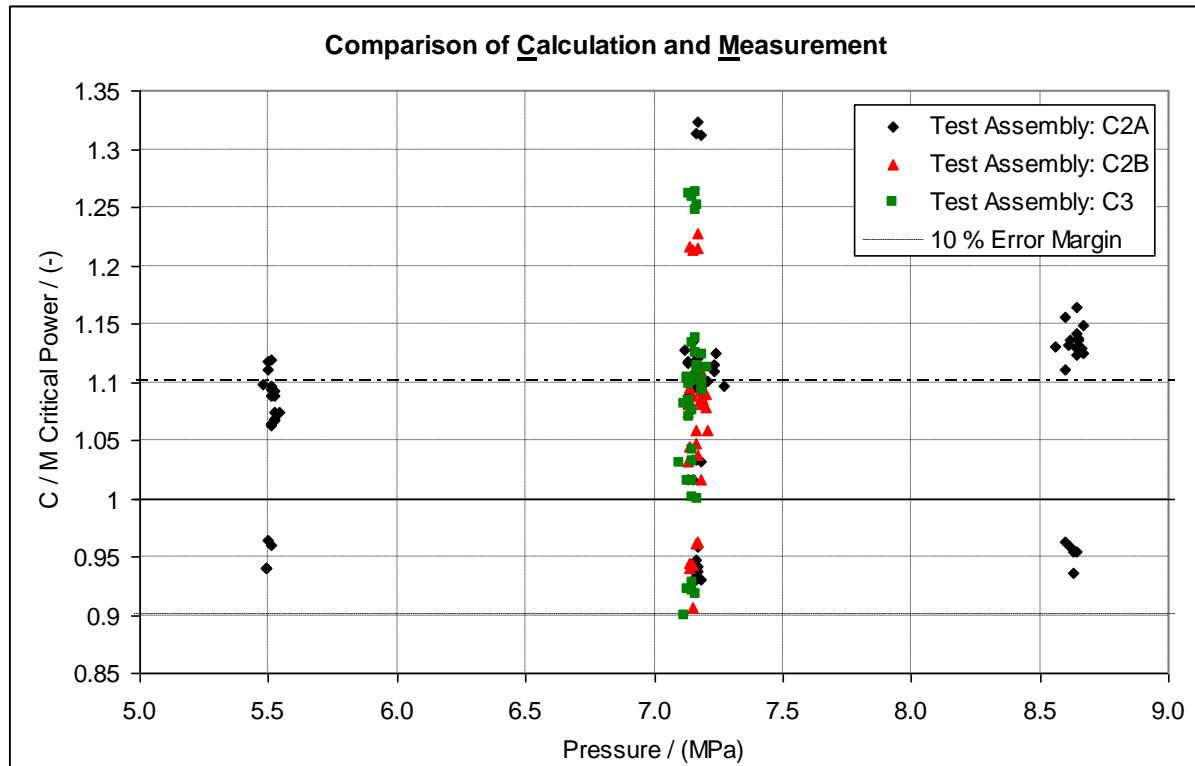


Fig. 6.41: Ratio of prediction (C) and measurement (M) dependent on pressure

The comparison of predicted critical power with the measurement is summarized in Fig. 6.42. The results shown in this figure confirm the earlier observation that TRACE tends in general to overpredict critical power.

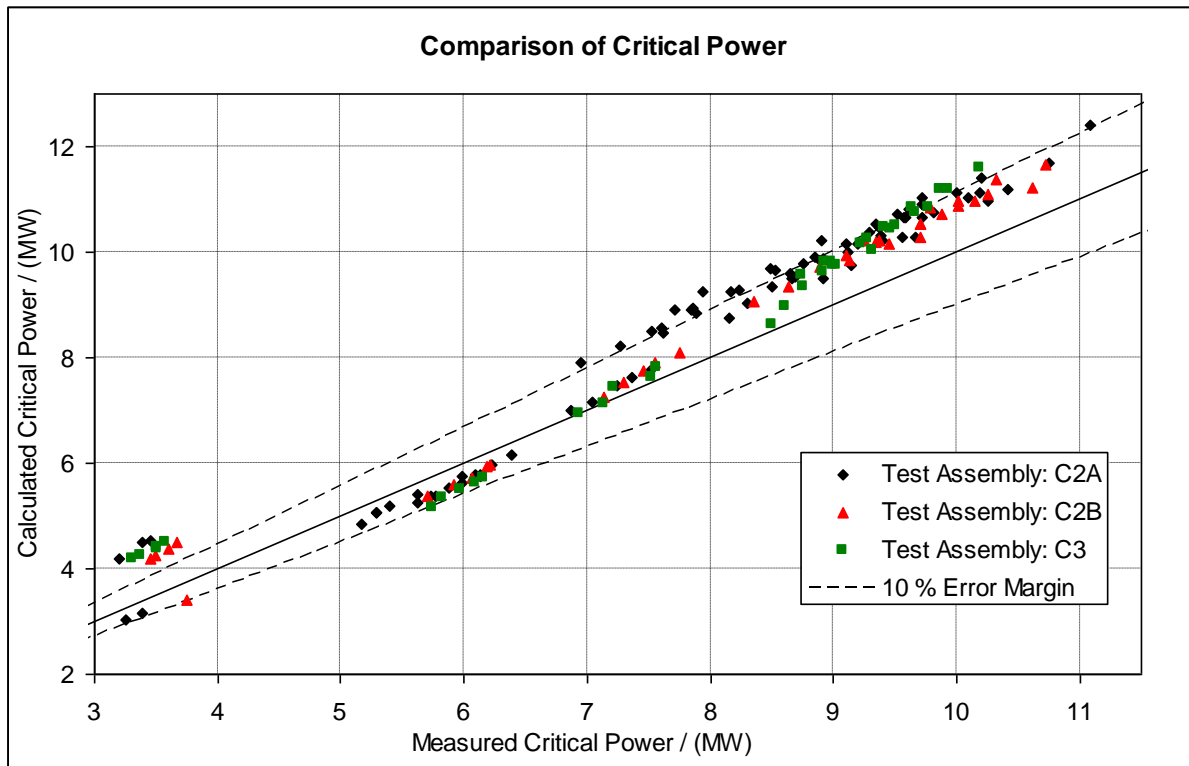


Fig. 6.42: Ratio of prediction (C) and measurement (M) dependent on pressure

In addition selected parameter like the heat transfer coefficient and the cladding temperature for each test are given in Fig. 6.43 to Fig. 6.50. The temperature fluctuation before the critical power conditions is caused in the TRACE calculations by the switching between the two flow regimes nucleate boiling and film boiling. Afterwards for example for test SA510600 (refer to Fig. 6.43), the shown fluctuation is caused by the switch of the heat transfer regime between transition boiling and film boiling with the transition boiling regime increasingly dominating the film boiling regime for approximately 427 s. The heat transfer coefficient of the transition boiling decreased with rising overheating as shown in Fig. 6.44, Fig. 6.46, Fig. 6.48 and Fig. 6.50. The time evolution of the cladding temperature and of the heat transfer coefficient of all simulated tests shows clearly the expected behaviour i.e. shows an increase of the temperature of the heater with a simultaneous decrease of the heat transfer coefficient.

The CPU times were approximately 88 s, 162 s, 83 s and 269 s for the test calculations SA510600, SA610600, SA810600 and SC610500 respectively.

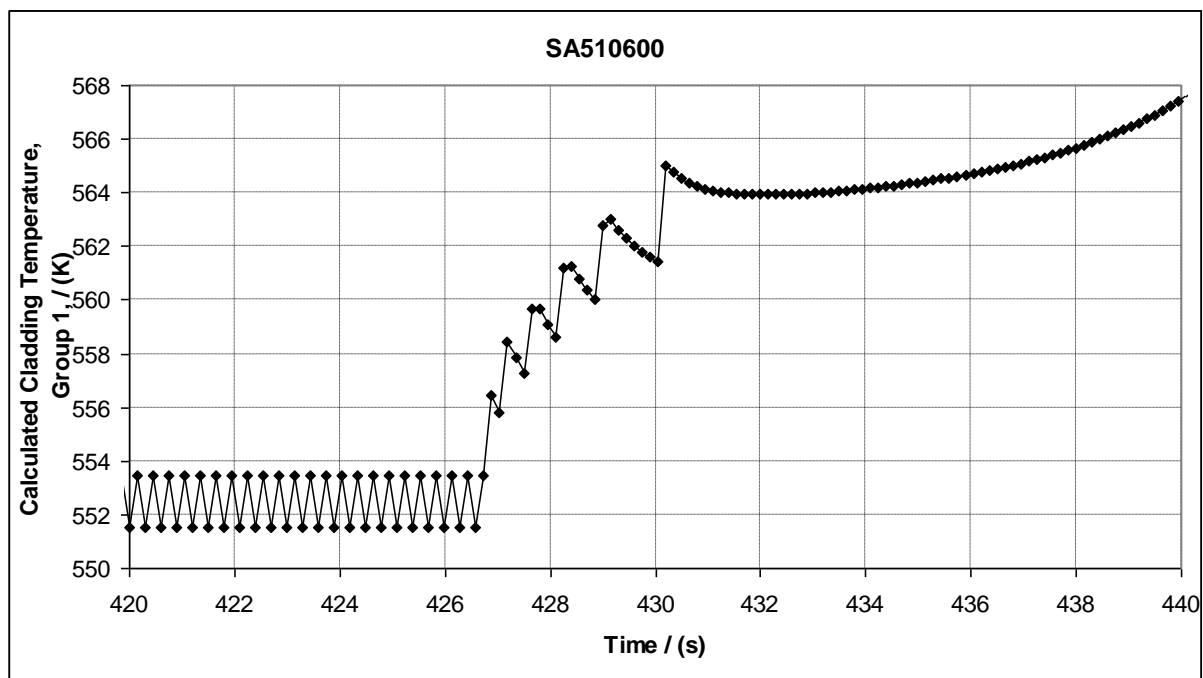


Fig. 6.43: Temperature rise due to dry out of test SA510600

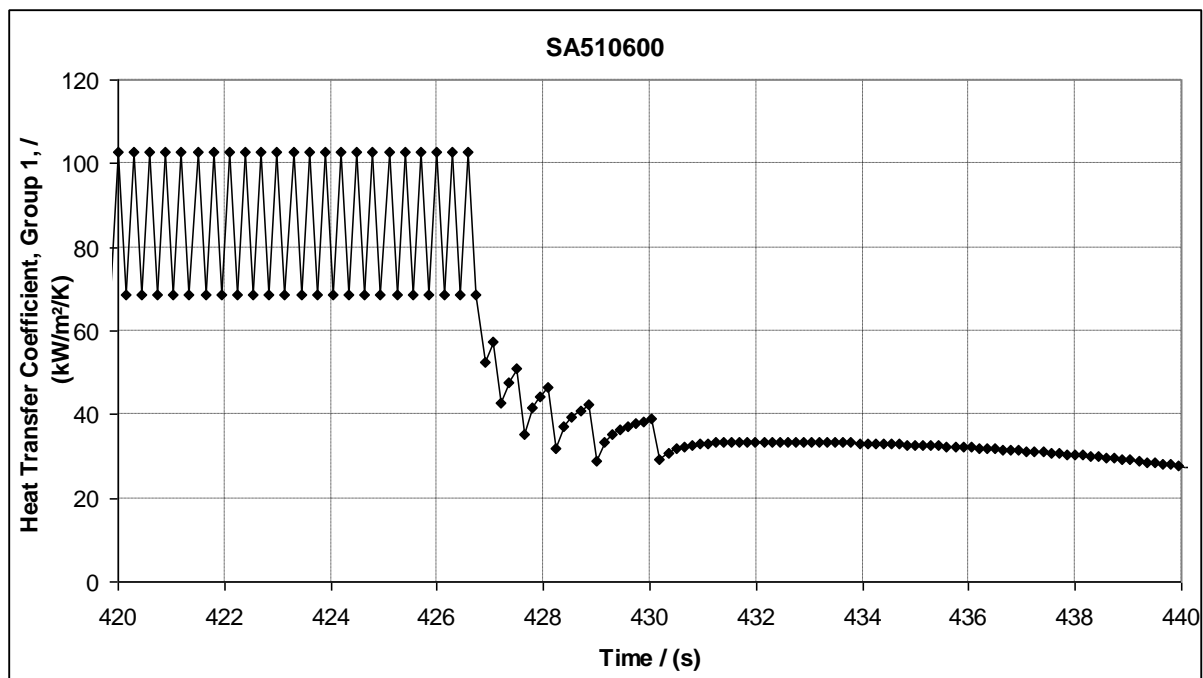


Fig. 6.44: Progression of the heat transfer coefficient of test SA510600

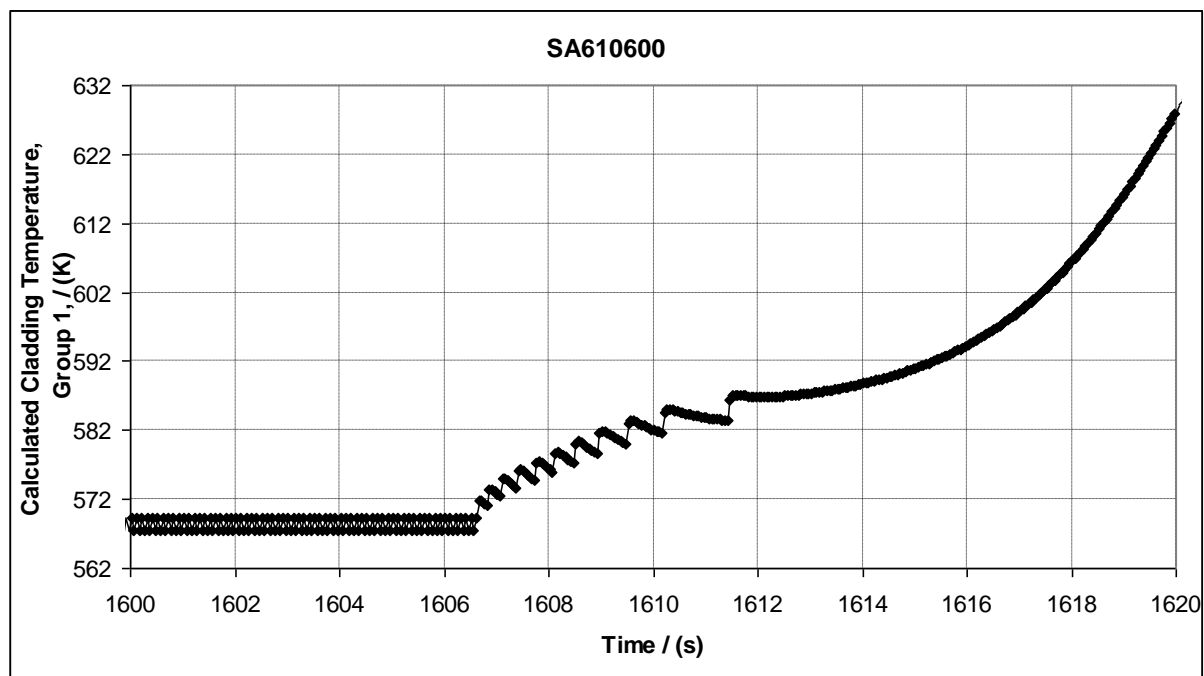


Fig. 6.45: Temperature rise due to dry out of test SA610600

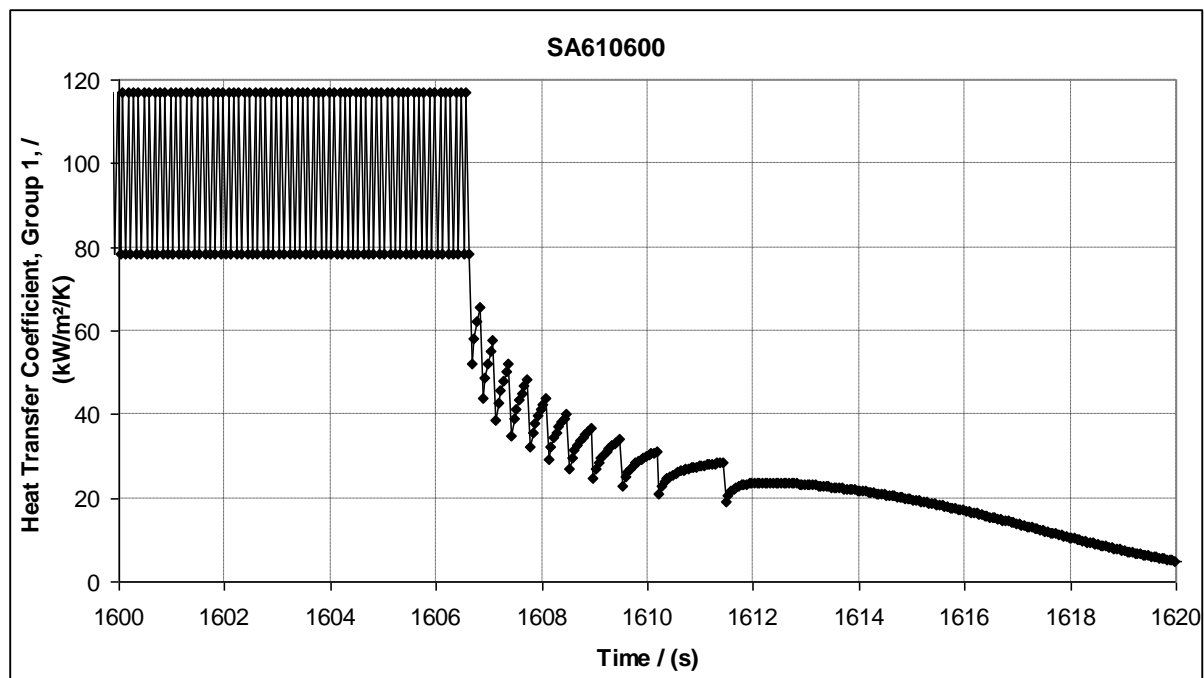


Fig. 6.46: Progression of the heat transfer coefficient of test SA610600

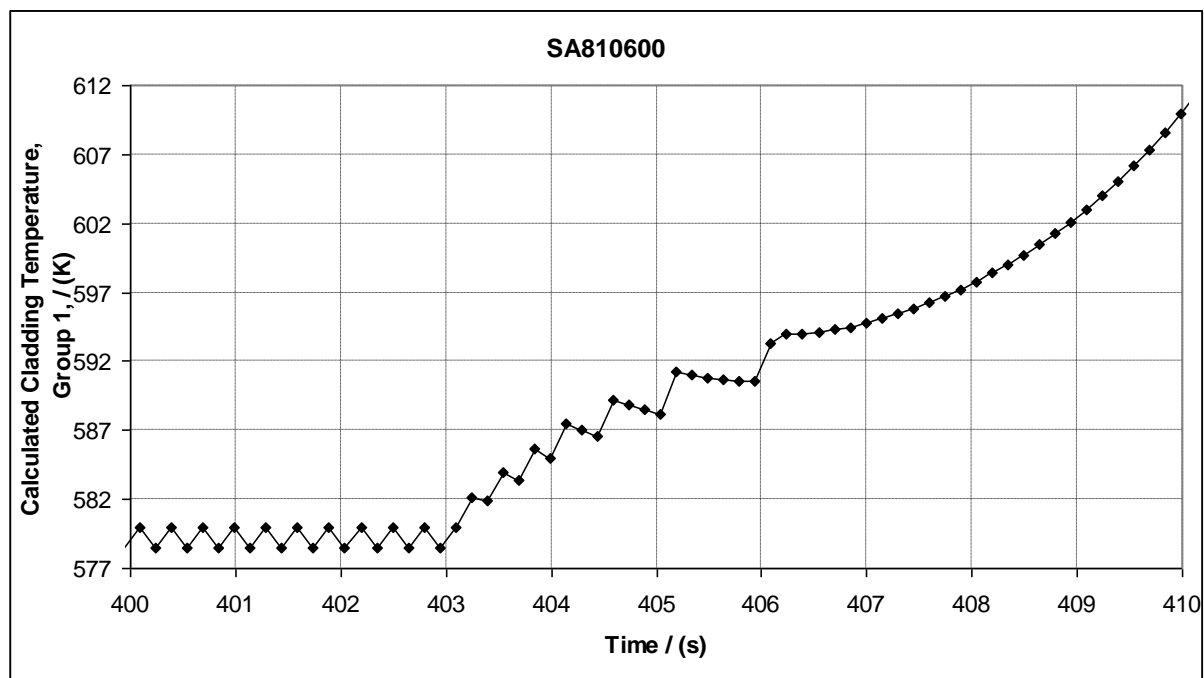


Fig. 6.47: Temperature rise due to dry out of test SA810600

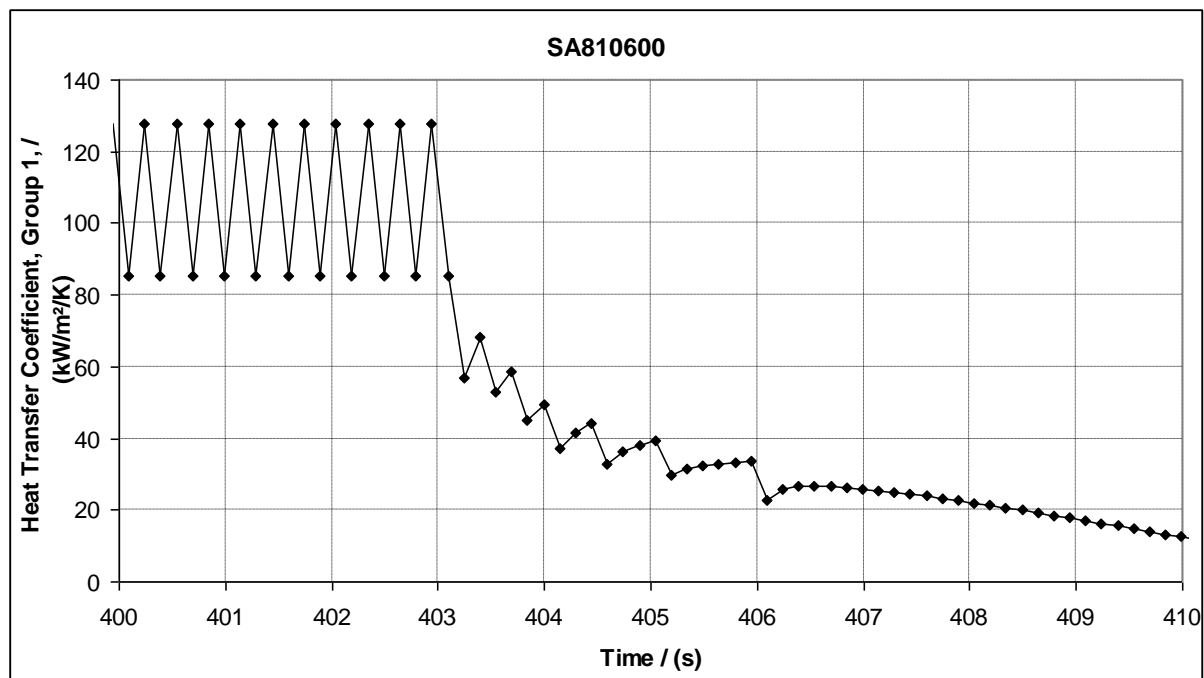


Fig. 6.48: Progression of the heat transfer coefficient of test SA810600

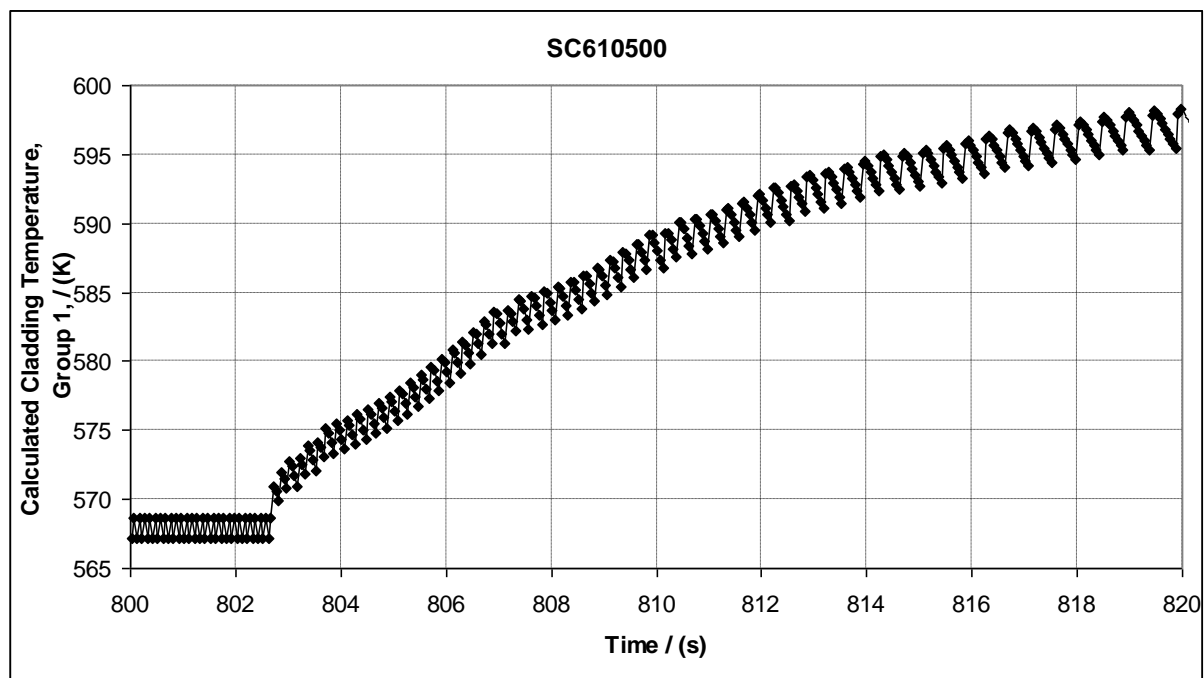


Fig. 6.49: Temperature rise due to dry out of test SC610500

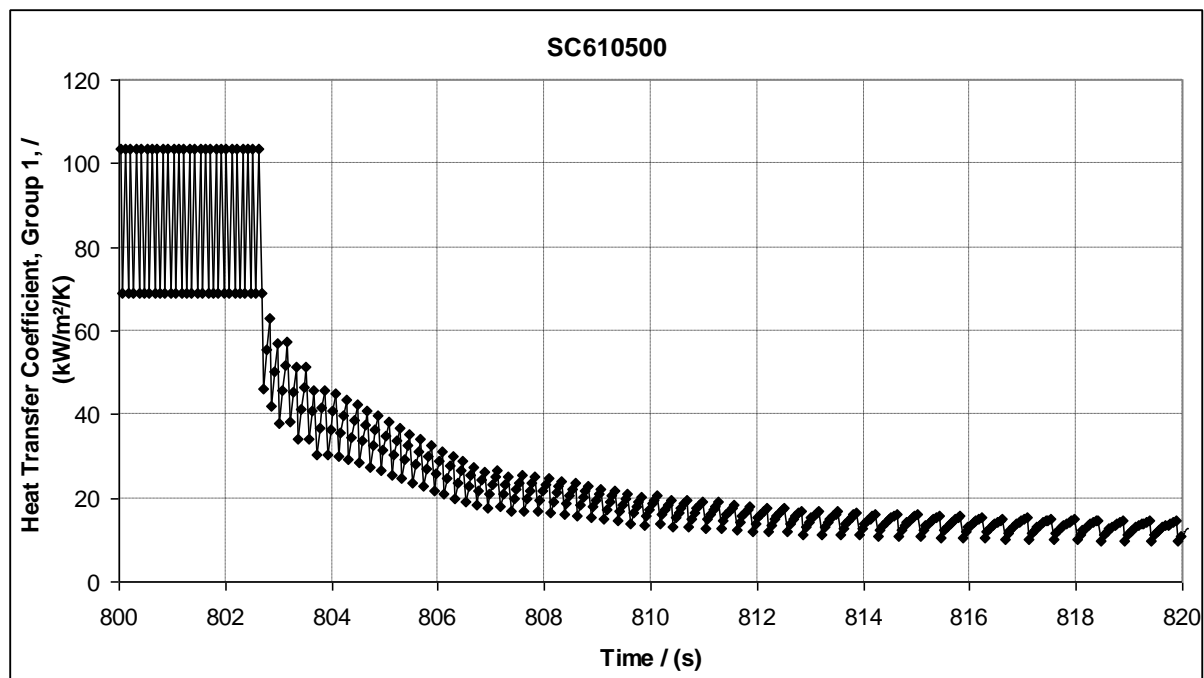


Fig. 6.50: Progression of the heat transfer coefficient of test SC610500

6.2.3 TRACE Results for Transient Test TGA10008

A transient calculation was performed considering the time dependent boundary conditions given for the turbine trip transient. The CPU time was approximately 469 s for this calculation. The boundary condition used in TRACE such as output for the flow rate, total power, bundle outlet pressure and bundle inlet temperature are shown in Fig. 3.7, Fig. 3.8, Fig. 3.9 and Fig. 3.10.

In Fig. 6.51 the measured inlet pressure with the pressure calculated by TRACE are compared showing a good agreement. The comparison of measured bundle outlet temperature with the calculated outlet liquid and vapor temperature is shown in Fig. 6.52. For this specific test as can be seen in Fig. 6.51 and Fig. 6.52 the trend of the predicted liquid temperature follows the trend of the measured and predicted bundle pressure while the measured liquid temperature does not. The calculated liquid temperature shows an early increase of 2 s compared to the measured temperature. One reason may be the fact that TRACE overpredicts the heat transfer coefficient already before reaching the power peak.

In Fig. 6.53 and Fig. 6.54 the exact position of the thermocouples on the heater rod surface can be observed. The couple notation is described in section 2.3. In Fig. 6.55 the surface heater temperature measured by thermocouples located on positions with similar thermohydraulic conditions are plotted. It can be observed that the temperature readings of all four thermocouples are quite similar during the time frame of the power peak. But before and after this power peak a deviation of up to 5 K is noted among them. In addition the surface temperature measured by the thermocouples 45-B240 and 59-B45, (refer to Fig. 6.56), which are under the same thermal conditions is very close to each other.

In Fig. 6.57 a comparison of the averaged surface temperature of the heater group one which was calculated taking into account the six thermocouple signals and the predicted surface temperature is given. There is a large underprediction of the cladding temperature by TRACE of about 13 K already at the beginning of the transient. In addition TRACE is not able to predict the rapid increase of the heater temperature caused by the power jump and mass flow rate reduction. A re-evaluation of the steady state calculation seems here to be necessary.

In Fig. 6.58 a comparison of predicted axial temperature distribution for the heater group 1 is presented for two time points after 10 s and at 24.6 s. It can be clearly seen that there is no dryout to be observed at the time point 24.6 s.

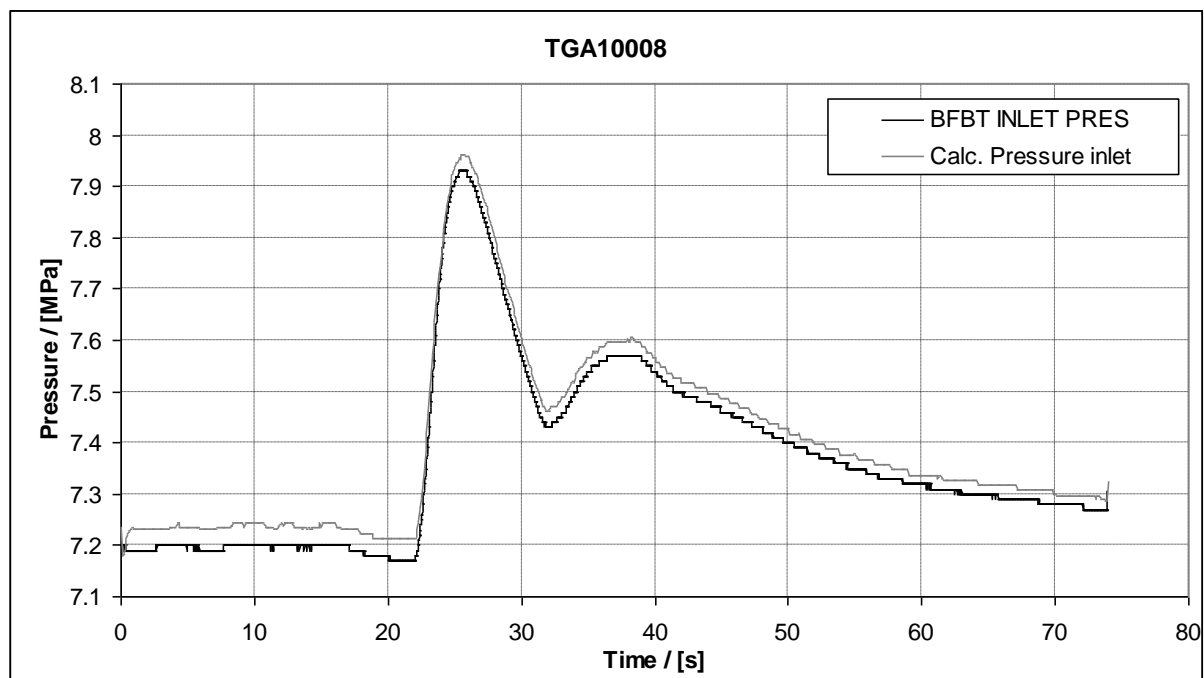


Fig. 6.51: Comparison between measured inlet pressure and calculation

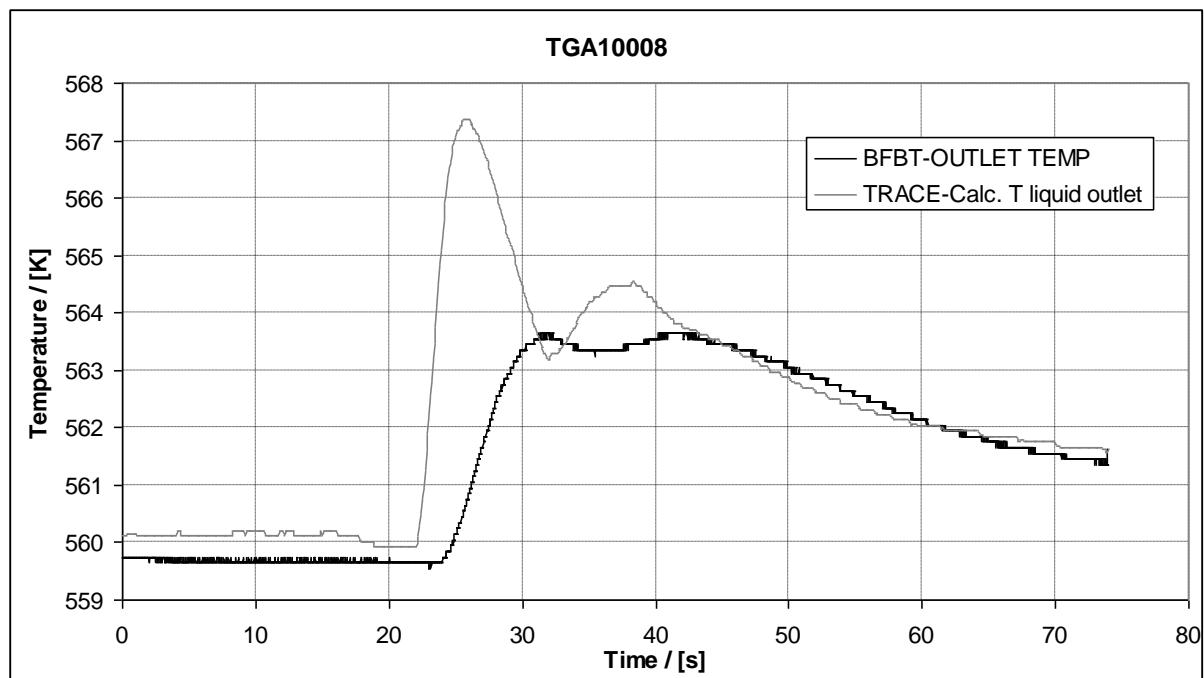


Fig. 6.52: Comparison between measured fluid outlet temperature and calculation

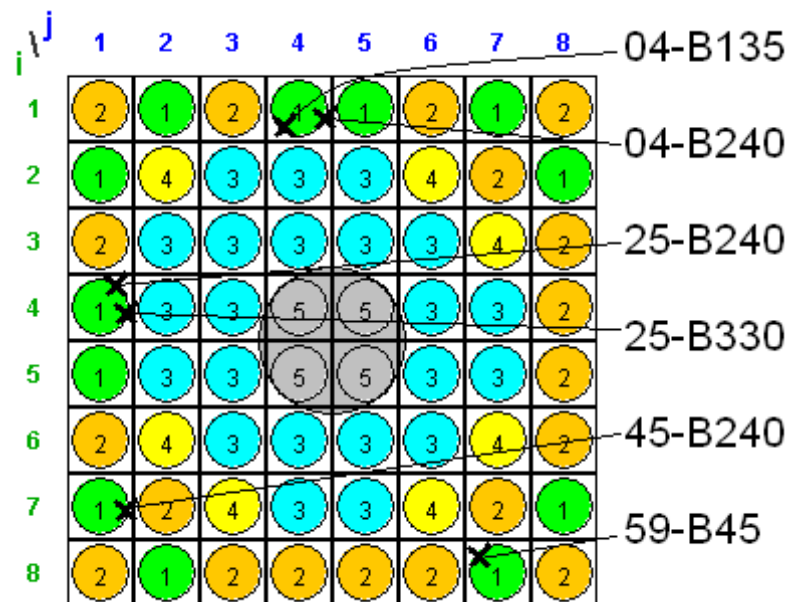


Fig. 6.53: Positions of thermocouples [1]

Node Spacer Elevation

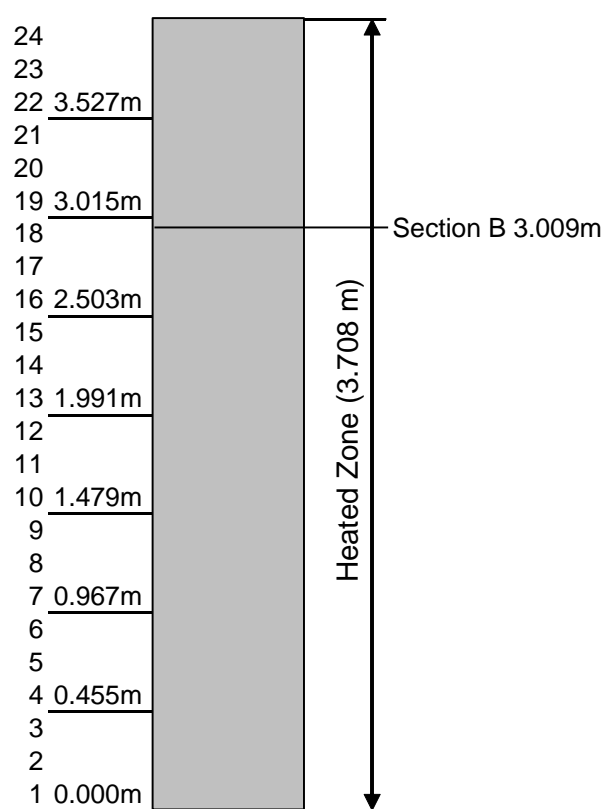


Fig. 6.54: Elevation of thermocouples [1]

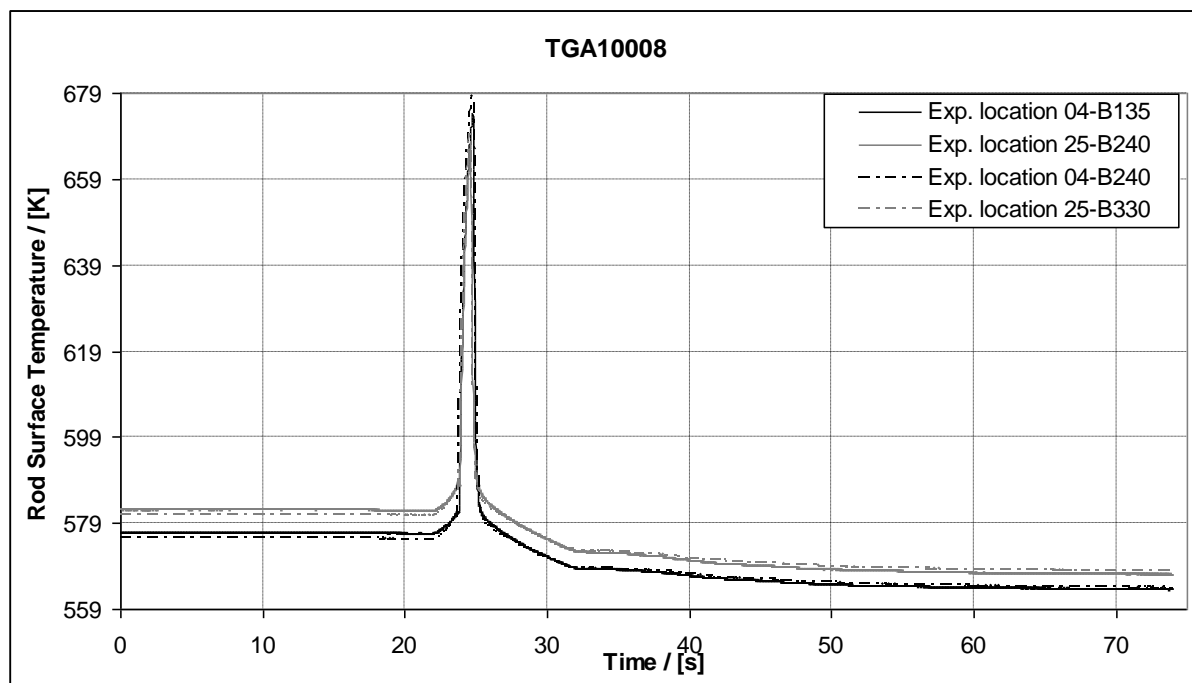


Fig. 6.55: Temperatures of symmetric thermocouple positions to each other

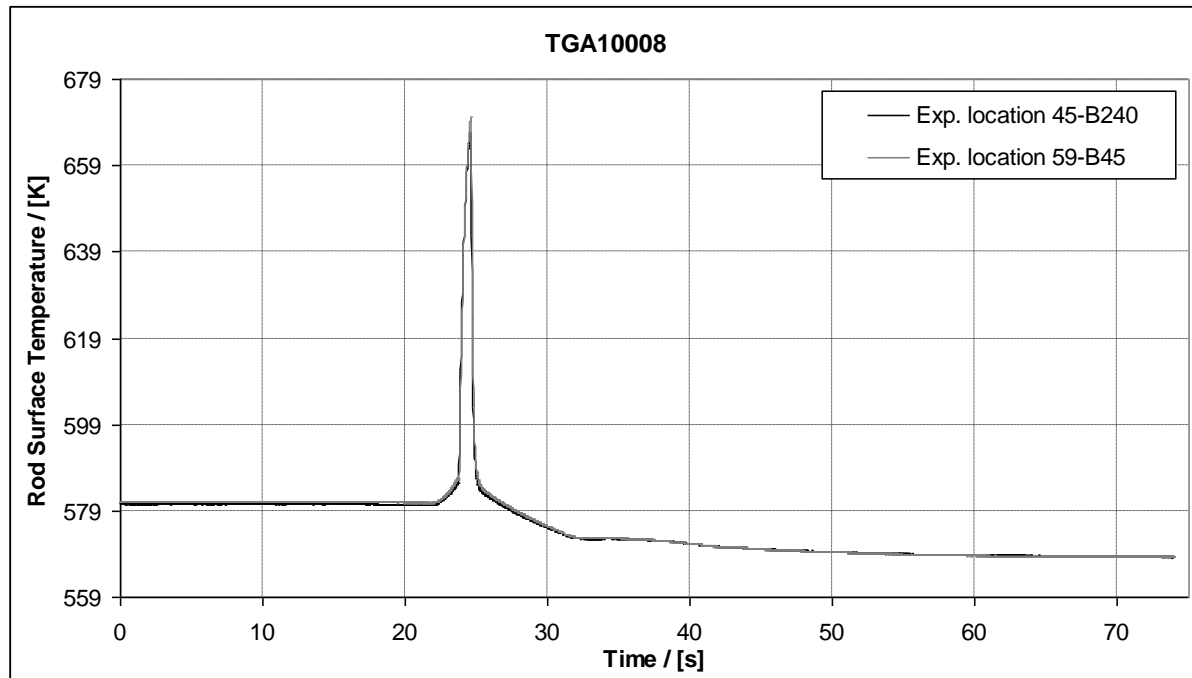


Fig. 6.56: View of further comparable measured thermocouple temperatures

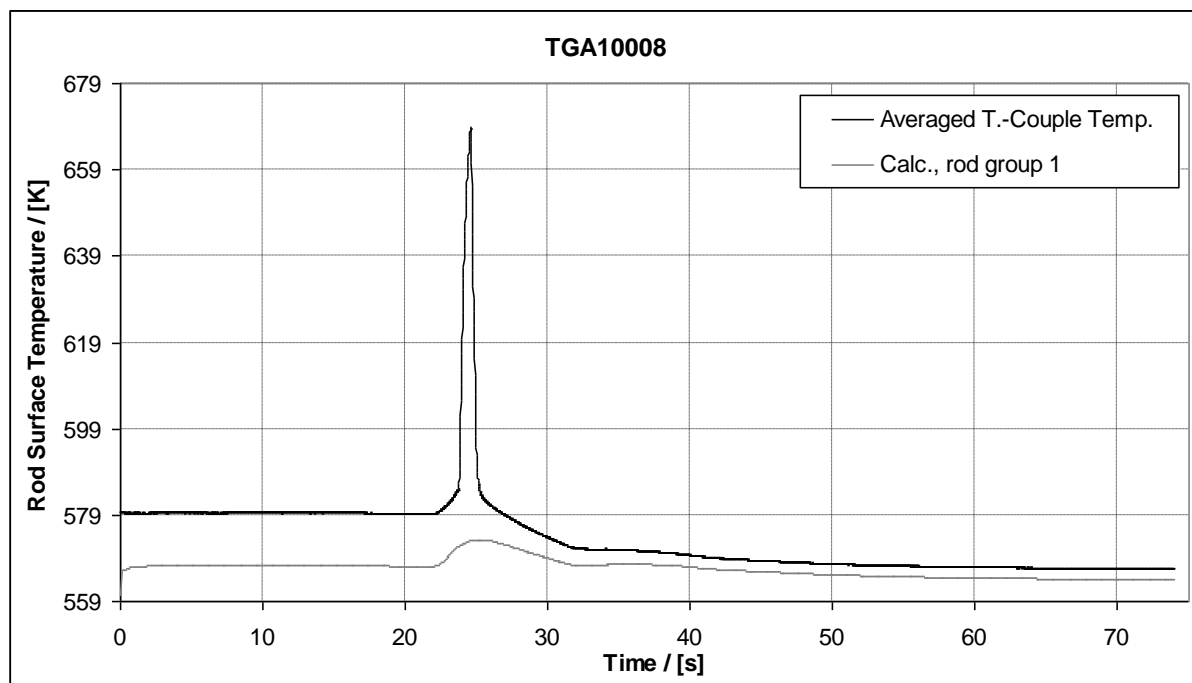


Fig. 6.57: Comparison between the averaged thermocouple temperature and calculation

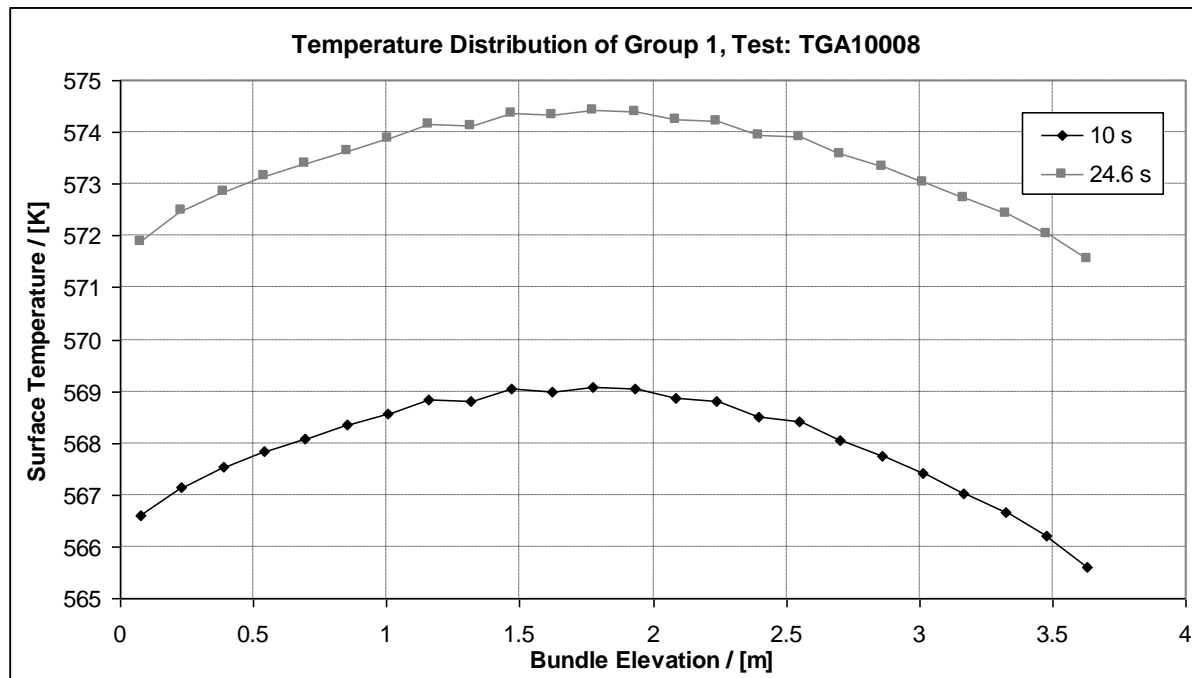


Fig. 6.58: Axial temperature distribution

7 Conclusions

Based on the TRACE models developed to simulate BWR-relevant experiments performed at the NUPEC BFBT test facility selected void and critical power tests were chosen for verification calculations with the TRACE version V50RC2.

From the comparison of the predicted parameters with the existing experimental data the following conclusion can be drawn:

- In case of the steady state void fraction BFBT test, TRACE predicts quite well the void fraction at the bundle outlet (RSME: 0.039). But it tends to underpredict the void fraction measured at the elevation of 2.73 m. Here the RSME between the prediction and the measured data is 0.078. It is worth to note that this deviation is almost at the lower limit of the measurement error band, however the trend to underprediction is quite clear.
- In case of the transient void fraction (BFBT) tests simulating a turbine trip transient the trends of the void fractions measured at four elevations could be fully reproduced by TRACE qualitatively in a very good manner. The TRACE predictions agree quantitatively very good with the void fraction obtained from the test data except for low mass flow rate and void fractions below 0.15. For void fractions between 0.45 and 0.8 and high mass flow rates and heat fluxes the agreement between predictions and void fraction data is reasonable good with deviations below 15 %.
- For the stationary critical power tests, TRACE overpredicts the measured critical power for pressure values ranging from 5.5 MPa to 8.6 MPa. The RSME by TRACE is 0.82 MW.
- In case of the transient critical power tests, the TRACE predictions follow qualitatively well the inlet pressure but do not follow the measured fluid temperatures at the bundle outlet. In addition, the measured rapid increase of the cladding temperature caused by the sudden increase of the power (boundary condition) could not be reproduced by TRACE. The program only shows a temperature increase of 6 K compared to 89 K seen from the tests. A reason for that may be the overprediction of the heat transfer coefficient already during the steady state calculation and the heat transfer selected by the program before the power peak occurs.

In general it can be concluded that the two phase flow models of TRACE which are relevant for BWR simulations are able to predict the void fraction and critical power with reasonable accuracy. Moreover the correlations for the void fraction prediction in TRACE at low mass flow rates and subcooled boiling conditions should be examined in detail for possible improvements.

8 References

- [1] B. Neykov, F. Aydogan, L. Hochreiter, K. Ivanov, H. Utsuno, F. Kasahara, E.Sartori, M. Martin, "NUPEC BWR Full-size Fine-mesh Bundle Test (BFBT) Benchmark, Volume I: Specifications", OECD 2006, NEA No. 6212, NEA/NSC/DOC(2005)5
- [2] German Atomic Energy Act, "Gesetz über die friedliche Verwendung der Kernenergie und den Schutz gegen ihre Gefahren (Atomgesetz), § 19a Sicherheitsüberprüfung", in the version from 31.10.2006
- [3] The Federal Assembly of the Swiss Confederation, SR 732.1 „Nuclear Energy Act (NEA)“, Art.22e, Die Bundesbehörden der Schweizerischen Eidgenossenschaft, 21. März 2003
- [4] "The Atomic Energy Act of 1954", as Amended in NUREG-0980, 30.08.1954
- [5] TRACE V5.0 User's Manual, Division of System Analysis, Office of Nuclear Regulatory Research, U. S. Nuclear Regulatory Commission, Washington, DC 20555-0001
- [6] BMWi, 2005, "Further Development and Verification/Validation of Computational Programs for Reactor Safety", Gesellschaft für Anlagen und Reaktorsicherheit (GRS) mbH
- [7] F. Cadinu, T. Kozlowski, T.-N. Dinh, "RELAP5 Performance in Predicting Critical Power in a BWR Fuel Bundle" , Royal Institute of Technology, Nuclear Power Safety, Stockholm, Sweden, Transactions- American Nuclear Society, Vol. 95, 650-651, 2006

Appendix A Input Deck Listing for Test 4101-53

```

free format
*
*
*****
* main data *
*****
*
*      numtcr          ieos        inopt        nmat        id2o
           1             0            1            3            0
*
*
*****
* namelist data *
*****
*
&inopts
  dtstrt=-1.0,
  graphlevel="full",
  iadded=0,
  iddiag=4,
  ikfac=1,
  inlab=3,
  iogrf=0,
  ioinp=0,
  iolab=0,
  ipowr=1,
  isscvt=1,
  nosets=0,
  nsdl=0,
  nsdu=0,
  usesjc=3,
  xtvres=4,
  npower=1
&end
*
*****
* Model Flags *
*****
*
*      dstep          timet
           0            0.0
*      stdyst         transi       ncomp       njun        ipak
           1             0            4            2            1
*      epso            epss
           1.0E-3        1.0E-3
*      oitmax         sitmax       isolut      ncontr      nccfl
           10            10            0            0            0
*      ntsv            ntcb         ntcf        ntrp        ntcp
           1              0            0            0            0
*
*****
* component-number data *
*****
*
* Component input order (IORDER)
*-- type ---- num ----- name ----- +   jun1   jun2   jun3
* FILL    *    100 s * Inlet          +     10
* CHAN    *    200 s * Heizstabbuendel +     10     20
* POWER   *    201 s * Power          +
* BREAK   *    300 e * Outlet         +     20
*
*
*****
* material-properties data *

```

Appendix A

```
*****
*
*      Nichrome/Constantan Boron Nitride    Inconel 600
* matb *          51           52           53e
* ptbln *         131           0           109e
*
*      temp / K rho / kg/m³ cp / J/kg/K   k / W/m/K epsilon / (-)
255.38      8393.4  45.36430405  28.91173756  0.0
255.39      8393.4  53.8531741   28.91178586  0.0
255.4017801 8393.4  59.8448108   28.91184275  0.0
255.421441  8393.4  66.52408757  28.9119377   0.0
255.4508766 8393.4  73.32029572  28.91207985  0.0
255.4941879 8393.4  80.30748763  28.91228902  0.0
255.5561734 8393.4  87.45558234  28.91258837  0.0
255.6428864 8393.4  94.75259312  28.91300715  0.0
255.7617114 8393.4  102.1855615  28.913581   0.0
255.9215533 8393.4  109.7431223  28.91435294  0.0
256.1330052 8393.4  117.414934  28.91537413  0.0
256.4085224 8393.4  125.1915412  28.91670471  0.0
256.76259   8393.4  133.0641741  28.91841464  0.0
257.2118807 8393.4  141.0245431  28.92058445  0.0
257.7753933 8393.4  149.0646113  28.92330587  0.0
258.4745584 8393.4  157.176339  28.92668242  0.0
259.3332935 8393.4  165.3513921  28.9308296   0.0
260.3779793 8393.4  173.5808084  28.9358748   0.0
261.6373257 8393.4  181.854621  28.94195669  0.0
263.1420819 8393.4  190.161443  28.94922376  0.0
264.9245434 8393.4  198.4880339  28.95783198  0.0
267.0178041 8393.4  206.8188781  28.96794117  0.0
269.4547179 8393.4  215.135833  28.97971   0.0
272.2665569 8393.4  223.4179212  28.9932895  0.0
275.4814117 8393.4  231.641358  29.00881532  0.0
279.1224469 8393.4  239.7799042  29.02639934  0.0
283.2062072 8393.4  247.8056037  29.04612145  0.0
287.7412292 8393.4  255.6899013  29.06802288  0.0
292.7272218 8393.4  263.4050474  29.09210224  0.0
298.1550064 8393.4  270.9256079  29.11831518  0.0
304.0072676 8393.4  278.2298458  29.14657809  0.0
310.2599956 8393.4  285.3007542  29.17677501  0.0
316.8843636 8393.4  292.126601  29.20876674  0.0
323.8487283 8393.4  298.7009546  29.24240044  0.0
331.1204764 8393.4  305.022271  29.27751862  0.0
338.66753   8393.4  311.0931808  29.31396636  0.0
346.4594357 8393.4  316.9196327  29.35159659  0.0
354.46805   8393.4  322.5100252  29.39027339  0.0
362.667884  8393.4  327.874415  29.42987367  0.0
371.0361963 8393.4  333.0238504  29.4702876  0.0
379.5529136 8393.4  337.9698432  29.51141823  0.0
388.2004494 8393.4  342.7239725  29.55318064  0.0
396.9634707 8393.4  347.2976025  29.59550078  0.0
405.8286474 8393.4  351.7016925  29.63831426  0.0
414.7844055 8393.4  355.9466773  29.6815652  0.0
423.820697  8393.4  360.0424014  29.72520506  0.0
432.9287919 8393.4  363.99809  29.7691917   0.0
442.1010946 8393.4  367.8223468  29.81348842  0.0
451.3309833 8393.4  371.5231687  29.85806324  0.0
460.6126724 8393.4  375.1079718  29.90288823  0.0
469.9410943 8393.4  378.5836238  29.94793891  0.0
479.3117979 8393.4  381.9564793  29.99319379  0.0
488.7208634 8393.4  385.2324163  30.03863393  0.0
498.1648285 8393.4  388.4168728  30.08424261  0.0
507.640627  8393.4  391.5148809  30.13000503  0.0
517.1455355 8393.4  394.5311008  30.17590804  0.0
526.6771285 8393.4  397.4698508  30.22193991  0.0
536.2332397 8393.4  400.3351366  30.2680902   0.0
545.8119294 8393.4  403.130677  30.31434952  0.0
555.4114562 8393.4  405.8599289  30.36070948  0.0
565.0302529 8393.4  408.5261085  30.40716249  0.0
574.6669053 8393.4  411.1322121  30.45370174  0.0
```

584.3201347	8393.4	413.6810341	30.50032105	0.0
593.9887818	8393.4	416.1751838	30.54701481	0.0
603.6717937	8393.4	418.6171003	30.59377795	0.0
613.3682117	8393.4	421.0090664	30.64060583	0.0
623.0771611	8393.4	423.3532212	30.68749423	0.0
632.7978427	8393.4	425.6515712	30.73443929	0.0
642.5295242	8393.4	427.9060007	30.78143747	0.0
652.271534	8393.4	430.1182813	30.82848554	0.0
662.0232545	8393.4	432.2900802	30.8755805	0.0
671.7841172	8393.4	434.4229684	30.92271961	0.0
681.5535978	8393.4	436.5184273	30.96990034	0.0
691.3312119	8393.4	438.5778556	31.01712034	0.0
701.1165114	8393.4	440.602575	31.06437747	0.0
710.9090809	8393.4	442.5938357	31.11166971	0.0
720.7085351	8393.4	444.5528214	31.15899519	0.0
730.514516	8393.4	446.480654	31.20635219	0.0
740.3266904	8393.4	448.3783972	31.25373911	0.0
750.1447478	8393.4	450.2470613	31.30115443	0.0
759.9683985	8393.4	452.0876057	31.34859677	0.0
769.7973723	8393.4	453.900943	31.39606482	0.0
779.6314159	8393.4	455.6879416	31.44355735	0.0
789.4702927	8393.4	457.4494285	31.49107322	0.0
799.3137806	8393.4	459.1861919	31.53861136	0.0
809.1616715	8393.4	460.8989837	31.58617077	0.0
819.0137696	8393.4	462.5885215	31.63375049	0.0
828.869891	8393.4	464.2554907	31.68134964	0.0
838.7298627	8393.4	465.9005463	31.72896739	0.0
848.5935217	8393.4	467.5243151	31.77660294	0.0
858.4607141	8393.4	469.1273966	31.82425556	0.0
868.3312948	8393.4	470.710365	31.87192455	0.0
878.2051269	8393.4	472.2737707	31.91960923	0.0
888.0820807	8393.4	473.8181413	31.96730899	0.0
897.9620337	8393.4	475.3439829	32.01502324	0.0
907.8448698	8393.4	476.8517813	32.0627514	0.0
917.7304789	8393.4	478.3420033	32.11049296	0.0
927.6187568	8393.4	479.8150971	32.15824741	0.0
937.5096044	8393.4	481.271494	32.20601427	0.0
947.4029277	8393.4	482.7116085	32.25379309	0.0
957.2986373	8393.4	484.13584	32.30158343	0.0
967.1966483	8393.4	485.5445726	32.34938488	0.0
977.0968797	8393.4	486.9381766	32.39719706	0.0
986.9992545	8393.4	488.3170089	32.44501959	0.0
996.9036993	8393.4	489.6814135	32.49285212	0.0
1006.810144	8393.4	491.0317223	32.5406943	0.0
1016.718522	8393.4	492.3682557	32.58854582	0.0
1026.62877	8393.4	493.691323	32.63640637	0.0
1036.540826	8393.4	495.0012228	32.68427565	0.0
1046.454632	8393.4	496.2982439	32.73215339	0.0
1056.370133	8393.4	497.5826652	32.78003931	0.0
1066.287275	8393.4	498.8547567	32.82793316	0.0
1076.206008	8393.4	500.1147793	32.87583469	0.0
1086.126283	8393.4	501.3629858	32.92374366	0.0
1096.048053	8393.4	502.5996207	32.97165986	0.0
1105.971272	8393.4	503.8249208	33.01958305	0.0
1115.895899	8393.4	505.0391158	33.06751304	0.0
1125.821891	8393.4	506.2424279	33.11544963	0.0
1135.74921	8393.4	507.4350729	33.16339262	0.0
1145.677816	8393.4	508.6172597	33.21134184	0.0
1155.607674	8393.4	509.7891913	33.25929709	0.0
1165.538749	8393.4	510.9510645	33.30725822	0.0
1175.471006	8393.4	512.1030704	33.35522507	0.0
1185.404413	8393.4	513.2453945	33.40319746	0.0
1195.338939	8393.4	514.378217	33.45117526	0.0
1205.274553	8393.4	515.501713	33.49915832	0.0
1215.211227	8393.4	516.6160527	33.54714649	0.0
1225.148932	8393.4	517.7214014	33.59513964	0.0
1235.087642	8393.4	518.8179201	33.64313765	0.0
1245.027331	8393.4	519.905765	33.69114038	0.0
1254.967973	8393.4	520.9850885	33.73914772	0.0e

Appendix A

```

*
*      rhonum      sphnum      condnum      emisnum
*           1          1          1          1
*
*      rho
*
*      toffset      tlower      tupper      a0      a1
*           0.0        242.15    1256.15    2002.0    0.0
*      a2          a3          a4          a5
*           0.0        0.0        0.0        0.0
*
*      Specific Heat
*
*      toffset      tlower      tupper      a0      a1
*   255.3722222    242.15    1256.15    760.59    3.2319
*      a2          a3          a4          a5
*   -2.8092096E-3  9.2705472E-7    0.0        0.0
*
*      Thermal Conductivity
*
*      toffset      tlower      tupper      a0      a1
*   255.3722222    242.15    1256.15    25.27    -2.457E-3
*      a2          a3          a4          a5
*           0.0        0.0        0.0        0.0
*
*      Emissivity
*
*      toffset      tlower      tupper      a0      a1
*           0.0        242.15    1256.15    0.0        0.0
*      a2          a3          a4          a5
*           0.0        0.0        0.0        0.0
*
*      temp / K    rho / kg/m³  cp / J/kg/K  k / W/m/K epsilon / (-)
  242.15      8432.452933  420.1273328  13.66698989  0.0
  251.6322368  8428.775415  423.3033658  13.80229546  0.0
  261.1144736  8425.096782  426.4275069  13.93956998  0.0
  270.6122485  8421.411003  429.5088785  14.07884191  0.0
  280.1241792  8417.71861   432.5493405  14.21990931  0.0
  289.6493957  8414.019936  435.5495915  14.36258726  0.0
  299.1874373  8410.315154  438.509339   14.50670672  0.0
  308.7381734  8406.604312  441.4274702  14.65211355  0.0
  318.3017309  8402.887355  444.3022143  14.79866747  0.0
  327.8784278  8399.164155  447.131295  14.94624095  0.0
  337.4687131  8395.434533  449.912074  15.09471818  0.0
  347.0731126  8391.698279  452.6416843  15.24399405  0.0
  356.6921798  8387.955172  455.317154  15.39397316  0.0
  366.3264527  8384.204999  457.9355209  15.54456892  0.0
  375.9764166  8380.447565  460.4939392  15.69570276  0.0
  385.642473   8376.682707  462.9897767  15.84730339  0.0
  395.3249138  8372.910307  465.4207049  15.99930617  0.0
  405.023902   8369.130294  467.7847803  16.15165262  0.0
  414.7394585  8365.342655  470.0805176  16.30428996  0.0
  424.4714541  8361.547433  472.3069546  16.45717086  0.0
  434.219608   8357.744734  474.4637072  16.61025314  0.0
  443.9834902  8353.934718  476.5510157  16.76349966  0.0
  453.7625294  8350.117602  478.5697802  16.91687824  0.0
  463.5560238  8346.293656  480.5215859  17.07036157  0.0
  473.3631557  8342.463194  482.4087168  17.22392729  0.0
  483.1830077  8338.626569  484.2341582  17.37755794  0.0
  493.0145795  8334.784167  486.0015884  17.53124097  0.0
  502.8568057  8330.936401  487.7153581  17.68496878  0.0
  512.7085719  8327.083703  489.3804593  17.83873862  0.0
  522.5687298  8323.226518  491.0024844  17.99255256  0.0
  532.4361093  8319.365302  492.5875739  18.14641729  0.0
  542.3095289  8315.500514  494.1423573  18.30034395  0.0
  552.1878016  8311.632616  495.6738839  18.45434786  0.0
  562.069739   8307.762074  497.1895485  18.60844819  0.0
  571.9541514  8303.88935   498.6970098  18.76266757  0.0
  581.8398467  8300.014913  500.2041044  18.91703166  0.0

```

Appendix A

591.7256257	8296.139232	501.7187571	19.07156865	0.0
601.610278	8292.26278	503.2488884	19.22630881	0.0
611.492576	8288.386041	504.8023198	19.38128393	0.0
621.3712707	8284.509506	506.3866792	19.53652683	0.0
631.2450888	8280.633675	508.0093062	19.69207088	0.0
641.1127316	8276.759061	509.6771594	19.84794952	0.0
650.9728781	8272.886185	511.3967269	20.00419589	0.0
660.8241919	8269.015574	513.1739405	20.16084247	0.0
670.6653317	8265.147759	515.014096	20.31792082	0.0
680.4949675	8261.283267	516.9217806	20.47546142	0.0
690.3118006	8257.422613	518.9008079	20.63349354	0.0
700.1145885	8253.56629	520.954163	20.79204531	0.0
709.9021725	8249.71476	523.0839578	20.9511437	0.0
719.6735092	8245.868439	525.2913972	21.11081477	0.0
729.4277029	8242.027685	527.5767567	21.27108386	0.0
739.1640389	8238.192786	529.9393725	21.43197585	0.0
748.8820159	8234.363947	532.3776411	21.5935155	0.0
758.5813768	8230.541275	534.8890309	21.75572774	0.0
768.2621356	8226.724771	537.4701025	21.91863795	0.0
777.9246003	8222.914321	540.1165371	22.0822723	0.0
787.5693907	8219.109686	542.823172	22.24665788	0.0
797.1974499	8215.310502	545.5840408	22.41182289	0.0
806.810049	8211.516271	548.3924183	22.57779665	0.0
816.4087858	8207.726369	551.2408669	22.74460953	0.0
825.9955749	8203.940044	554.1212853	22.91229276	0.0
835.5726322	8200.156426	557.0249579	23.08087803	0.0
845.1424507	8196.374531	559.9426047	23.25039705	0.0
854.7077703	8192.593279	562.8644332	23.42088081	0.0
864.2715397	8188.811507	565.7801913	23.59235873	0.0
873.8368717	8185.027982	568.6792251	23.76485762	0.0
883.4069912	8181.241428	571.5505414	23.9384004	0.0
892.9851768	8177.450546	574.3828803	24.11300462	0.0
902.5746952	8173.654039	577.1648	24.28868077	0.0
912.1787295	8169.850643	579.8847785	24.46543043	0.0
921.8003027	8166.039155	582.5313378	24.64324411	0.0
931.442196	8162.218465	585.0931957	24.82209906	0.0
941.1068657	8158.387594	587.5594515	25.00195685	0.0
950.7963598	8154.54572	589.9198111	25.18276098	0.0
960.5122396	8150.692215	592.1648573	25.36443451	0.0
970.2555095	8146.826672	594.2863701	25.54687782	0.0
980.0265626	8142.948925	596.2776988	25.72996674	0.0
989.8251458	8139.059063	598.1341883	25.91355113	0.0
999.6503528	8135.157436	599.853655	26.09745405	0.0
1009.500648	8131.244646	601.4369087	26.28147168	0.0
1019.373925	8127.32152	602.8883116	26.46537408	0.0
1029.267596	8123.389078	604.2163633	26.64890665	0.0
1039.178703	8119.448488	605.4343009	26.83179226	0.0
1049.104043	8115.50102	606.5607036	27.01373356	0.0
1059.040261	8111.548002	607.6200928	27.19441512	0.0
1068.983903	8107.590804	608.6435205	27.37350461	0.0
1078.931355	8103.630865	609.6691396	27.5506523	0.0
1088.878623	8099.669771	610.7427353	27.72548789	0.0
1098.820884	8095.709446	611.9181818	27.89761398	0.0
1108.75172	8091.752449	613.2577311	28.06659544	0.0
1118.661969	8087.802435	614.8319691	28.23194452	0.0
1128.538142	8083.864792	616.7191465	28.39310271	0.0
1138.360428	8079.947435	619.0034459	28.54942188	0.0
1148.100499	8076.061686	621.7716163	28.70015043	0.0
1157.719565	8072.223056	625.1074256	28.8444336	0.0
1167.167562	8068.451578	629.0837546	28.98134028	0.0
1176.384535	8064.771254	633.753093	29.1099273	0.0
1185.305125	8061.208273	639.1385699	29.22934244	0.0
1193.865999	8057.788038	645.228714	29.33894765	0.0
1202.014468	8054.531723	651.97867	29.43842508	0.0
1209.715441	8051.453481	659.3181457	29.52782549	0.0
1216.954372	8048.559257	667.1633178	29.60754191	0.0
1223.735773	8045.84737	675.4285496	29.67822447	0.0
1230.078757	8043.310291	684.0348571	29.74067254	0.0
1236.011652	8040.936788	692.9142758	29.79573712	0.0

Appendix A

```

1241.567263 8038.713825 702.0109382 29.84425044 0.0
1246.779398 8036.627949 711.2802036 29.8869842 0.0
1251.680706 8034.666158 720.6869605 29.92463059 0.0
1256.3015 8032.816372 730.2037853 29.95779783 0.0e
*
*
*****
* Starting Signal Variable Section of Model *
*****
*
*      idsv      isvn      ilcn      icnl      icn2
202          0          0          0          0
*****
* Finished Signal Variable Section of Model *
*****
*
*
*
*****
*      type      num      userid      component name
fill           100          1          Inlet
*      jun1      ifty      ioff
10            5          0
*      iftr      ifsv      nftb      nfsv      nfrf
0              202          5          0          0
*      twtold     rfmx      concin     felv
0.0           1.0E20        0.0        0.0
*      dxin      volin     alpin      vlin      tlin
0.1545       1.462034E-3    0.0        0.0      551.35
*      pin       pain      flowin     vvin      tvin
7.23E6        0.0        15.180556   0.0        561.21
*      vmscl     vvsc1
1.0           1.0
*
*      vmtbv *      0.0        15.180556s
*      vmtbv *      1.0        15.180556s
*      vmtbv *      2.0        15.180556s
*      vmtbv *      3.0        15.180556s
*      vmtbv *      1.0E6      15.180556e
*
*
*****
*      type      num      userid      component name
chan          200          0          Heizstabbuendel
*      ncell     nodes      jun1      jun2      epsw
25            3          10          20      1.0E-4
*      nsides
2
* Water Rod inlet junction
*      nclk      junlk      ncmpto      nclkto      nlevto
1              210          0          0          0
*      theta
0.0
* Water Rod outlet junction
*      nclk      junlk      ncmpto      nclkto      nlevto
24            220          0          0          0
*      theta
0.0
*      ichf      iconc      iaxcnd      liqlev      nhcom
2              0          0          0          0
*      width      th       houtl      houtv      toutl
0.516265     3.0E-3        0.0        0.0      560.0
*      toutv     advbwrf     quadsym     numwrds      nvfrays
560.0         1            2            1            0
*      ngrp      nchans     nodesr      nrow      ncrz
5              1            22           8            24
*      icrnk     icrlh      nmwrxx      nfci      nfcil
0              0            0            0            0
*      fmon      reflood     nzmax      nzmaxw      ibeam
0              0            100          100          0

```

```

*      dznht      dznhtw      dtxht1      dtxht2
*      1.0E-3      1.0E-3      2.0          10.0
*      hgapo      pdrat      pldr      fucrac      norad
*      6300.0      1.3170732      0.0          1.0          1
*      emcif1      emcif2      emcif3      noani
*      0.0          0.0          0.0          0
*      emcof1      emcof2      emcof3
*      0.0          0.0          0.0
* dx   *      0.1545      0.1545      0.1545      0.1545s
* dx   *      0.1e
* vol  *      1.46203E-3  1.46203E-3  1.46203E-3  1.46203E-3s
* vol  *      9.463E-4e
* fa   *      9.463E-3      9.463E-3      9.463E-3      9.463E-3s
* fa   *      9.463E-3      9.463E-3e
* kfac *      0.0          0.0          0.0          1.2s
* kfac *      0.0          0.0          1.2          0.0s
* kfac *      0.0          0.0          1.2          0.0s
* kfac *      0.0          1.2          0.0          0.0s
* kfac *      1.2          0.0          0.0          0.0s
* kfac *      1.2          0.0          0.0          1.2s
* kfac *      0.0          0.0e
* grav *      1.0          1.0          1.0          1.0s
* grav *      1.0          1.0e
* hd   *      0.012869321  0.012869321  0.012869321  0.012869321s
* hd   *      0.012869321  0.012869321e
* nff *      1            1            1            1s
* alp *      0.0          0.0          0.0          0.0s
* alp *      0.0          0.0          0.0          0.0s
* alp *      0.0          5.41E-5    7.30103E-4  2.69308E-3s
* alp *      6.18904E-3  0.013886783  0.024535041  0.035519812s
* alp *      0.06131376  0.090480253  0.12046678  0.13963521s
* alp *      0.1756786   0.20165347   0.21196781  0.2472679s
* alp *      0.24149102e
* vl   *      2.1174169   2.121114   2.1248493  2.1286104s
* vl   *      2.1324015   2.1362128   2.1400487  2.143914s
* vl   *      2.1477985   2.1517069   2.1557441  2.1610169s
* vl   *      2.1687918   2.1794279   2.1987281  2.2241719s
* vl   *      2.2500119   2.3095551   2.3790746  2.4546595s

```

Appendix A

```

* vl    * 2.5034192  2.6063759  2.6846077  2.7131131s
* vl    * 2.8331542  2.8091443e
* vv    * 2.1174169  2.1264186  2.1301541  2.1362457s
* vv    * 2.137707   2.1415179  2.1476967  2.1492195s
* vv    * 2.1531036  2.1795301  2.3069837  2.3799672s
* vv    * 2.5214603  2.8647115  2.6529737  2.6579468s
* vv    * 2.9164801  2.7815588  2.8612576  2.9479535s
* vv    * 3.2514815  3.1650176  3.2562573  3.5718422s
* vv    * 3.4781263  3.6450925e
* tl    * 552.002   552.651   553.298   553.942s
* tl    * 554.586   555.228   555.867   556.506s
* tl    * 557.143   557.777   558.398   558.996s
* tl    * 559.555   560.058   560.502   560.88s
* tl    * 561.074   561.131   561.137   561.126s
* tl    * 561.096   561.075   561.055   561.02s
* tl    * 560.888e
* tv    * 561.241   561.224   561.206   561.169s
* tv    * 561.151   561.134   561.096   561.079s
* tv    * 561.061   561.044   561.006   560.989s
* tv    * 560.971   560.933   560.915   560.896s
* tv    * 560.856   560.838   560.818   560.797s
* tv    * 560.748   560.729   560.708   560.654s
* tv    * 560.636e
* p     * 7.233494E6 7.231621E6 7.229749E6 7.225831E6s
* p     * 7.22396E6  7.22209E6  7.218164E6  7.216295E6s
* p     * 7.214428E6 7.21256E6  7.208622E6  7.206754E6s
* p     * 7.204884E6 7.200922E6 7.199034E6  7.197133E6s
* p     * 7.193092E6 7.19113E6  7.18913E6  7.187089E6s
* p     * 7.182706E6 7.180569E6 7.17842E6  7.173769E6s
* p     * 7.171845E6e
* pa    * 0.0        0.0        0.0        0.0s
* pa    * 0.0e
* qppp * f 0.0e
* mat   * 53         53e
* tw    * 553.929   553.929   553.929   556.284   556.284s
* tw    * 556.284   558.616   558.616   558.616   560.742s
* tw    * 560.742   560.742   560.731   560.731   560.731s
* tw    * 560.72    560.72    560.72    560.709   560.709s
* tw    * 560.709   560.698   560.698   560.698   560.687s
* tw    * 560.687   560.687   560.677   560.677   560.677s
* tw    * 560.666   560.666   560.666   560.655   560.655s
* tw    * 560.655   560.644   560.644   560.644   560.633s
* tw    * 560.633   560.633   560.622   560.622   560.622s
* tw    * 560.611   560.611   560.611   560.601   560.601s
* tw    * 560.601   560.59    560.59    560.59    560.579s
* tw    * 560.579   560.579   560.568   560.568   560.568s
* tw    * 560.557   560.557   560.557   560.546   560.546s
* tw    * 560.546   560.535   560.535   560.535   560.525s
* tw    * 560.525   560.525   560.516   560.516   560.516e
* rdx   * 12.0      19.0      22.0      7.0      1.0e
* radrd * 0.0       4.41667E-4 8.83333E-4 1.325E-3 1.76667E-3s
* radrd * 2.20833E-3 2.65E-3  2.81667E-3 2.98333E-3 3.15E-3s
* radrd * 3.31667E-3 3.48333E-3 3.65E-3  3.85E-3 4.05E-3s
* radrd * 4.25E-3   4.45E-3  4.65E-3  4.85E-3 5.28333E-3s
* radrd * 5.71667E-3 6.15E-3e
* matrd * 52         52         52         52s
* matrd * 52         52         51         51s
* matrd * 51         51         51         51s
* matrd * 52         52         52         52s
* matrd * 52         52         53         53s
* matrd * 53e
* nfax  * 3          3          3          3s
* nfax  * 3          3          3          3s
* nfax  * 3          3          3          3s

```

*	nfax *	3	3	3	3s
*	nfax *	3	3	3	3s
*	nfax *	3	3	3	3e
*	rftn *	668.425	668.425	668.425	668.425s
*	rftn *	668.425	668.425	668.425	668.425s
*	rftn *	666.585	663.101	658.135	651.824s
*	rftn *	644.282	636.212	628.553	621.266s
*	rftn *	614.318	607.678	601.319	584.353s
*	rftn *	568.614	553.929	670.714	670.714s
*	rftn *	670.714	670.714	670.714	670.714s
*	rftn *	670.714	670.714	668.876	665.395s
*	rftn *	660.434	654.129	646.595	638.523s
*	rftn *	630.863	623.576	616.627	609.985s
*	rftn *	603.626	586.677	570.954	556.284s
*	rftn *	672.981	672.981	672.981	672.981s
*	rftn *	672.981	672.981	672.981	672.981s
*	rftn *	671.145	667.667	662.711	656.412s
*	rftn *	648.885	640.812	633.152	625.863s
*	rftn *	618.913	612.271	605.911	588.979s
*	rftn *	573.271	558.616	675.048	675.048s
*	rftn *	675.048	675.048	675.048	675.048s
*	rftn *	675.048	675.048	673.213	669.739s
*	rftn *	664.787	658.494	650.973	642.899s
*	rftn *	635.238	627.949	620.997	614.355s
*	rftn *	607.994	591.077	575.384	560.742s
*	rftn *	675.038	675.038	675.038	675.038s
*	rftn *	675.038	675.038	675.038	675.038s
*	rftn *	673.203	669.728	664.776	658.483s
*	rftn *	650.962	642.889	635.227	627.938s
*	rftn *	620.987	614.344	607.983	591.066s
*	rftn *	575.373	560.731	675.027	675.027s
*	rftn *	675.027	675.027	675.027	675.027s
*	rftn *	675.027	675.027	673.192	669.717s
*	rftn *	664.766	658.472	650.952	642.878s
*	rftn *	635.216	627.927	620.976	614.333s
*	rftn *	607.972	591.055	575.362	560.72s
*	rftn *	675.017	675.017	675.017	675.017s
*	rftn *	675.017	675.017	675.017	675.017s
*	rftn *	673.181	669.707	664.755	658.462s
*	rftn *	650.941	642.867	635.206	627.917s
*	rftn *	620.966	614.323	607.962	591.045s
*	rftn *	575.352	560.709	675.006	675.006s
*	rftn *	675.006	675.006	675.006	675.006s
*	rftn *	675.006	675.006	673.171	669.696s
*	rftn *	664.745	658.451	650.93	642.857s
*	rftn *	635.195	627.906	620.955	614.312s
*	rftn *	607.951	591.034	575.341	560.699s
*	rftn *	674.995	674.995	674.995	674.995s
*	rftn *	674.995	674.995	674.995	674.995s
*	rftn *	673.16	669.686	664.734	658.441s
*	rftn *	650.92	642.846	635.184	627.895s
*	rftn *	620.944	614.301	607.941	591.023s
*	rftn *	575.33	560.688	674.985	674.985s
*	rftn *	674.985	674.985	674.985	674.985s
*	rftn *	674.985	674.985	673.15	669.675s
*	rftn *	664.723	658.43	650.909	642.835s
*	rftn *	635.174	627.885	620.934	614.291s
*	rftn *	607.93	591.012	575.319	560.677s
*	rftn *	674.974	674.974	674.974	674.974s
*	rftn *	674.974	674.974	674.974	674.974s
*	rftn *	673.139	669.665	664.713	658.419s
*	rftn *	650.898	642.825	635.163	627.874s
*	rftn *	620.923	614.28	607.919	591.002s
*	rftn *	575.308	560.666	674.964	674.964s
*	rftn *	674.964	674.964	674.964	674.964s
*	rftn *	674.964	674.964	673.129	669.654s
*	rftn *	664.702	658.409	650.888	642.814s
*	rftn *	635.152	627.863	620.912	614.269s
*	rftn *	607.909	590.991	575.298	560.655s

Appendix A

*	rftn *	674.953	674.953	674.953	674.953s
*	rftn *	674.953	674.953	674.953	674.953s
*	rftn *	673.118	669.643	664.692	658.398s
*	rftn *	650.877	642.803	635.142	627.853s
*	rftn *	620.902	614.259	607.898	590.98s
*	rftn *	575.287	560.644	674.943	674.943s
*	rftn *	674.943	674.943	674.943	674.943s
*	rftn *	674.943	674.943	673.108	669.633s
*	rftn *	664.681	658.387	650.867	642.793s
*	rftn *	635.131	627.842	620.891	614.248s
*	rftn *	607.887	590.97	575.276	560.634s
*	rftn *	674.932	674.932	674.932	674.932s
*	rftn *	674.932	674.932	674.932	674.932s
*	rftn *	673.097	669.622	664.67	658.377s
*	rftn *	650.856	642.782	635.121	627.831s
*	rftn *	620.88	614.238	607.877	590.959s
*	rftn *	575.265	560.623	674.922	674.922s
*	rftn *	674.922	674.922	674.922	674.922s
*	rftn *	674.922	674.922	673.086	669.612s
*	rftn *	664.66	658.366	650.845	642.771s
*	rftn *	635.11	627.821	620.87	614.227s
*	rftn *	607.866	590.948	575.254	560.612s
*	rftn *	674.911	674.911	674.911	674.911s
*	rftn *	674.911	674.911	674.911	674.911s
*	rftn *	673.076	669.601	664.649	658.356s
*	rftn *	650.835	642.761	635.099	627.81s
*	rftn *	620.859	614.216	607.856	590.937s
*	rftn *	575.244	560.601	674.901	674.901s
*	rftn *	674.901	674.901	674.901	674.901s
*	rftn *	674.901	674.901	673.065	669.591s
*	rftn *	664.639	658.345	650.824	642.75s
*	rftn *	635.089	627.8	620.849	614.206s
*	rftn *	607.845	590.927	575.233	560.59s
*	rftn *	674.89	674.89	674.89	674.89s
*	rftn *	674.89	674.89	674.89	674.89s
*	rftn *	673.055	669.58	664.628	658.334s
*	rftn *	650.813	642.739	635.078	627.789s
*	rftn *	620.838	614.195	607.834	590.916s
*	rftn *	575.222	560.579	674.879	674.879s
*	rftn *	674.879	674.879	674.879	674.879s
*	rftn *	674.879	674.879	673.044	669.569s
*	rftn *	664.617	658.324	650.803	642.729s
*	rftn *	635.067	627.778	620.827	614.184s
*	rftn *	607.824	590.905	575.211	560.568s
*	rftn *	674.869	674.869	674.869	674.869s
*	rftn *	674.869	674.869	674.869	674.869s
*	rftn *	673.034	669.559	664.607	658.313s
*	rftn *	650.792	642.718	635.057	627.768s
*	rftn *	620.817	614.174	607.813	590.895s
*	rftn *	575.201	560.558	674.858	674.858s
*	rftn *	674.858	674.858	674.858	674.858s
*	rftn *	674.858	674.858	673.023	669.548s
*	rftn *	664.596	658.302	650.781	642.707s
*	rftn *	635.046	627.757	620.806	614.163s
*	rftn *	607.802	590.884	575.19	560.547s
*	rftn *	674.848	674.848	674.848	674.848s
*	rftn *	674.848	674.848	674.848	674.848s
*	rftn *	673.013	669.538	664.586	658.292s
*	rftn *	650.771	642.697	635.035	627.746s
*	rftn *	620.795	614.152	607.792	590.873s
*	rftn *	575.179	560.536	674.837	674.837s
*	rftn *	674.837	674.837	674.837	674.837s
*	rftn *	674.837	674.837	673.002	669.527s
*	rftn *	664.575	658.281	650.76	642.686s
*	rftn *	635.025	627.736	620.785	614.142s
*	rftn *	607.781	590.862	575.168	560.525e
*	rftn *	668.425	668.425	668.425	668.425s
*	rftn *	668.425	668.425	668.425	668.425s
*	rftn *	666.585	663.101	658.135	651.824s

*	rftn *	644.282	636.212	628.553	621.266s
*	rftn *	614.318	607.678	601.319	584.353s
*	rftn *	568.614	553.929	670.714	670.714s
*	rftn *	670.714	670.714	670.714	670.714s
*	rftn *	670.714	670.714	668.876	665.395s
*	rftn *	660.434	654.129	646.595	638.523s
*	rftn *	630.863	623.576	616.627	609.985s
*	rftn *	603.626	586.677	570.954	556.284s
*	rftn *	672.981	672.981	672.981	672.981s
*	rftn *	672.981	672.981	672.981	672.981s
*	rftn *	671.145	667.667	662.711	656.412s
*	rftn *	648.885	640.812	633.152	625.863s
*	rftn *	618.913	612.271	605.911	588.979s
*	rftn *	573.271	558.616	675.048	675.048s
*	rftn *	675.048	675.048	675.048	675.048s
*	rftn *	675.048	675.048	673.213	669.739s
*	rftn *	664.787	658.494	650.973	642.899s
*	rftn *	635.238	627.949	620.997	614.355s
*	rftn *	607.994	591.077	575.384	560.742s
*	rftn *	675.038	675.038	675.038	675.038s
*	rftn *	675.038	675.038	675.038	675.038s
*	rftn *	673.203	669.728	664.776	658.483s
*	rftn *	650.962	642.889	635.227	627.938s
*	rftn *	620.987	614.344	607.983	591.066s
*	rftn *	575.373	560.731	675.027	675.027s
*	rftn *	675.027	675.027	675.027	675.027s
*	rftn *	675.027	675.027	673.192	669.717s
*	rftn *	664.766	658.472	650.952	642.878s
*	rftn *	635.216	627.927	620.976	614.333s
*	rftn *	607.972	591.055	575.362	560.72s
*	rftn *	675.017	675.017	675.017	675.017s
*	rftn *	675.017	675.017	675.017	675.017s
*	rftn *	673.181	669.707	664.755	658.462s
*	rftn *	650.941	642.867	635.206	627.917s
*	rftn *	620.966	614.323	607.962	591.045s
*	rftn *	575.352	560.709	675.006	675.006s
*	rftn *	675.006	675.006	675.006	675.006s
*	rftn *	675.006	675.006	673.171	669.696s
*	rftn *	664.745	658.451	650.93	642.857s
*	rftn *	635.195	627.906	620.955	614.312s
*	rftn *	607.951	591.034	575.341	560.699s
*	rftn *	674.995	674.995	674.995	674.995s
*	rftn *	674.995	674.995	674.995	674.995s
*	rftn *	673.16	669.686	664.734	658.441s
*	rftn *	650.92	642.846	635.184	627.895s
*	rftn *	620.944	614.301	607.941	591.023s
*	rftn *	575.33	560.688	674.985	674.985s
*	rftn *	674.985	674.985	674.985	674.985s
*	rftn *	674.985	674.985	673.15	669.675s
*	rftn *	664.723	658.43	650.909	642.835s
*	rftn *	635.174	627.885	620.934	614.291s
*	rftn *	607.93	591.012	575.319	560.677s
*	rftn *	674.974	674.974	674.974	674.974s
*	rftn *	674.974	674.974	674.974	674.974s
*	rftn *	673.139	669.665	664.713	658.419s
*	rftn *	650.898	642.825	635.163	627.874s
*	rftn *	620.923	614.28	607.919	591.002s
*	rftn *	575.308	560.666	674.964	674.964s
*	rftn *	674.964	674.964	674.964	674.964s
*	rftn *	674.964	674.964	673.129	669.654s
*	rftn *	664.702	658.409	650.888	642.814s
*	rftn *	635.152	627.863	620.912	614.269s
*	rftn *	607.909	590.991	575.298	560.655s
*	rftn *	674.953	674.953	674.953	674.953s
*	rftn *	674.953	674.953	674.953	674.953s
*	rftn *	673.118	669.643	664.692	658.398s
*	rftn *	650.877	642.803	635.142	627.853s
*	rftn *	620.902	614.259	607.898	590.98s
*	rftn *	575.287	560.644	674.943	674.943s

Appendix A

*	rftn *	674.943	674.943	674.943	674.943s
*	rftn *	674.943	674.943	673.108	669.633s
*	rftn *	664.681	658.387	650.867	642.793s
*	rftn *	635.131	627.842	620.891	614.248s
*	rftn *	607.887	590.97	575.276	560.634s
*	rftn *	674.932	674.932	674.932	674.932s
*	rftn *	674.932	674.932	674.932	674.932s
*	rftn *	673.097	669.622	664.67	658.377s
*	rftn *	650.856	642.782	635.121	627.831s
*	rftn *	620.88	614.238	607.877	590.959s
*	rftn *	575.265	560.623	674.922	674.922s
*	rftn *	674.922	674.922	674.922	674.922s
*	rftn *	674.922	674.922	673.086	669.612s
*	rftn *	664.66	658.366	650.845	642.771s
*	rftn *	635.11	627.821	620.87	614.227s
*	rftn *	607.866	590.948	575.254	560.612s
*	rftn *	674.911	674.911	674.911	674.911s
*	rftn *	674.911	674.911	674.911	674.911s
*	rftn *	673.076	669.601	664.649	658.356s
*	rftn *	650.835	642.761	635.099	627.81s
*	rftn *	620.859	614.216	607.856	590.937s
*	rftn *	575.244	560.601	674.901	674.901s
*	rftn *	674.901	674.901	674.901	674.901s
*	rftn *	674.901	674.901	673.065	669.591s
*	rftn *	664.639	658.345	650.824	642.75s
*	rftn *	635.089	627.8	620.849	614.206s
*	rftn *	607.845	590.927	575.233	560.59s
*	rftn *	674.89	674.89	674.89	674.89s
*	rftn *	674.89	674.89	674.89	674.89s
*	rftn *	673.055	669.58	664.628	658.334s
*	rftn *	650.813	642.739	635.078	627.789s
*	rftn *	620.838	614.195	607.834	590.916s
*	rftn *	575.222	560.579	674.879	674.879s
*	rftn *	674.879	674.879	674.879	674.879s
*	rftn *	674.879	674.879	673.044	669.569s
*	rftn *	664.617	658.324	650.803	642.729s
*	rftn *	635.067	627.778	620.827	614.184s
*	rftn *	607.824	590.905	575.211	560.568s
*	rftn *	674.869	674.869	674.869	674.869s
*	rftn *	674.869	674.869	674.869	674.869s
*	rftn *	673.034	669.559	664.607	658.313s
*	rftn *	650.792	642.718	635.057	627.768s
*	rftn *	620.817	614.174	607.813	590.895s
*	rftn *	575.201	560.558	674.858	674.858s
*	rftn *	674.858	674.858	674.858	674.858s
*	rftn *	674.858	674.858	673.023	669.548s
*	rftn *	664.596	658.302	650.781	642.707s
*	rftn *	635.046	627.757	620.806	614.163s
*	rftn *	607.802	590.884	575.19	560.547s
*	rftn *	674.848	674.848	674.848	674.848s
*	rftn *	674.848	674.848	674.848	674.848s
*	rftn *	673.013	669.538	664.586	658.292s
*	rftn *	650.771	642.697	635.035	627.746s
*	rftn *	620.795	614.152	607.792	590.873s
*	rftn *	575.179	560.536	674.837	674.837s
*	rftn *	674.837	674.837	674.837	674.837s
*	rftn *	674.837	674.837	673.002	669.527s
*	rftn *	664.575	658.281	650.76	642.686s
*	rftn *	635.025	627.736	620.785	614.142s
*	rftn *	607.781	590.862	575.168	560.525e
*	rftn *	668.425	668.425	668.425	668.425s
*	rftn *	668.425	668.425	668.425	668.425s
*	rftn *	666.585	663.101	658.135	651.824s
*	rftn *	644.282	636.212	628.553	621.266s
*	rftn *	614.318	607.678	601.319	584.353s
*	rftn *	568.614	553.929	670.714	670.714s
*	rftn *	670.714	670.714	670.714	670.714s
*	rftn *	670.714	670.714	668.876	665.395s
*	rftn *	660.434	654.129	646.595	638.523s

*	rftn *	630.863	623.576	616.627	609.985s
*	rftn *	603.626	586.677	570.954	556.284s
*	rftn *	672.981	672.981	672.981	672.981s
*	rftn *	672.981	672.981	672.981	672.981s
*	rftn *	671.145	667.667	662.711	656.412s
*	rftn *	648.885	640.812	633.152	625.863s
*	rftn *	618.913	612.271	605.911	588.979s
*	rftn *	573.271	558.616	675.048	675.048s
*	rftn *	675.048	675.048	675.048	675.048s
*	rftn *	675.048	675.048	673.213	669.739s
*	rftn *	664.787	658.494	650.973	642.899s
*	rftn *	635.238	627.949	620.997	614.355s
*	rftn *	607.994	591.077	575.384	560.742s
*	rftn *	675.038	675.038	675.038	675.038s
*	rftn *	675.038	675.038	675.038	675.038s
*	rftn *	673.203	669.728	664.776	658.483s
*	rftn *	650.962	642.889	635.227	627.938s
*	rftn *	620.987	614.344	607.983	591.066s
*	rftn *	575.373	560.731	675.027	675.027s
*	rftn *	675.027	675.027	675.027	675.027s
*	rftn *	675.027	675.027	673.192	669.717s
*	rftn *	664.766	658.472	650.952	642.878s
*	rftn *	635.216	627.927	620.976	614.333s
*	rftn *	607.972	591.055	575.362	560.72s
*	rftn *	675.017	675.017	675.017	675.017s
*	rftn *	675.017	675.017	675.017	675.017s
*	rftn *	673.181	669.707	664.755	658.462s
*	rftn *	650.941	642.867	635.206	627.917s
*	rftn *	620.966	614.323	607.962	591.045s
*	rftn *	575.352	560.709	675.006	675.006s
*	rftn *	675.006	675.006	675.006	675.006s
*	rftn *	675.006	675.006	673.171	669.696s
*	rftn *	664.745	658.451	650.93	642.857s
*	rftn *	635.195	627.906	620.955	614.312s
*	rftn *	607.951	591.034	575.341	560.699s
*	rftn *	674.995	674.995	674.995	674.995s
*	rftn *	674.995	674.995	674.995	674.995s
*	rftn *	673.16	669.686	664.734	658.441s
*	rftn *	650.92	642.846	635.184	627.895s
*	rftn *	620.944	614.301	607.941	591.023s
*	rftn *	575.33	560.688	674.985	674.985s
*	rftn *	674.985	674.985	674.985	674.985s
*	rftn *	674.985	674.985	673.15	669.675s
*	rftn *	664.723	658.43	650.909	642.835s
*	rftn *	635.174	627.885	620.934	614.291s
*	rftn *	607.93	591.012	575.319	560.677s
*	rftn *	674.974	674.974	674.974	674.974s
*	rftn *	674.974	674.974	674.974	674.974s
*	rftn *	673.139	669.665	664.713	658.419s
*	rftn *	650.898	642.825	635.163	627.874s
*	rftn *	620.923	614.28	607.919	591.002s
*	rftn *	575.308	560.666	674.964	674.964s
*	rftn *	674.964	674.964	674.964	674.964s
*	rftn *	674.964	674.964	673.129	669.654s
*	rftn *	664.702	658.409	650.888	642.814s
*	rftn *	635.152	627.863	620.912	614.269s
*	rftn *	607.909	590.991	575.298	560.655s
*	rftn *	674.953	674.953	674.953	674.953s
*	rftn *	674.953	674.953	674.953	674.953s
*	rftn *	673.118	669.643	664.692	658.398s
*	rftn *	650.877	642.803	635.142	627.853s
*	rftn *	620.902	614.259	607.898	590.98s
*	rftn *	575.287	560.644	674.943	674.943s
*	rftn *	674.943	674.943	674.943	674.943s
*	rftn *	674.943	674.943	673.108	669.633s
*	rftn *	664.681	658.387	650.867	642.793s
*	rftn *	635.131	627.842	620.891	614.248s
*	rftn *	607.887	590.97	575.276	560.634s
*	rftn *	674.932	674.932	674.932	674.932s

Appendix A

*	rftn *	674.932	674.932	674.932	674.932s
*	rftn *	673.097	669.622	664.67	658.377s
*	rftn *	650.856	642.782	635.121	627.831s
*	rftn *	620.88	614.238	607.877	590.959s
*	rftn *	575.265	560.623	674.922	674.922s
*	rftn *	674.922	674.922	674.922	674.922s
*	rftn *	674.922	674.922	673.086	669.612s
*	rftn *	664.66	658.366	650.845	642.771s
*	rftn *	635.11	627.821	620.87	614.227s
*	rftn *	607.866	590.948	575.254	560.612s
*	rftn *	674.911	674.911	674.911	674.911s
*	rftn *	674.911	674.911	674.911	674.911s
*	rftn *	673.076	669.601	664.649	658.356s
*	rftn *	650.835	642.761	635.099	627.81s
*	rftn *	620.859	614.216	607.856	590.937s
*	rftn *	575.244	560.601	674.901	674.901s
*	rftn *	674.901	674.901	674.901	674.901s
*	rftn *	674.901	674.901	673.065	669.591s
*	rftn *	664.639	658.345	650.824	642.75s
*	rftn *	635.089	627.8	620.849	614.206s
*	rftn *	607.845	590.927	575.233	560.59s
*	rftn *	674.89	674.89	674.89	674.89s
*	rftn *	674.89	674.89	674.89	674.89s
*	rftn *	673.055	669.58	664.628	658.334s
*	rftn *	650.813	642.739	635.078	627.789s
*	rftn *	620.838	614.195	607.834	590.916s
*	rftn *	575.222	560.579	674.879	674.879s
*	rftn *	674.879	674.879	674.879	674.879s
*	rftn *	674.879	674.879	673.044	669.569s
*	rftn *	664.617	658.324	650.803	642.729s
*	rftn *	635.067	627.778	620.827	614.184s
*	rftn *	607.824	590.905	575.211	560.568s
*	rftn *	674.869	674.869	674.869	674.869s
*	rftn *	674.869	674.869	674.869	674.869s
*	rftn *	673.034	669.559	664.607	658.313s
*	rftn *	650.792	642.718	635.057	627.768s
*	rftn *	620.817	614.174	607.813	590.895s
*	rftn *	575.201	560.558	674.858	674.858s
*	rftn *	674.858	674.858	674.858	674.858s
*	rftn *	674.858	674.858	673.023	669.548s
*	rftn *	664.596	658.302	650.781	642.707s
*	rftn *	635.046	627.757	620.806	614.163s
*	rftn *	607.802	590.884	575.19	560.547s
*	rftn *	674.848	674.848	674.848	674.848s
*	rftn *	674.848	674.848	674.848	674.848s
*	rftn *	673.013	669.538	664.586	658.292s
*	rftn *	650.771	642.697	635.035	627.746s
*	rftn *	620.795	614.152	607.792	590.873s
*	rftn *	575.179	560.536	674.837	674.837s
*	rftn *	674.837	674.837	674.837	674.837s
*	rftn *	674.837	674.837	673.002	669.527s
*	rftn *	664.575	658.281	650.76	642.686s
*	rftn *	635.025	627.736	620.785	614.142s
*	rftn *	607.781	590.862	575.168	560.525e
*	rftn *	668.425	668.425	668.425	668.425s
*	rftn *	668.425	668.425	668.425	668.425s
*	rftn *	666.585	663.101	658.135	651.824s
*	rftn *	644.282	636.212	628.553	621.266s
*	rftn *	614.318	607.678	601.319	584.353s
*	rftn *	568.614	553.929	670.714	670.714s
*	rftn *	670.714	670.714	670.714	670.714s
*	rftn *	670.714	670.714	668.876	665.395s
*	rftn *	660.434	654.129	646.595	638.523s
*	rftn *	630.863	623.576	616.627	609.985s
*	rftn *	603.626	586.677	570.954	556.284s
*	rftn *	672.981	672.981	672.981	672.981s
*	rftn *	672.981	672.981	672.981	672.981s
*	rftn *	671.145	667.667	662.711	656.412s
*	rftn *	648.885	640.812	633.152	625.863s

*	rftn *	618.913	612.271	605.911	588.979s
*	rftn *	573.271	558.616	675.048	675.048s
*	rftn *	675.048	675.048	675.048	675.048s
*	rftn *	675.048	675.048	673.213	669.739s
*	rftn *	664.787	658.494	650.973	642.899s
*	rftn *	635.238	627.949	620.997	614.355s
*	rftn *	607.994	591.077	575.384	560.742s
*	rftn *	675.038	675.038	675.038	675.038s
*	rftn *	675.038	675.038	675.038	675.038s
*	rftn *	673.203	669.728	664.776	658.483s
*	rftn *	650.962	642.889	635.227	627.938s
*	rftn *	620.987	614.344	607.983	591.066s
*	rftn *	575.373	560.731	675.027	675.027s
*	rftn *	675.027	675.027	675.027	675.027s
*	rftn *	675.027	675.027	673.192	669.717s
*	rftn *	664.766	658.472	650.952	642.878s
*	rftn *	635.216	627.927	620.976	614.333s
*	rftn *	607.972	591.055	575.362	560.72s
*	rftn *	675.017	675.017	675.017	675.017s
*	rftn *	675.017	675.017	675.017	675.017s
*	rftn *	673.181	669.707	664.755	658.462s
*	rftn *	650.941	642.867	635.206	627.917s
*	rftn *	620.966	614.323	607.962	591.045s
*	rftn *	575.352	560.709	675.006	675.006s
*	rftn *	675.006	675.006	675.006	675.006s
*	rftn *	675.006	675.006	673.171	669.696s
*	rftn *	664.745	658.451	650.93	642.857s
*	rftn *	635.195	627.906	620.955	614.312s
*	rftn *	607.951	591.034	575.341	560.699s
*	rftn *	674.995	674.995	674.995	674.995s
*	rftn *	674.995	674.995	674.995	674.995s
*	rftn *	673.16	669.686	664.734	658.441s
*	rftn *	650.92	642.846	635.184	627.895s
*	rftn *	620.944	614.301	607.941	591.023s
*	rftn *	575.33	560.688	674.985	674.985s
*	rftn *	674.985	674.985	674.985	674.985s
*	rftn *	674.985	674.985	673.15	669.675s
*	rftn *	664.723	658.43	650.909	642.835s
*	rftn *	635.174	627.885	620.934	614.291s
*	rftn *	607.93	591.012	575.319	560.677s
*	rftn *	674.974	674.974	674.974	674.974s
*	rftn *	674.974	674.974	674.974	674.974s
*	rftn *	673.139	669.665	664.713	658.419s
*	rftn *	650.898	642.825	635.163	627.874s
*	rftn *	620.923	614.28	607.919	591.002s
*	rftn *	575.308	560.666	674.964	674.964s
*	rftn *	674.964	674.964	674.964	674.964s
*	rftn *	674.964	674.964	673.129	669.654s
*	rftn *	664.702	658.409	650.888	642.814s
*	rftn *	635.152	627.863	620.912	614.269s
*	rftn *	607.909	590.991	575.298	560.655s
*	rftn *	674.953	674.953	674.953	674.953s
*	rftn *	674.953	674.953	674.953	674.953s
*	rftn *	673.118	669.643	664.692	658.398s
*	rftn *	650.877	642.803	635.142	627.853s
*	rftn *	620.902	614.259	607.898	590.98s
*	rftn *	575.287	560.644	674.943	674.943s
*	rftn *	674.943	674.943	674.943	674.943s
*	rftn *	674.943	674.943	673.108	669.633s
*	rftn *	664.681	658.387	650.867	642.793s
*	rftn *	635.131	627.842	620.891	614.248s
*	rftn *	607.887	590.97	575.276	560.634s
*	rftn *	674.932	674.932	674.932	674.932s
*	rftn *	674.932	674.932	674.932	674.932s
*	rftn *	673.097	669.622	664.67	658.377s
*	rftn *	650.856	642.782	635.121	627.831s
*	rftn *	620.88	614.238	607.877	590.959s
*	rftn *	575.265	560.623	674.922	674.922s
*	rftn *	674.922	674.922	674.922	674.922s

Appendix A

* rftn *	674.922	674.922	673.086	669.612s
* rftn *	664.66	658.366	650.845	642.771s
* rftn *	635.11	627.821	620.87	614.227s
* rftn *	607.866	590.948	575.254	560.612s
* rftn *	674.911	674.911	674.911	674.911s
* rftn *	674.911	674.911	674.911	674.911s
* rftn *	673.076	669.601	664.649	658.356s
* rftn *	650.835	642.761	635.099	627.81s
* rftn *	620.859	614.216	607.856	590.937s
* rftn *	575.244	560.601	674.901	674.901s
* rftn *	674.901	674.901	674.901	674.901s
* rftn *	674.901	674.901	673.065	669.591s
* rftn *	664.639	658.345	650.824	642.75s
* rftn *	635.089	627.8	620.849	614.206s
* rftn *	607.845	590.927	575.233	560.59s
* rftn *	674.89	674.89	674.89	674.89s
* rftn *	674.89	674.89	674.89	674.89s
* rftn *	673.055	669.58	664.628	658.334s
* rftn *	650.813	642.739	635.078	627.789s
* rftn *	620.838	614.195	607.834	590.916s
* rftn *	575.222	560.579	674.879	674.879s
* rftn *	674.879	674.879	674.879	674.879s
* rftn *	674.879	674.879	673.044	669.569s
* rftn *	664.617	658.324	650.803	642.729s
* rftn *	635.067	627.778	620.827	614.184s
* rftn *	607.824	590.905	575.211	560.568s
* rftn *	674.869	674.869	674.869	674.869s
* rftn *	674.869	674.869	674.869	674.869s
* rftn *	673.034	669.559	664.607	658.313s
* rftn *	650.792	642.718	635.057	627.768s
* rftn *	620.817	614.174	607.813	590.895s
* rftn *	575.201	560.558	674.858	674.858s
* rftn *	674.858	674.858	674.858	674.858s
* rftn *	674.858	674.858	673.023	669.548s
* rftn *	664.596	658.302	650.781	642.707s
* rftn *	635.046	627.757	620.806	614.163s
* rftn *	607.802	590.884	575.19	560.547s
* rftn *	674.848	674.848	674.848	674.848s
* rftn *	674.848	674.848	674.848	674.848s
* rftn *	673.013	669.538	664.586	658.292s
* rftn *	650.771	642.697	635.035	627.746s
* rftn *	620.795	614.152	607.792	590.873s
* rftn *	575.179	560.536	674.837	674.837s
* rftn *	674.837	674.837	674.837	674.837s
* rftn *	674.837	674.837	673.002	669.527s
* rftn *	664.575	658.281	650.76	642.686s
* rftn *	635.025	627.736	620.785	614.142s
* rftn *	607.781	590.862	575.168	560.525e
* rdppwr *	0.0	0.0	0.0	0.0s
* rdppwr *	0.0	1.0	1.0	1.0
* rdppwr *	1.0	1.0	1.0	0.0
* rdppwr *	0.0	0.0	0.0	0.0
* rdppwr *	0.0	0.0e		
* cpowr *	1.3	1.15	0.89	0.45e
* radpw *	1.0	1.0	1.0	1.0
* radpw *	1.0	1.0	1.0	1.0
* radpw *	1.0	1.0	1.0	1.0
* radpw *	1.0	1.0	1.0	1.0
* radpw *	1.0	1.0	1.0	1.0e
* fpuo2 *	0.0	0.0	0.0	0.0e
* ftd *	1.0	1.0	1.0	1.0e
* gmix * f	0.0e			
* pgapt *	0.0	0.0	0.0	0.0e
* burn *	0.0	0.0	0.0	0.0s
* burn *	0.0	0.0	0.0	0.0s
* burn *	0.0	0.0	0.0	0.0s
* burn *	0.0	0.0	0.0	0.0s
* burn *	0.0	0.0	0.0	0.0s
* burn *	0.0	0.0	0.0	0.0s
* burn *	0.0	0.0	0.0	0.0e

```

* burn *      0.0      0.0      0.0      0.0s
* burn *      0.0      0.0      0.0      0.0e
* burn *      0.0      0.0      0.0      0.0s
* burn *      0.0      0.0      0.0      0.0e
* burn *      0.0      0.0      0.0      0.0s
* burn *      0.0      0.0      0.0      0.0e
* burn *      0.0      0.0      0.0      0.0s
* mrod *      2       1       2       1       1s
* mrod *      2       1       2       1       4s
* mrod *      3       3       3       4       2s
* mrod *      1       2       3       3       3s
* mrod *      3       3       4       2       1s
* mrod *      3       3       5       5       3s
* mrod *      3       2       1       3       3s
* mrod *      5       5       3       3       2s
* mrod *      2       4       3       3       3s
* mrod *      3       4       2       1       2s
* mrod *      4       3       3       4       2s
* mrod *      1       2       1       2       2s
* mrod *      2       2       1       2       6e
*      partial length rods
*      i           j           levrod
*      -1
*
*      water rods *
*      i           j           flag        xloc        yloc
*      4           4           1          0.06625   -0.06625
*      4           5           1          0.0          0.0
*      5           4           1          0.0          0.0
*      5           5           1          0.0          0.0
-1
*      water rod data sets
*
*      igeom      wrnodes
*      1           3
*      wrinlet    wroutlet     dia        sidea      sideb
*      1           24          0.034     0.0         0.0
*      th         rcorner     flowarea   flwareai   flwareao
*      0.001      0.0          9.079203E-4 9.079203E-4 9.079203E-4
*      hd         hdri        hdro       thrmdiai  thrmdiao
*      0.032      0.032       0.032     0.032      0.032
*      wrflossi   wrflosso   wrrlossi  wrrlosso
*      1.0E20     1.0E20     1.0E20
*      matwr *    53          53e
*      tw *       553.929    553.929    553.929    556.284   556.284s
*      tw *       556.284    558.616    558.616    558.616    560.742s
*      tw *       560.742    560.742    560.731    560.731    560.731s
*      tw *       560.72     560.72     560.72     560.709    560.709s
*      tw *       560.709    560.698    560.698    560.698    560.687s
*      tw *       560.687    560.687    560.677    560.677    560.677s
*      tw *       560.666    560.666    560.666    560.655    560.655s
*      tw *       560.655    560.644    560.644    560.644    560.633s
*      tw *       560.633    560.633    560.622    560.622    560.622s
*      tw *       560.611    560.611    560.611    560.601    560.601s
*      tw *       560.601    560.59     560.59     560.59     560.579s
*      tw *       560.579    560.579    560.568    560.568    560.568s
*      tw *       560.557    560.557    560.557    560.546    560.546s
*      tw *       560.546    560.535    560.535    560.535    560.525s

```

Appendix A

```

*      tw     *      560.525      560.525e
*
*
*****      type      num      userid      component name
break          300          1          Outlet
*      junl      ibty      isat      ioff      adjpress
*          20          1          0          1          0
*      ibtr      ibsv      nbtb      nbsv      nbrf
*          0          202          5          0          0
*      dxin      volin      alpin      tin      pin
*      0.1545  1.462034E-3  0.124      560.551  7.17E6
*      pain      concin      rbmx      poff      belv
*      0.0          0.0      1.0E20  0.0          0.0
*      pscl      tlscl      tvscl      pascl      conscl
*          1.0          1.0          1.0          1.0          1.0
*      ptb      0.0      7.17E6s
*      ptb      1.0      7.17E6s
*      ptb      2.0      7.17E6s
*      ptb      3.0      7.17E6s
*      ptb      1.0E6  7.17E6e
*
*
*****
*      Starting Power Components      *
*****
*
*****      type      num      userid      component name
power          201          1          Power
*      numpwr      chanpow      1
*      htnum      200e
*      irpwty      ndgx      ndhx      nrt5      nhist
*          6          0          0          100          0
*      irpwtr      irpws5      nrpwtb      nrpws5      nrpwrf
*          0          202          4          0          0
*      izpwtr      izpws5      nzpwtb      nzpws5      nzpwrf
*          0          202          4          0          0
*      ipwrad      ipwdep      promheat      decaheat      wt bypass
*          0          0          0.0          0.0          0.0
*      nzpwz      nzpwi      nfpwt      nrpw5      nrpwi
*          0          0          0          1          0
*      react      tneut      rpwoff      rrpwm5      rpwsc5
*          0.0          0.0          0.0          1.0E20          1.0
*      rpowri      zpwin      zpwoff      rzpwm5
*      1.24E6          0.0          -1.0E19          1.0E20
*      extsou      pldr      pdrat      fucrac
*          0.0          0.0          1.0          1.0
*      zpwtb1*      0.0s
*      zpwtb1*      1.0          1.0          1.0          1.0          1.0s
*      zpwtb2*      1.0s
*      zpwtb2*      1.0          1.0          1.0          1.0          1.0s
*      zpwtb3*      2.0s
*      zpwtb3*      1.0          1.0          1.0          1.0          1.0s
*      zpwtb4*      1.0E6s
*      zpwtb4*      1.0          1.0          1.0          1.0          1.0s
*      zpwtb4*      1.0          1.0          1.0          1.0          1.0s
*      zpwtb4*      1.0          1.0          1.0          1.0          1.0s

```

```
* zpwtb4*      1.0      1.0      1.0      1.0      1.0s
* zpwtb4*      1.0      1.0      1.0      1.0e
* rpwtbr*      0.0      1.24E6s
* rpwtbr*      5.0      1.24E6s
* rpwtbr*     60.0      1.24E6s
* rpwtbr*    1.0E6      1.24E6e
*****
*      Finished Power Components      *
*****
*
*
*
end
*
*****
* Timestep Data *
*****
*      dtmin      dtmax      tend      rtwfp
*      1.0E-4      1.0E-3     1000.0     10.0
*      edint      gfint      dmpint      sedint
*                  1.0          0.1       100.0        1.0
*
*      endflag
*                  -1.0
```